DYNAMICS OF AEROSPACE VEHICLES

LANGLEY
GRANT
IN-18-CR
1572
P 114

Final Technical Report

For

NASA Grant NAG 1-758

On Research Performed For the

NASA Langley Reseach Center
Hampton, VA

Technical Monitors:
Mr. P. D. Arbuckle
Mr. C. S. Buttrill

Principle Investigator

Dr. David K. Schmidt
Aerospace Research Center
College of Engineering and Applied Sciences
Arizona State University
Tempe, AZ 85287-8006

April 1, 1991

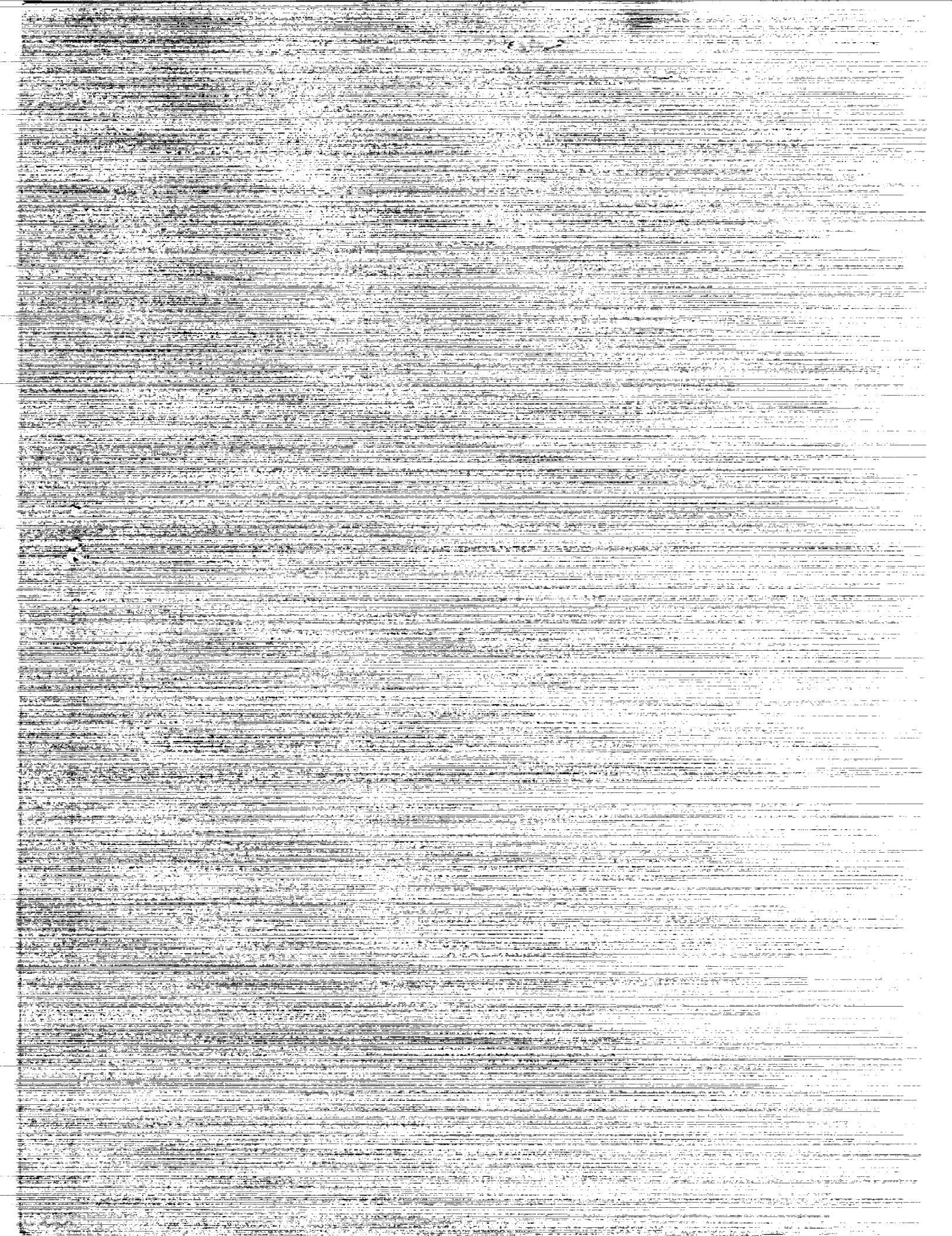

Final Technical Report

DYNAMICS OF AEROSPACE VEHICLES
(NAG 1 - 758)

Project Period May, 1987 - Sept., 1990.

This constitutes the final technical report for the subject grant. The grant was administered through Purdue University, and the principle investigator was Dr. David K. Schmidt. Dr. Schmidt pursued the grant research activities at Purdue until August, 1988. From August, 1988 until the end of the project period, the research activities of the grant were performed at Arizona State University, under a subcontract arrangement with Purdue University. During this period, the principle investigator and graduate researchers supported by the project were all affiliated with Arizona State University's College of Engineering and Applied Sciences, located in Tempe, Arizona 85287.

The graduate researchers supported by the grant include the following:

Mr. Brett Newman, Research Associate in ASU's Aerospace Research Center. Mr. Newman is also pursuing a Doctorate in Aerospace Engineering from Purdue University.

Mr. Shawn Molodow, Research Associate in ASU's Aerospace Research Center. Mr. Molodow received the M.S. in Aerospace Engineering from ASU in Dec. 1990. Thesis entitled "A Dynamics and Control Study of an Elastic Inverted Pendulum."

Conference papers presented, reporting technical results from this grant are as follows:

1) Schmidt, D.K. and Newman, B.,"Modeling, Model Simplification and Stability Robustness With Aeroelastic Vehicles," AIAA Paper 88-4079, Presented at the Guidance, Nav. and Control Conf., Minneapolis, Minn., August, 1988.

2) Schmidt, D.K., "Modeling Flexible Aircraft for Dynamic Analysis and Control Synthesis," Aerospace Computational Control Workshop, Williamsburg, VA, July, 1988. Proceedings in NASA Tech Memo, 101578.

3) Schmidt, D.K. and Newman, B., "On The Control of Elastic Vehicles - Model Simplification and Stability Robustness," AIAA Paper 89-3558, Presented at the Guid., Nav., and Control Conference, Boston, Mass., August, 1989.

4) Schmidt, D.K., "Multivariable Frequency-Weighted Order Reduction Algorithm For Control Synthesis," Aerospace Computational Control Workshop, Oxnard, CA, August, 1989. Proceedings in JPL Publication 89-45.

5) Schmidt, D. K. and Newman, B. "Multivariable Flight Control Synthesis and Literal Robustness Analysis for an Aeroelastic Vehicle," AIAA Paper 90-3446,

Guidance, Nav., and Control Conf., Portland OR, August, 1990. (Included as Appendix A to this report.)

6) Waszak, M.R., Buttrill, C.S., and Schmidt, D.K., "Modeling and Model Simplification of Aeroelastic Vehicles," Proceedings of the 17th Congress of International Council of the Aeronautical Sciences, Stockholm, Sweden, Sept. 1990. (Proceedings available from the AIAA.)

The following paper, which will appear in an archival journal, reports additional grant technical results:

Newman, B. and Schmidt, D.K., "Numerical and Literal Aeroelastic-Vehicle-Model Reduction for Feedback Control Synthesis," accepted for publication in the *Journal of Guidance, Control, and Dynamics*. Publication anticipated in 1991. (Included as Appendix B to this report.)

Also, conference papers 3 and 5 above have been submitted for publication in the *Journal of Guidance, Control, and Dynamics*.

Finally, an oral interim report was presented at the Langley Research Center in July, 1989. The presentation was given by the principle investigator, and was entitled "Dynamics of Aerospace Vehicles." Copies of the slides for this presentation are included as Appendix C to this report.

Appendix A

MULTIVARIABLE FLIGHT CONTROL SYNTHESIS AND LITERAL ROBUSTNESS ANALYSIS FOR AN AEROELASTIC VEHICLE*

David K. Schmidt** and Brett Newman***
Department of Mechanical and Aerospace Engineering
Arizona State University
Tempe, AZ 85287-6106

Abstract

The vehicle to be augmented is representative of a large supersonic transport, with first fuselage aeroelastic mode frequency at six rad/sec, very close to the two rad/sec short-period mode. An integrated flight- and aeroelastic-mode control law is synthesized using a previously developed model-following synthesis approach. This technique, designed to yield a desired closed-loop rather than an open-loop loop shape, involves a specific LQR formulation leading to the model-following state-feedback gains. Then the use of asymptotic loop transfer recovery is utilized to obtain the compensation that recovers the LQR robustness properties, and which leads to an output-feedback control law. A classically designed control law is also developed for comparison purposes. The resulting closed-loop systems are then evaluated in terms of their performance and multivariable stability robustness, measured in terms of the appropriate singular values. This evaluation includes the use of approximate literal expressions for those singular values, expressed in terms of literal expressions for the poles and zeros in the vehicle transfer-function matrix. It is found that the control laws possess roughly equivalent performance and stability robustness, and the characteristics limiting this robustness are traced to some specific loop gains and the frequency and damping of the open-loop aeroelastic mode dipole. Furthermore, closed-form literal expressions for these characteristics are presented in terms of the stability derivatives of the vehicle. Insight from such an analysis would be hard to obtain from a strictly numerical procedure.

---

* As Presented at the 1990 AIAA G.N.&C. Conf., Portland Or., Aug.,1990.
** Professor of Engr.; Assoc. Fellow AIAA
*** Research Assoc.; also Doctoral Candidate, School of Aero and Astro, Purdue Univ.; Student Member AIAA

1. Introduction

The supersonic and hypersonic capabilities of advanced aerospace vehicles and the use of extremely light metallic or composite materials in them can lead to vehicles with significant dynamic coupling between the rigid-body and elastic motions. Ref. 1 and 2, for example, specifically addressed this coupling at the earliest stage of system modeling and flight-control synthesis.

Augmentation of an aeroelastic vehicle's open-loop dynamics via feedback is often necessary to provide sufficient levels of stability and performance (e.g., handling qualities). Feedback is used to stabilize the attitude and or aeroelastic responses (such as static aerodynamic instability or flutter) or just augment damping. Crossfeeds may also be used to improve the dynamic responses. And the control-law must ensure this stability and performance in the presence of vehicle modeling errors (i.e., robustness). For aeroelastic vehicle applications, modeling errors can arise from uncertainty in the aerodynamic model and neglected high-frequency structural modes both leading to uncertainty in the pole/zero locations in the vehicle transfer functions, for example.Such control objectives have been noted in the literature[3-9].

If possible, the vehicle model (used in control synthesis) should aid in the understanding and thereby provide insight regarding the vehicle physics, exposing key dynamic characteristics and their causes. This can be achieved by developing literal expressions for the vehicle transfer functions (gains, zeros, and poles) in terms of vehicle model parameters, such as stability and control derivatives or vibrational characteristics, which have their genesis in the fundamental vehicle geometric shape and structural layout.[2,9,10] Models of this type can be an extremely powerful tool in open-loop or closed-loop design.[11]

The control synthesis for an aeroelastic vehicle, and the systems' analyses specifically using a literal model, is the subject of this paper. An aeroelastic vehicle model is briefly presented and deficiencies in the vehicle dynamics are noted. Control objectives are stated and sufficient conditions ensuring an acceptable design are given. A new approach to implicit model following (IMF) control synthesis[12,13] is briefly discussed and applied to the vehicle model. A classical control synthesis approach is also considered for the purposes of comparison. The resulting compensators and closed-loop

systems are analyzed with a literal model to expose sources of system characteristics that limit the closed-loop system stability robustness. It will be shown, for example, that major among these critical characteristics are the frequency and damping of the vehicles first aeroelastic mode dipole, and closed-form expressions for these terms are presented in terms of the vehicle stability derivatives.

2. The Vehicle Model For Feedback Synthesis

The configuration to be considered (from Refs. 2 and 10) is a large supersonic aircraft of reasonably conventional geometry with a low-aspect ratio swept wing, conventional tail, and canard. Controlled inputs consist of elevator δ_E and canard (located near the cockpit) deflection δ_C . The reference flight condition is level flight at Mach 0.6 and altitude 5,000 ft.

The complete non-linear modelling of this vehicle was the subject of Ref. 2, and the development of low order linear models for control synthesis was considered in Ref. 10. A fourth order state space realization and the corresponding transfer functions for this linear model are given in Tables 1 and 2. This model involves the small perturbation longitudinal dynamics of the effective short period and first aeroelastic modes. The responses of interest are the rigid-body angle of attack α, rigid-body pitch rate q, and pitch rate q' measured at the cockpit. Here, rigid-body α and q are the angle of attack and pitch rate associated with the vehicle mean axes. An approximate measurement of q can be obtained from a rate gyro located at the anti-node of the first elastic structural mode, and then lowpass filtering of the higher-frequency modes. The effects of such filtering will not be specifically addressed, but it would add additional phase loss in the loops, which is considered in the robustness analysis

A fourth-order model was developed to accurately approximate the appropriate frequency responses of a twelfth-order model, in the anticipated critical frequency range of 1 to 10 rad/s. Figures 1 thru 3 show some of these frequency responses from elevator input δ_E . (It is noted that the next significant unmodeled aeroelastic mode frequency is above 13 rad/sec.) From Table 2 and Figures 1 thru 3, the major open-loop dynamic deficiency is the level of damping of the short period and aeroelastic modes. Furthermore, the aeroelastic mode contributes significantly to the vehicle's dynamic responses.

3. Classical Control Synthesis

A classical design approach consists of sequential single loop closures, using root loci, and relying upon knowledge of the physics of the elastic aircraft for synthesis strategy.

Consider a 2 × 2 system from Table 2 with the following notation.

$$q(s) = g_{11}(s)\delta_E(s) + g_{12}(s)\delta_C(s) \qquad (1)$$
$$q'(s) = g_{21}(s)\delta_E(s) + g_{22}(s)\delta_C(s)$$

First, the q'/δ_C loop is closed to improve the aeroelastic mode damping. Recall q' and δ_C are a co-located sensor and actuator pair near the cockpit. The control law $\delta_C = \delta_C' - k_{22}q'$ yields

$$q = (g_{11} - \frac{k_{22}g_{12}g_{21}}{1 + k_{22}g_{22}})\delta_E + g_{12}(1 - \frac{k_{22}g_{22}}{1 + k_{22}g_{22}})\delta_C' \qquad (2)$$
$$q' = \frac{g_{21}}{1 + k_{22}g_{22}}\delta_E + \frac{g_{22}}{1 + k_{22}g_{22}}\delta_C'$$

The root locus for $1 + k_{22}\frac{n_{22}}{d}$, where n_{ij} and d are the numerator and denominator polynomials, respectively, of g_{ij}, is shown in Figure 4. A gain of k_{22} = 0.05 rad/rad/s increases the aeroelastic mode damping by over 60% of the open-loop value.

An elevator-to-canard crossfeed is now introduced to reduce aeroelastic mode excitation from the elevator. Interconnecting "up canard" with "up elevator" will reduce aeroelastic mode deflections from the elevator because the fuselage mode shape[2] is similar to the fundamental bending mode shape of a slender beam.

The crossfeed $\delta_C' = k_{cf}\,\delta_E$ yields

$$q = \frac{g_{11} + k_{22}(g_{11}g_{22} - g_{12}g_{21}) + k_{cf}\,g_{12}}{1 + k_{22}g_{22}}\delta_E \qquad (3)$$

This can be simplified with the identity[7]

$$\det[G] = \det\begin{bmatrix} g_{11} & g_{12} \\ g_{21} & g_{22} \end{bmatrix} = g_{11}g_{22} - g_{12}g_{21} = \frac{\Psi_G}{d} \qquad (4)$$

where ψ_G is the transmission zero polynomial corresponding to the plant in Eq. (1).

$$\psi_G(s) = 89(s + 0.081)(s + 0.46) \tag{5}$$

Substitution of Eq. (4) into Eq. (3) yields

$$q = \frac{n_{11} + k_{22}\psi_G + k_{cf}\, n_{12}}{d + k_{22}n_{22}}\,\delta_E \tag{6}$$

It is now evident the crossfeed has the effect of moving the zeros of the q/δ_E transfer function (with the q'/δ_C loop closed) from $n_{11} + k_{22}\psi_G$ to n_{12}. The root locus for $1 + k_{cf}\frac{n_{12}}{n_{11} + k_{22}\psi_G}$ is shown in Figure 5. A gain of $k_{cf} = -1.5$ rad/rad results in almost perfect pole-zero cancellation for the aeroelastic dipole in the effective q/δ_E transfer function.

Finally, the effective q/δ_E loop is closed to further improve the short period damping. The control law $\delta_E = p\delta - k_{11}q$ yields

$$q = \frac{p(g_{11} + k_{22}(g_{11}g_{22} - g_{12}g_{21}) + k_{cf}\, g_{12})}{1 + k_{22}g_{22} + k_{11}(g_{11} + k_{22}(g_{11}g_{22} - g_{12}g_{21}) + k_{cf}\, g_{12})}\,\delta \tag{7}$$

where p is the gain on the pilot input δ. The root locus for $1 + k_{11}\frac{n_{11} + k_{22}\psi_G + k_{cf}\, n_{12}}{d + k_{22}n_{22}}$ is shown in Figure 6, as well as the final closed-loop pole locations for a gain of $k_{11} = -0.05$ rad/rad/s.

With some block diagram manipulation, the closed-loop system can be represented as in Figure 7. Table 3 contains the effective closed-loop transfer functions corresponding to the pilot command δ, while Figures 1 thru 3 show the corresponding frequency responses for the augmented vehicle. Short-period damping has improved from $\zeta_{sp} = 0.36$ (see Table 2) to $\zeta_{sp} = 0.54$ (a 50% increase), while the first aeroelastic mode damping has improved from $\zeta_{f_1} = 0.073$ (see Table 2) to $\zeta_{f_1} = 0.12$ (a 64% increase). These improvements are apparent in the closed-loop frequency responses.

Significant improvement in the rigid-body (α and q) frequency response shapes is also achieved. Besides improved short period damping, the aeroelastic mode pole-zero "saw tooth" located near 6 rad/s in Figures 1

and 2 are virtually eliminated when compared to the corresponding open-loop behavior. This is a result of improved closed-loop pole-zero cancellations (see Table 3) as desired in the classical control synthesis. Or the aeroelastic mode has been rendered undisturbable from pilot input.

4. IMF Control Synthesis[12,13]

A newly developed technique for the synthesis of flight-control laws will now be outlined. Although LQR and LTR concepts are used in the formulation of the algorithm, this approach is fundamentally different from LQG/LTR methodology[4]. LQG/LTR addresses the problem of obtaining specified open-loop shapes, while the approach taken here is to synthesize a control law that yields a desired closed-loop shape.

The system to be controlled is represented as

$$\begin{aligned} \dot{x}(t) &= Ax(t) + Bu(t) \\ y(t) &= Hx(t) \end{aligned} \tag{8}$$

and the model of the desired dynamics to be followed is

$$\begin{aligned} \dot{x}_m(t) &= A_m x_m(t) + B_m \delta(t) \\ y_m(t) &= H_m x_m(t) \\ \dot{\delta} &= -100.\,\delta \end{aligned} \tag{9}$$

where δ represents the input from the pilot. The error vector

$$e(t) = y(t) - y_m(t) \tag{10}$$

is constrained to be governed by stable, homogeneous dynamics

$$\dot{e}(t) = -Ge(t) \tag{11}$$

where G is to be selected in the synthesis process. The model-following control law is obtained by solving the LQR problem with the following objective function.

$$J = \int_0^\infty [(\dot{e} + Ge)^T Q(\dot{e} + Ge) + u^T R u]\, dt \qquad (12)$$

If the product HB is square and invertible, and the same for $H_m B_m$, and if G is chosen as $G = - H_m A_m H_m^{-1}$, then perfect model following is achieved asymptotically as R in Eqn. 7 approaches the null matrix. If this is the case, then the closed-loop poles approach the model poles (for G as defined above) and any open-loop plant finite transmission zeros (or their stable mirror image).[12]

The solution to this problem is the first step of the control law synthesis, yielding the state-feedback control law

$$u = Kx + K_\delta \delta \qquad (13)$$

For the elastic aircraft model in Table 1, rigid-body angle of attack and pitch rate, α and q, are the responses selected for model following, so that the handling characteristics will be improved. Also it is desirable that the response approximate that of a rigid vehicle. With this selection, the open-loop plant transmission zeros are located at -23. 1/s and 35. 1/s, and HB is square and invertible.

The model of the desired dynamics is chosen to be

$$\alpha_m(s)/\delta(s) = -3.5/(s + 0.89 \pm j0.91)$$

$$q_m(s)/\delta(s) = -3.3(s + 0.36)/(s + 0.89 \pm j0.91)$$

Note that the short-period mode is well damped. With this selection, H_m is square and also invertible. The short-period poles will approach those of the model, the aeroelastic mode poles will move toward the plant transmission zeros (or their stable mirror images via the optimal control formulation), and the α and q time and frequency responses will be shaped to better approximate those of a rigid vehicle.

With the state feedback gains K and K_δ so determined, compensators will now be synthesized using the loop transfer recovery procedure[4,7,13], which will then yield the output-feedback loop structure in Figure 9. Although the α and q responses were those used in the model-following step, they are not the measurements to be used for feedback. The feedback measurements are the same used for the classical design, q' and q. This

selection leads to minimum phase transmission zeros, for the loop-transfer recovery, located at -0.081 and -0.46 1/s.

Figure 8 shows the resulting feedback compensators, prefilter stick gains, and closed-loop structure after the loop-transfer recovery procedure is completed, and some straight-forward pole-zero cancellations are performed on the compensators. Note the compensators consist of relatively simple lead-lag and lag-lead filters of second order. Table 3 contains the effective closed-loop transfer functions corresponding to the pilot command δ, while Figures 1 thru 3 show the corresponding frequency responses. Short period damping has improved from $\zeta_{sp} = 0.36$ to $\zeta_{sp} = 0.45$ (25% increase) while the first aeroelastic mode damping has improved from $\zeta_{f_1} = 0.073$ to $\zeta_{f_1} = 0.12$ (64% increase).

These improvements are also apparent in the closed-loop frequency responses. Besides improved short-period damping, the aeroelastic mode pole-zero "saw tooth" located near 6 rad/s in the angle-of-attack and pitch-rate responses in Figures 1 and 2 is reduced by roughly 10 db, when compared to the corresponding open-loop response. This is a result of improved closed-loop pole-zero cancellations (see Table 3) as desired in the IMF control synthesis (i.e., following a rigid-body model).

5. Robustness Analysis

Now consider the generic feedback loop structure in Figure 9, which is a generalization of the closed-loop systems in Figures 7 and 8, with response vector y, control inputs u, commands y_c , and plant, compensator, and prefilter transfer function matrices G(s), K(s), and P(s), respectively. The feedback compensation in Figure 9 is assumed to be synthesized with a design model G(s), but the "true" plant transfer function is taken to be G'(s). Specifically, consider generic phase loss in each input channel to the plant, or let

$$G'(s) = G(s)\,(e^{-\tau s} I) \qquad (14)$$

This phase loss can represent, for example, unmodeled high-frequency dynamics originating from structural modes, actuators, sensors, etc. Rewriting G'(s) as

$$G'(s) = G(s)(I + E(s)) \tag{15}$$

it can be shown that

$$E(s) = (e^{-\tau s} - 1)\, I \tag{16}$$

where E(s) is the so called plant input multiplicative error.[4]

The "true" closed-loop system poles are roots of the "true" characteristic equation, obtained from

$$\det[I + K(s)G(s)(I + E(s))] = 0 \tag{17}$$

If the nominal closed-loop system is stable and the required number of encirclements of the critical point in Nyquist stability theory is the same for both nominal and "true" systems, then a sufficient condition, developed from Eq. (17), guaranteeing closed-loop stability under E(s)[4] is

$$\bar{\sigma}[E(j\omega)] < \underline{\sigma}[I + (K(j\omega)G(j\omega))^{-1}] \quad , \quad 0 \le \omega \le \infty \tag{18}$$

Eq. (18) is an indication of the system's multivariable stability robustness margin.

Figure 10 indicates the stability robustness of the classically designed closed-loop system, with the effect of multiplicative error due to generic phase loss in each input channel displayed as well. Note from Figure 10 the characteristic limiting the stability robustness is the dip in $\underline{\sigma}[I + (KG)^{-1}]$ near 6 rad/s. In fact, the phase loss allowed using this criteria is limited to $\tau \le 0.3$ s.

Figure 11 indicates the stability robustness properties of the IMF design, again with the effect of generic phase loss displayed. Note again a similar characteristic limiting the robustness of this loop. Here the allowable phase loss is $\tau \le 0.35$ s, only slightly better than the previous result.

The question now turns to the causes for this limiting characteristic. Literal expressions for the vehicle transfer function poles and zeros in Table 2 are available from Ref. 10 for further analysis. Before this, however, a literal

expression for $\underline{\sigma}[I + (KG)^{-1}]$ is necessary. The approach to be taken here is similar to that presented in Ref. 11.

With reference to Figure 9, consider a 2 × 2 closed-loop system with

$$K(j\omega) = \begin{bmatrix} k_{11} & k_{12} \\ k_{21} & k_{22} \end{bmatrix}, \quad G(j\omega) = \begin{bmatrix} g_{11} & g_{12} \\ g_{21} & g_{22} \end{bmatrix}, \quad I + (K(j\omega)G(j\omega))^{-1} = \begin{bmatrix} a_{11} & a_{12} \\ a_{21} & a_{22} \end{bmatrix} \tag{19}$$

where

$$\begin{aligned} a_{11} &= 1 + \frac{k_{21}g_{12} + k_{22}g_{22}}{\Delta} \\ a_{12} &= -\frac{k_{11}g_{12} + k_{12}g_{22}}{\Delta} \\ a_{21} &= -\frac{k_{21}g_{11} + k_{22}g_{21}}{\Delta} \\ a_{22} &= 1 + \frac{k_{11}g_{11} + k_{12}g_{21}}{\Delta} \\ \Delta &= \det[KG] = [k_{11}k_{22} - k_{12}k_{21}]\,[g_{11}g_{22} - g_{12}g_{21}] \end{aligned} \tag{20}$$

The minimum and maximum singular values of $I + (KG)^{-1}$ are given as

$$\begin{aligned} \underline{\sigma}[I + (KG)^{-1}] &= \underline{\lambda}^{1/2}\,[(I + (KG)^{-1})(I + (KG)^{-1})^*] \\ \overline{\sigma}[I + (KG)^{-1}] &= \overline{\lambda}^{1/2}\,[(I + (KG)^{-1})(I + (KG)^{-1})^*] \end{aligned} \tag{21}$$

where $\underline{\lambda}$ and $\overline{\lambda}$ denote the minimum and maximum eigenvalues, respectively. $\underline{\lambda}$ and $\overline{\lambda}$ solve

$$\det[\lambda I - (I + (KG)^{-1})(I + (KG)^{-1})^*] = \lambda^2 - (\underline{\lambda} + \overline{\lambda})\lambda + \underline{\lambda}\overline{\lambda} = 0 \tag{22}$$

where

$$\begin{aligned} \underline{\lambda} + \overline{\lambda} &= |a_{11}|^2 + |a_{12}|^2 + |a_{21}|^2 + |a_{22}|^2 \\ \underline{\lambda}\overline{\lambda} &= |a_{11}a_{22} - a_{12}a_{21}|^2 \end{aligned} \tag{23}$$

If $\underline{\lambda} \ll \overline{\lambda}$, then from Eq. (23) $\underline{\lambda}$ is approximately given as

$$\underline{\lambda} \approx \frac{|a_{11}a_{22} - a_{12}a_{21}|^2}{|a_{11}|^2 + |a_{12}|^2 + |a_{21}|^2 + |a_{22}|^2} \qquad (24)$$

or

$$\underline{\sigma}[I + (KG)^{-1}] \approx \frac{|a_{11}a_{22} - a_{12}a_{21}|}{(|a_{11}|^2 + |a_{12}|^2 + |a_{21}|^2 + |a_{22}|^2)^{1/2}} \qquad (25)$$

From inspection of Figures 10 and 11, it can be seen that the condition $\underline{\lambda} \ll \overline{\lambda}$ (or $\underline{\sigma} \ll \overline{\sigma}$) is reasonably satisfied.

Substitution of Eq. (20) into the numerator and denominator of Eq. (25) yields

$$|a_{11}a_{22} - a_{12}a_{21}| = \left|\frac{1}{\Delta}\right| \cdot |1 + k_{11}g_{11} + k_{12}g_{21} + k_{21}g_{12} + k_{22}g_{22} + \Delta| \qquad (26)$$

$$|a_{11}|^2 + |a_{12}|^2 + |a_{21}|^2 + |a_{22}|^2 = \left|\frac{1}{\Delta}\right|^2 \cdot (|k_{21}g_{12} + k_{22}g_{22} + \Delta|^2 +$$
$$|k_{11}g_{12} + k_{12}g_{21}|^2 + |k_{21}g_{11} + k_{22}g_{21}|^2 + |k_{11}g_{11} + k_{12}g_{21} + \Delta|^2)$$

These can be further simplified with the following observation[7]

$$1 + k_{11}g_{11} + k_{12}g_{21} + k_{21}g_{12} + k_{22}g_{22} + \Delta = \det[I + KG] = \frac{\phi_{cl}}{\phi_{ol}} \qquad (27)$$

$$\Delta = \det[KG] = \frac{\psi_K \psi_G}{\phi_{ol}}$$

where ϕ_{cl} and ϕ_{ol} are the system's closed-loop and open-loop characteristic polynomials, respectively, and ψ_K and ψ_G are the compensator and plant transmission zero polynomials, respectively. With the notation

$$k_{ij}g_{pq} = \frac{n_{k_{ij}} n_{g_{pq}}}{\phi_{ol}} \quad , \quad i,j,p,q = 1,2$$

where $n_{k_{ij}}$ and $n_{g_{pq}}$ are the numerator polynomials of k_{ij} and g_{pq} ,respectively, substitution of Eqs. (26) and (27) into Eq. (25) yields the following literal expression for $\underline{\sigma}[I + (KG)^{-1}]$.

$$\underline{\sigma}[I + (KG)^{-1}] \approx \frac{|\phi_{cl}|}{(|n_{11}|^2 + |n_{12}|^2 + |n_{21}|^2 + |n_{22}|^2)^{1/2}} \qquad (28)$$

$$n_{11} = n_{k_{21}} n_{g_{12}} + n_{k_{22}} n_{g_{22}} + \psi_K \psi_G$$
$$n_{12} = n_{k_{11}} n_{g_{12}} + n_{k_{12}} n_{g_{22}}$$
$$n_{21} = n_{k_{21}} n_{g_{11}} + n_{k_{22}} n_{g_{21}}$$
$$n_{22} = n_{k_{11}} n_{g_{11}} + n_{k_{12}} n_{g_{21}} + \psi_K \psi_G$$

Observe that the "zeros" of $\underline{\sigma}[I + (KG)^{-1}]$ are nothing more than the closed-loop poles, while the "poles" of $\underline{\sigma}[I + (KG)^{-1}]$ depend on the plant's and compensator's transfer-function zeros as well as their transmission zeros. This result was first noted in Ref. 11, but the transmission zeros $\psi_K \psi_G$ were related to the so called coupling numerators.

Now consider the classically designed closed-loop system shown in Figure 7. Here

$$g_{11} = q(s)/\delta_E(s) \qquad k_{11} = n_{k_{11}} = \delta_E/q$$
$$g_{12} = q(s)/\delta_C(s) \qquad k_{12} = n_{k_{12}} = 0$$
$$g_{21} = q'(s)/\delta_E(s) \qquad k_{21} = n_{k_{21}} = \delta_C/q$$
$$g_{22} = q'(s)/\delta_C(s) \qquad k_{22} = n_{k_{22}} = \delta_C/q'$$
$$\psi_G(s) = 89(s + 0.081)(s + 0.46) \qquad \psi_K = k_{11}k_{22} - k_{12}k_{21}$$

with g_{ij} available from Table 2 and k_{ij} available from Figure 7. Substitution of the above quantities into Eq. (28) yields

$$\underline{\sigma}[I+(KG)^{-1}] \approx \frac{|(j\omega + 0.70 \pm j1.1)(j\omega + 0.75 \pm j6.0)|}{0.94\,|(j\omega + 0.22)(j\omega + 3.1 \pm j3.8)|} \qquad (29)$$

It is evident that the augmented first aeroelastic mode poles, denoted

$$s^2 + (2\zeta\omega)_{cl_2} s + (\omega^2)_{cl_2} = s^2 + 1.5s + 37 = s + 0.75 \pm j6.0 \qquad (30)$$

and their low damping are responsible for the previously discussed critical stability robustness feature near 6 rad/s in Figure 10.

From the classical design (see Section 3) and Figure 4, these poles are primarily a function of the q'/δ_C loop closure. With increasing q'/δ_C root

locus gain k_{22} , these augmented aeroelastic mode poles originate from their open-loop locations

$$s^2 + (2\zeta\omega)_{f_1} s + (\omega^2)_{f_1} = s^2 + 0.88s + 36 = s + 0.44 \pm j6.0 \qquad (31)$$

and migrate towards their corresponding aeroelastic mode zeros in the q'/δ_C transfer function (see Table 2), denoted as

$$s^2 + {}_{f_1}(2\zeta\omega)^{\delta c}_{q'} s + {}_{f_1}(\omega^2)^{\delta c}_{q'} = s^2 + 1.5s + 8.9 = s + 0.73 \pm j2.9 \qquad (32)$$

Yielding the closed-loop locations in Eq. (30) for the selected value of k_{22} .

From Ref. 10, the open-loop natural frequency and damping terms of the aeroelastic mode poles and zeros in Eqs. (31) and (32) are approximately given by

$$(\omega^2)_{f_1} \approx (\omega_1^2 - F_{1\eta_1}) + \frac{(1 + \frac{Z_q}{V_{T_1}})M_{\eta_1} F_{1_\alpha}}{(\omega_1^2 - F_{1\eta_1})}$$
$$= \quad 35 \quad + \quad 2.0 \qquad (33)$$

$$(2\zeta\omega)_{f_1} \approx (2\zeta_1\omega_1 - F_{1\dot{\eta}_1}) + \frac{M_{\eta_1} F_{1_q} + [\frac{Z_{\eta_1}}{V_{T_1}} + (1 + \frac{Z_q}{V_{T_1}})M_{\dot{\eta}_1}]F_{1_\alpha}}{(\omega_1^2 - F_{1\eta_1})}$$
$$= \quad 0.62 \quad + \quad 0.35$$

$${}_{f_1}(\omega^2)^{\delta c}_{q'} \approx \frac{(\omega_1^2 - F_{1\eta_1})\, M_{\delta_c}}{M_{\delta_c} - \phi_1'(x)F_{1_{\delta c}}} - \frac{M_{\eta_1} + \phi_1'(x)(1 + \frac{Z_q}{V_{T_1}})M_\alpha}{\phi_1'(x)}$$
$$= \quad 2.0 \quad - \quad (-6.5) \qquad (34)$$

$${}_{f_1}(2\zeta\omega)^{\delta c}_{q'} \approx \frac{(2\zeta_1\omega_1 - F_{1\dot{\eta}_1})M_{\delta_c} + \phi_1'(x)M_q F_{1_{\delta c}}}{M_{\delta_c} - \phi_1'(x)F_{1_{\delta c}}} - \frac{\phi_1'(x)(1 + \frac{Z_q}{V_{T_1}})\frac{Z_\alpha}{V_{T_1}} M_\alpha F_{1_{\delta c}}}{(\omega_1^2 - F_{1\eta_1})M_{\delta_c}}$$
$$= \quad 0.82 \quad - \quad (-0.67)$$

with the following numerical values:

$\frac{Z_\alpha}{V_{T_1}} = -0.416 \ \ ft/s^2$ $\qquad (1 + \frac{Z_q}{V_{T_1}}) = 1.03$

$\frac{Z_{\eta_1}}{V_{T_1}} = -0.00267 \ \ 1/s$ $\qquad M_\alpha = -3.33 \ \ 1/s^2$

$M_q = -0.830 \ \ 1/s$ $\qquad M_{\eta_1} = -0.0655 \ \ 1/s^2$

$M_{\dot{\eta}_1} = -0.00390 \ \ 1/s$ $\qquad M_{\delta_C} = 0.809 \ \ 1/s^2$

$F_{1_\alpha} = -1{,}040 \ \ 1/s^2$ $\qquad F_{1_q} = -78.4 \ \ 1/s$

$F_{1_{\delta C}} = -631 \ \ 1/s^2$ $\qquad (\omega_1^2 - F_{1\eta_1}) = 34.8 \ \ 1/s^2$

$(2\zeta_1\omega_1 - F_{1\dot{\eta}_1}) = 0.621 \ \ 1/s$ $\qquad \phi_1'(x) = 0.021 \ \ ft/ft$

The above parameters are functions of the flight velocity V_{T_1}; rigid-body and aeroelastic aerodynamic stability derivatives Z_i , M_i , and F_{i_j} ; first in vacuo elastic mode shape, vibration frequency ω_1 and damping ratio ζ_1. These vehicle parameters appear explicitly in the linear equations of motion for the elastic aircraft[10] listed below.

$$\dot{\alpha} = \frac{Z_\alpha}{V_{T_1}}\alpha + (1 + \frac{Z_q}{V_{T_1}})q + \frac{Z_{\eta_1}}{V_{T_1}}\eta_1 + \frac{Z_{\dot{\eta}_1}}{V_{T_1}}\dot{\eta}_1 + \frac{Z_{\delta_E}}{V_{T_1}}\delta_E + \frac{Z_{\delta_C}}{V_{T_1}}\delta_C$$

$$\dot{q} = M_\alpha\alpha + M_q q + M_{\eta_1}\eta_1 + M_{\dot{\eta}_1}\dot{\eta}_1 + M_{\delta_E}\delta_E + M_{\delta_C}\delta_C \qquad (35)$$

$$\ddot{\eta}_1 = F_{1_\alpha}\alpha + F_{1_q}q - (\omega_1^2 - F_{1\eta_1})\eta_1 - (2\zeta_1\omega_1 - F_{1\dot{\eta}_1})\dot{\eta}_1 + F_{1_{\delta E}}\delta_E + F_{1_{\delta C}}\delta_C$$

$$q' = q - \phi_1'(x)\dot{\eta}_1$$

As seen from Eq. (33), the frequency of the open-loop aeroelastic mode poles is primarily due to the elastic mode structural frequency and aerodynamic stiffness (i.e., $(\omega_1^2 - F_{1\eta_1})$). Also, the inherent low damping in this mode is primarily due to the elastic mode structural and aerodynamic damping (i.e., $(2\zeta_1\omega_1 - F_{1\dot{\eta}_1})$). However, note also that approximately 1/3 of the total damping is due to aerodynamic coupling between the rigid and elastic degrees of freedom. It is now clear which key vehicle and compensator parameters contribute to the critical stability robustness properties of this closed-loop system.

Now consider the IMF design closed-loop system shown in Figure 8. Here

$g_{11} = q(s)/\delta_E(s)$ $\qquad k_{11} = \delta_E(s)/q(s)$

$$g_{12} = q(s)/\delta_C(s) \qquad k_{12} = \delta_E(s)/q'(s)$$
$$g_{21} = q'(s)/\delta_E(s) \qquad k_{21} = \delta_C(s)/q(s)$$
$$g_{22} = q'(s)/\delta_C(s) \qquad k_{22} = \delta_C(s)/q'(s)$$
$$\psi_C(s) = 89(s + 0.081)(s + 0.46) \qquad \psi_K(s) = 0.00091(s+0.060)(s+0.35\pm j0.21)(s-1.9)$$

with g_{ij} available from Table 2 and k_{ij} available from Figure 8. Substitution of the above quantities into Eq. (28) yields

$$\underline{\sigma}[I + (KG)^{-1}] \approx \frac{|(j\omega + 0.56 \pm j1.1)(j\omega + 0.73 \pm j5.8)|}{0.66\,|(j\omega + 0.83 \pm j1.0)(j\omega + 4.6)|} \qquad (36)$$

It is evident that again the augmented first aeroelastic mode poles

$$s^2 + (2\zeta\omega)_{cl_2}s + (\omega^2)_{cl_2} = s^2 + 1.5s + 34 = s + 0.73 \pm j5.8$$

and their low damping are responsible for the critical stability robustness feature near 6 rad/s in Figure 11. From the IMF design (see Section 4), these poles originate at their open-loop location and migrate toward the transmission zeros (or their stable mirror image) defined through the model-following formulation, as the control weighting in the loss function is reduced (or the loop gains are increased). Although literal approximations for these transmission zeros are still being developed, the above expressions for the open-loop aeroelastic poles again reveal the major source of these critical characteristics.

6. Conclusions

An integrated flight- and aeroelastic-mode control law was synthesized for a very flexible supersonic vehicle, using a previously developed model-following synthesis approach. This technique, designed to yield a desired closed-loop rather than an open-loop loop shapes, involves a specific LQR formulation leading to the model-following state-feedback gains. Then the use of asymptotic loop transfer recovery is utilized to obtain the compensation that recovers the LQR robustness properties, and which leads to an output-feedback control law. A classically designed control law was also developed for comparison purposes, and parallels between the results obtained with the two approaches are observed.

The resulting closed-loop systems were evaluated in terms of their performance and multivariable stability robustness, measured in terms of the appropriate singular values. This evaluation utilized approximate literal expressions for those singular values, expressed in terms of literal expressions for the poles and zeros of the vehicle transfer functions. It was found that both control laws possessed equivalent performance and stability robustness, and the characteristics limiting this robustness were in both cases traced to some specific step in the synthesis process, as well as the locations of critical open-loop poles and zeros (or transmission zeros). Furthermore, closed-form literal expressions for these characteristics were presented in terms of the stability derivatives of the vehicle. The insight gained from this analysis is considered invaluable to the control system designer, and unavailable from strictly numerical analysis.

7. Acknowledgements

This research was supported by NASA Langley Research Center under Grant NAG1-758. Mr. Douglas Arbuckle and Mr. Carey Buttrill have served as technical monitors. Thanks also goes out to Mr. John Schierman for his advice concerning the IMF procedure, to Mr. Shawn Molodow for development of the classical controller, and to Prof. Bong Wie for several fruitful conversations.

8. References

1. Bisplinghoff, R. L. and Ashley, H., "Principles Of Aeroelasticity," Dover Publications, 1962
2. Waszak, M. R. and Schmidt, D. K., "Flight Dynamics Of Aeroelastic Vehicles," *Journal Of Aircraft*, Vol. 25, No. 6, June, 1988
3. Schmidt, D. K. and Foxgrover, J. A., "Multivariable Flight Control Synthesis Approaches To Meet Handling Qualities Objectives," Proceedings Of The AIAA Guidance And Control Conference, Seattle, Wash., Aug. 1984
4. Doyle, J. C. and Stein, G., "Multivariable Feedback Design: Concepts For A Classical/Modern Synthesis," *IEEE Transactions On Automatic Control*, Vol. AC-26, Feb., 1981
5. McRuer, D., Ashkenas, I., and Graham, D., "Aircraft Dynamics And Automatic Control," Princeton University Press, 1973

6. Blakelock, J. H., "Automatic Control Of Aircraft And Missiles," John Wiley & Sons Inc., 1965
7. Kwakernaak, H. and Sivan, R., "Linear Optimal Control Systems," John Wiley & Sons, 1972
8. Doyle, J.C., et al, "State-Space Solutions To Standard H_2 And H_∞ Control Problems," Proceedings Of The American Control Conference, Atlanta, GA, June, 1988
9. Pearce, B.F., et al, "Analytical Study of Approximate Longitudinal Transfer Functions For A Flexible Airframe," ASD - TDR - 62 - 279, June, 1962.
10. Schmidt, D. K. and Newman, B., "Modeling, Model Simplification, And Stability Robustness With Aeroelastic Vehicles," AIAA-88-4079-CP, Proceedings Of The AIAA Guidance, Navigation, And Control Conference, Minneapolis, Minn. Aug.15-17, 1988. (To appear in the *Journal of Guidance, Control, and Dynamics.)*
11. McRuer, D.T., Meyers, T.T., and Thompson, P.M., "Literal Singular-Value-Based Flight Control System Design Techniques," Vol.12, No. 6, *Journal of Guidance, Control, and Dynamics,* Nov-Dec, 1989.
12. Anderson, M.R. and Schmidt, D.K., "The Significance Of Error Dynamics In Model-Following For Flight Control Design," AIAA-87-2311, Proceedings Of The AIAA Guidance, Navigation, And Control Conference, Monterey, Calif., Aug., 1987. (To appear in the *Journal of Guidance, Control, and Dynamics.)*
13. Schmidt, D.K., "Control System Design Research To Meet Aircraft Handling Qualities Requirements, Phase II," Final Report to the McDonnell Aircraft Co., Performed at Arizona State University, Dept. of Mech. and Aero. Engr., Tempe, AZ, July, 1989.

Table 1. Elastic Aircraft Model

$$\dot{x}(t) = Ax(t) + Bu(t)$$
$$y(t) = Cx(t)$$

$$y = \begin{bmatrix} \alpha \ \text{(rad)} \\ q \ \text{(rad/s)} \\ q' \ \text{(rad/s)} \end{bmatrix}, \quad u = \begin{bmatrix} \delta_E \ \text{(rad)} \\ \delta_C \ \text{(rad)} \end{bmatrix}$$

$$A = \begin{bmatrix} -0.517 & 3.85 & 0.150 & 4.24 \\ -9.39 & -0.318 & -0.523 & -4.67 \\ 0.0438 & 0.0164 & -0.0128 & -2.06 \\ -0.0591 & -0.0165 & 0.764 & -0.986 \end{bmatrix}$$

$$B = \begin{bmatrix} -292. & -182. \\ -598. & -424. \\ 53.7 & -31.2 \\ -38.4 & 17.7 \end{bmatrix}$$

$$C = \begin{bmatrix} 0.000480 & -0.0000247 & -0.0188 & -0.0286 \\ 0.00147 & 0.00170 & -0.0264 & 0.0549 \\ -0.0222 & -0.0213 & -0.0372 & 0.0687 \end{bmatrix}$$

Table 2. Elastic Aircraft Transfer Functions

$$\alpha(s)/\delta_E(s) = -0.036(s - 0.018 \pm j4.9)(s + 150.)/d(s) \quad \text{rad/rad}$$

$$q(s)/\delta_E(s) = -5.0(s + 0.36)(s + 0.11 \pm j4.9)/d(s) \quad \text{rad/s/rad}$$

$$q'(s)/\delta_E(s) = 15.(s + 0.040)(s - 2.9)(s + 4.0)/d(s) \quad \text{rad/s/rad}$$

$$\alpha(s)/\delta_C(s) = 0.0044(s + 1.8 \pm j9.0)(s + 200.)/d(s) \quad \text{rad/rad}$$

$$q(s)/\delta_C(s) = 0.80(s + 0.33)(s + 1.3 \pm j9.1)/d(s) \quad \text{rad/s/rad}$$

$$q'(s)/\delta_C(s) = 15.(s + 0.056)(s + 0.73 \pm j2.9)/d(s) \quad \text{rad/s/rad}$$

---

where $d(s) = (s + 0.47 \pm j1.2)(s + 0.44 \pm j6.0)$

Table 3. Closed-Loop Transfer Functions

Classical Control Synthesis

$$\alpha(s)/\delta(s) = 3.7(s + 0.70 \pm j5.9)(s + 160)/d(s) \quad \text{rad/rad}$$

$$q(s)/\delta(s) = 0.025(s + 0.35)(s + 0.71 \pm j5.9)/d(s) \quad \text{rad/s/rad}$$

$$q'(s)/\delta(s) = 5.1(s + 0.049)(s + 1.0 \pm j6.6)/d(s) \quad \text{rad/s/rad}$$

where $d(s) = (s + 0.70 \pm j1.1)(s + 0.75 \pm j6.0)$

IMF Control Synthesis

$$\alpha(s)/\delta(s) = -0.0062(s + 0.22 \pm j5.1)(s + 150)/d(s) \quad \text{rad/rad}$$

$$q(s)/\delta(s) = -0.87(s + 0.36)(s + 0.34 \pm j5.1)/d(s) \quad \text{rad/s/rad}$$

$$q'(s)/\delta(s) = 2.0(s + 0.042)(s - 3.6)(s + 4.5)/d(s) \quad \text{rad/s/rad}$$

where $d(s) = (s + 0.56 \pm j1.1)(s + 0.73 \pm j5.8)$

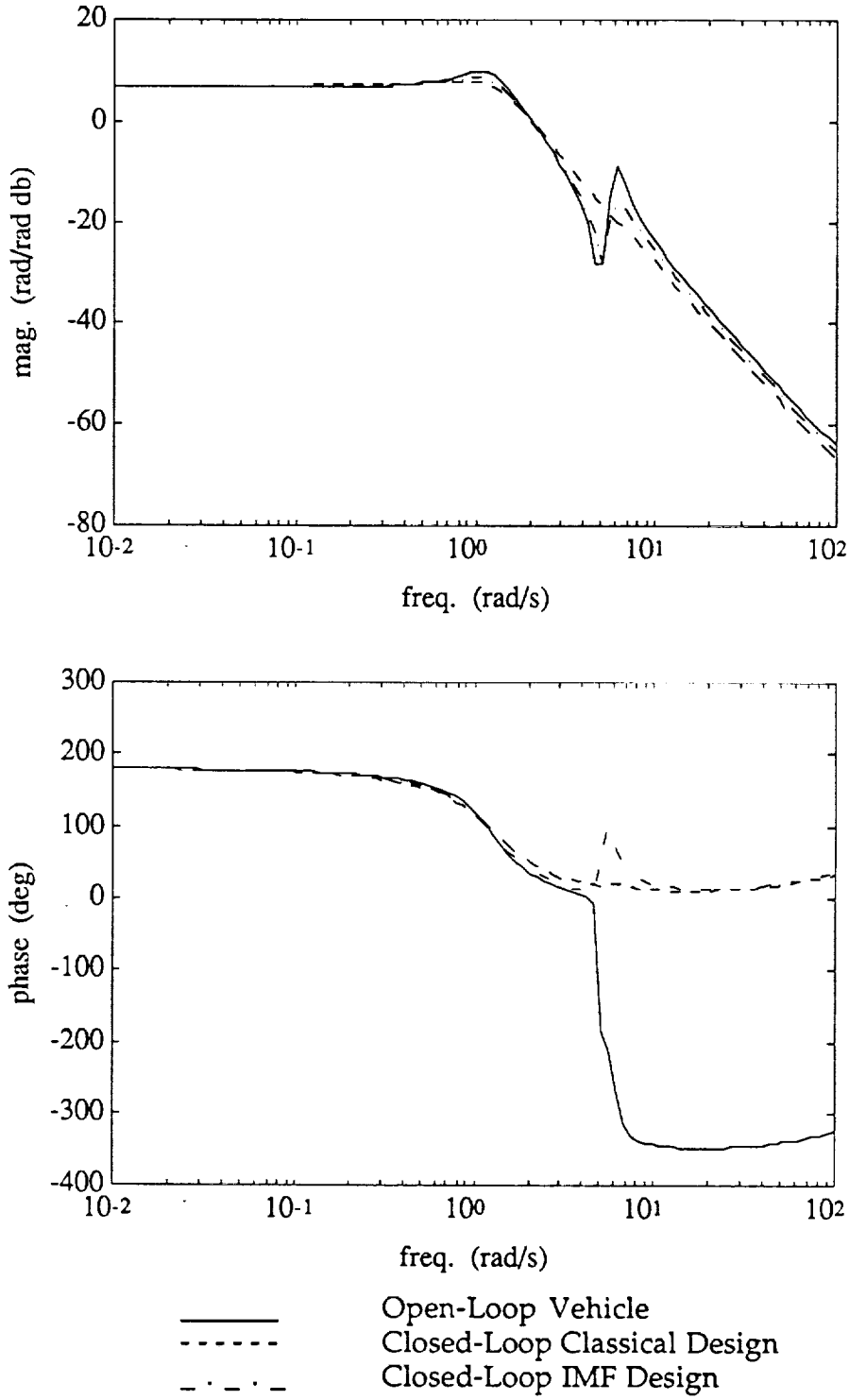

Figure 1. $\alpha(s)/\delta_E(s)$ And $\alpha(s)/\delta(s)$ Frequency Responses

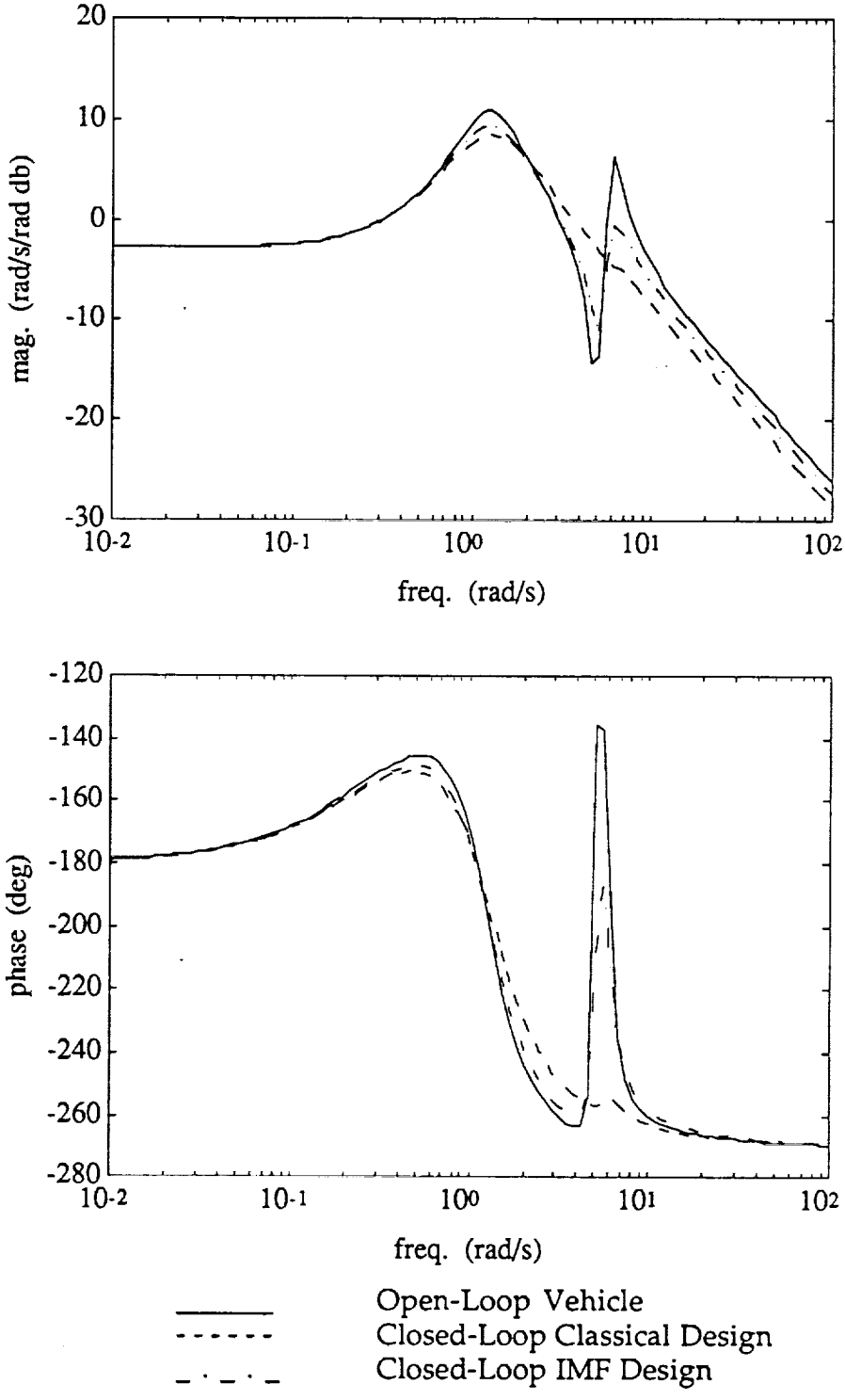

Figure 2. $q(s)/\delta_E(s)$ And $q(s)/\delta(s)$ Frequency Responses

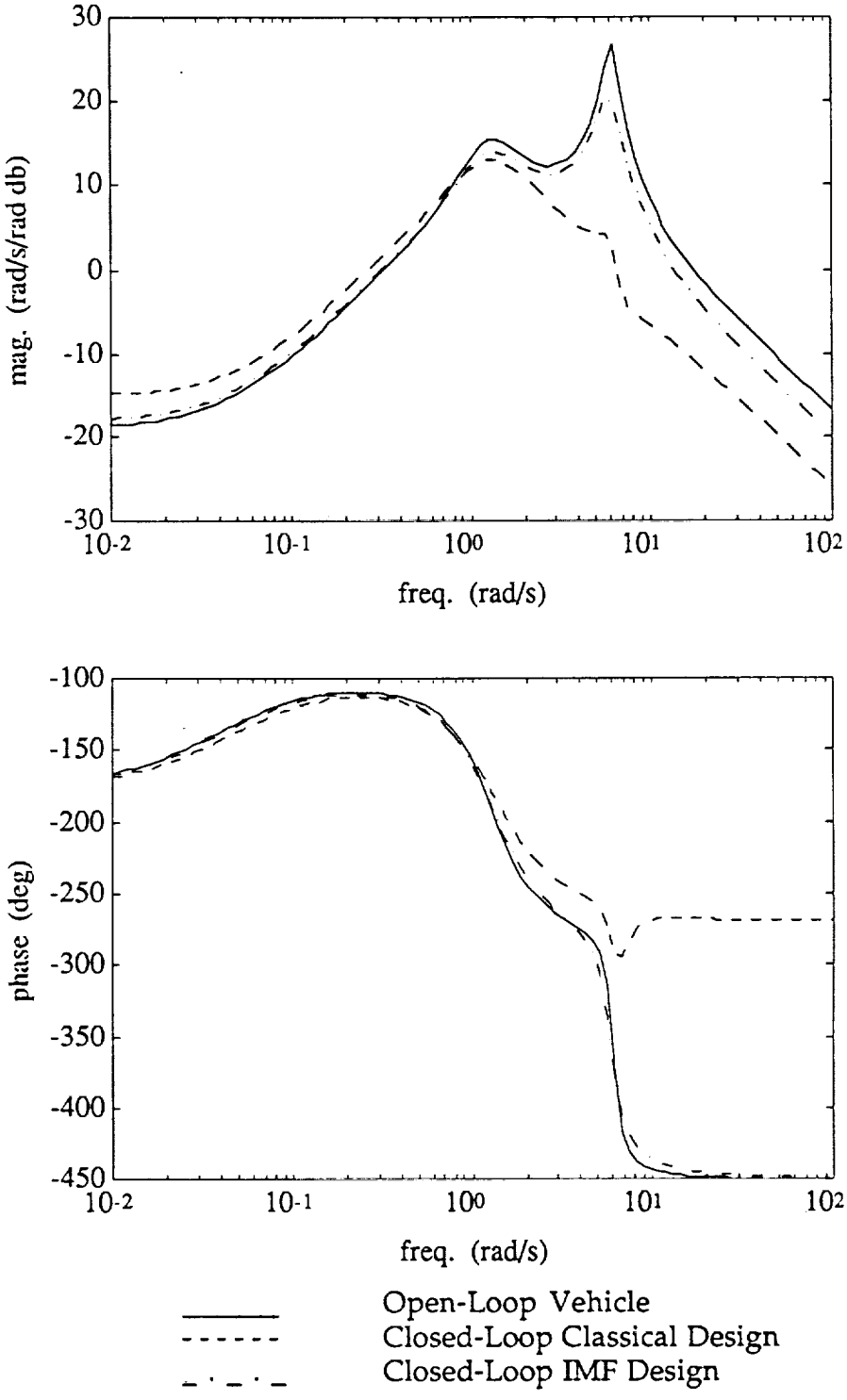

Figure 3. $q'(s)/\delta_E(s)$ And $q'(s)/\delta(s)$ Frequency Responses

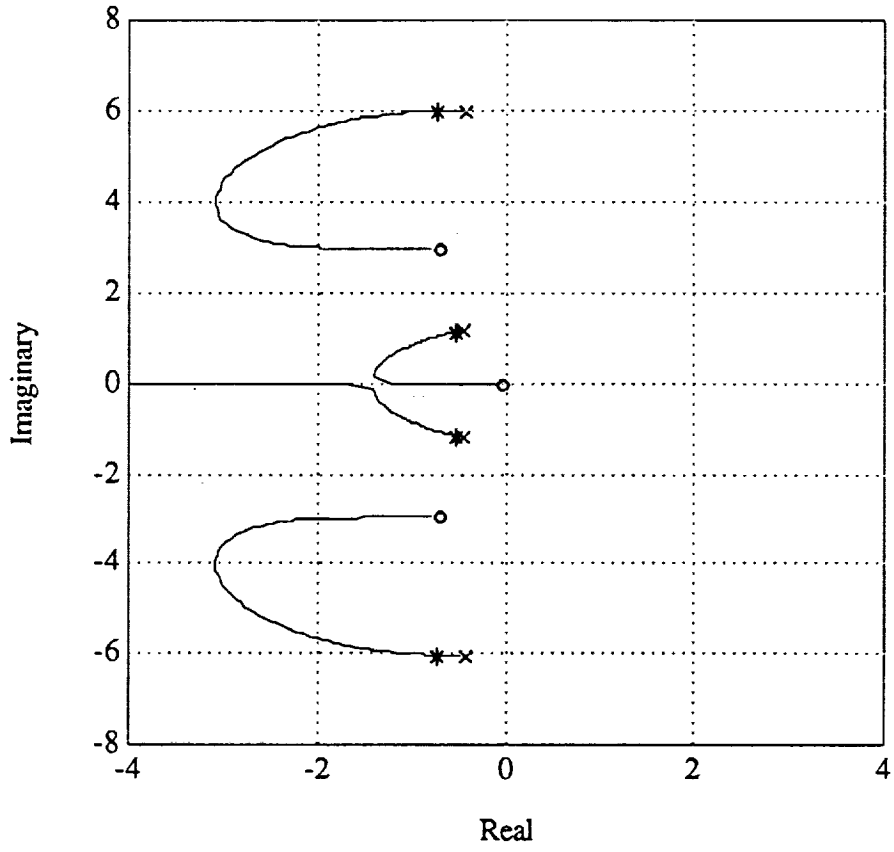

x : -0.47±j1.2
-0.44±j6.0

o : -0.056
-0.73±j2.9

* (k_{22} = 0.05) : -0.55±j1.1
-0.75±j6.0

Figure 4. Root Locus For q'/δ_C Loop Closure

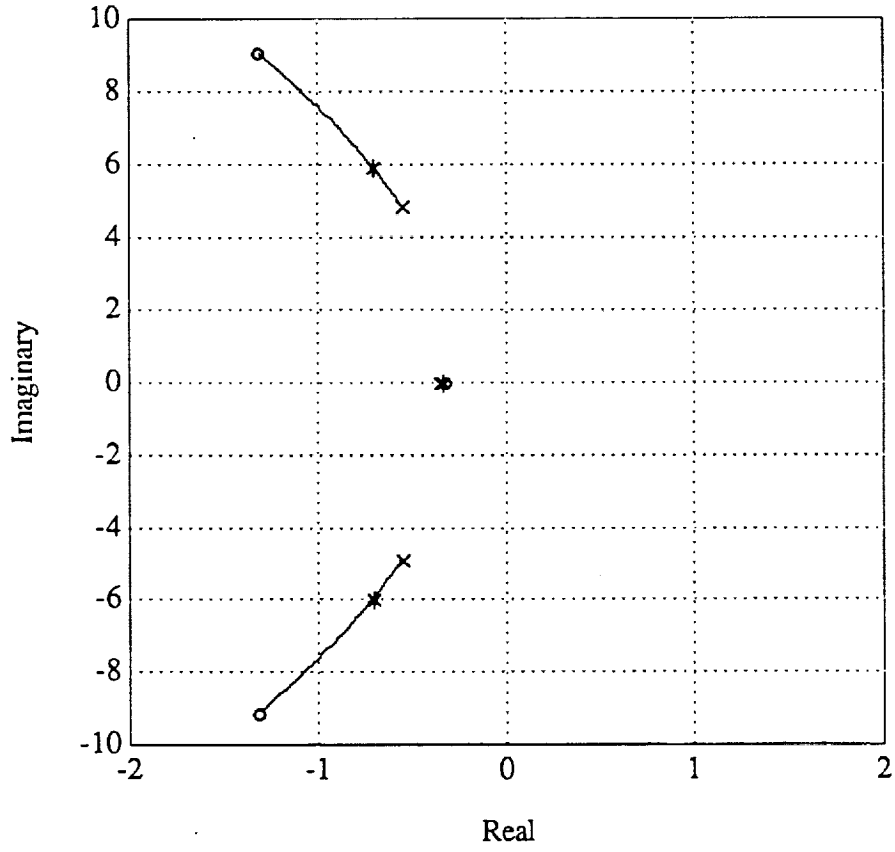

x : -0.36
-0.56±j4.9

o : -0.33
-1.3±j9.1

* (k_{cf} = -1.5) : -0.35
-0.71±j5.9

Figure 5. Zero Root Locus For δ_E To δ_C Crossfeed

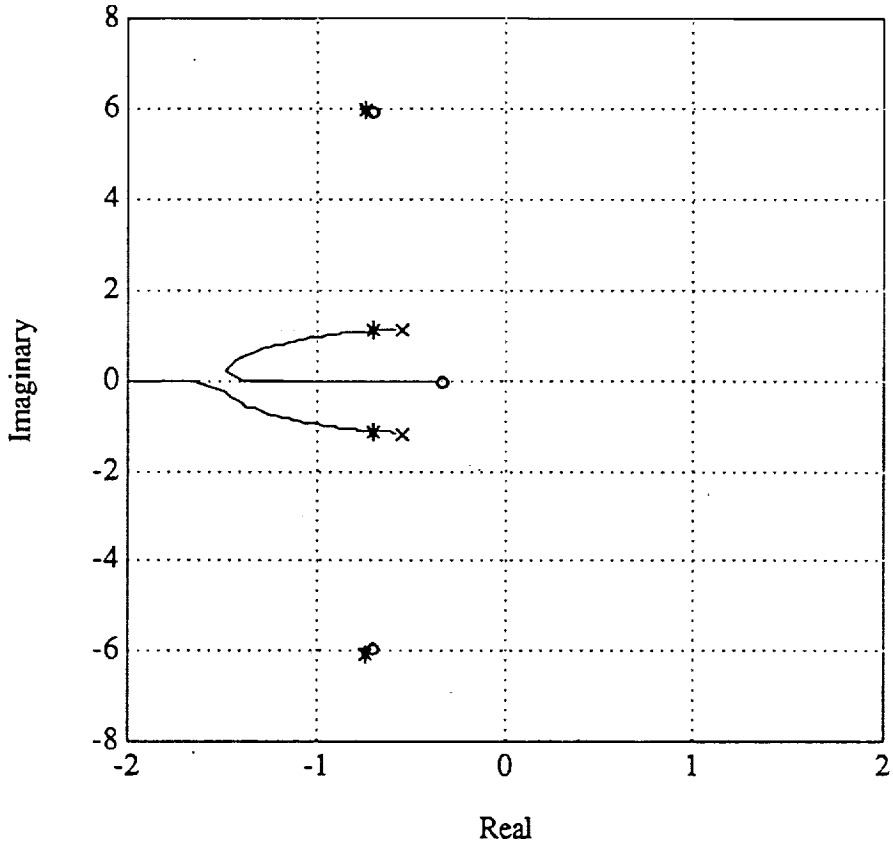

x : -0.55±j1.1
-0.75±j6.0

o : -0.35
-0.71±j5.9

* (k_{11} = -0.05) : -0.70±j1.1
-0.75±j6.0

Figure 6. Root Locus For q/δ_E Loop Closure

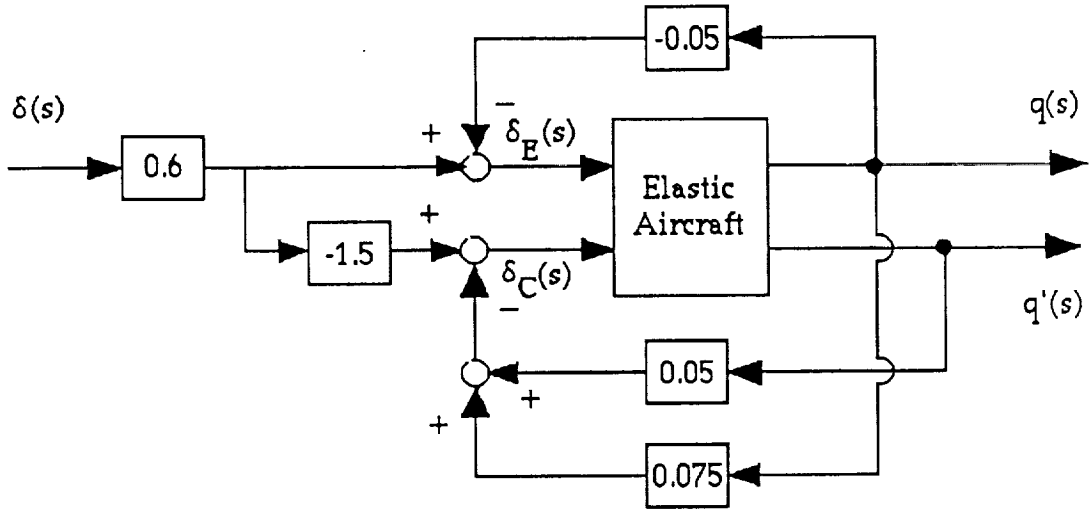

Figure 7. Classically Designed Closed-Loop System

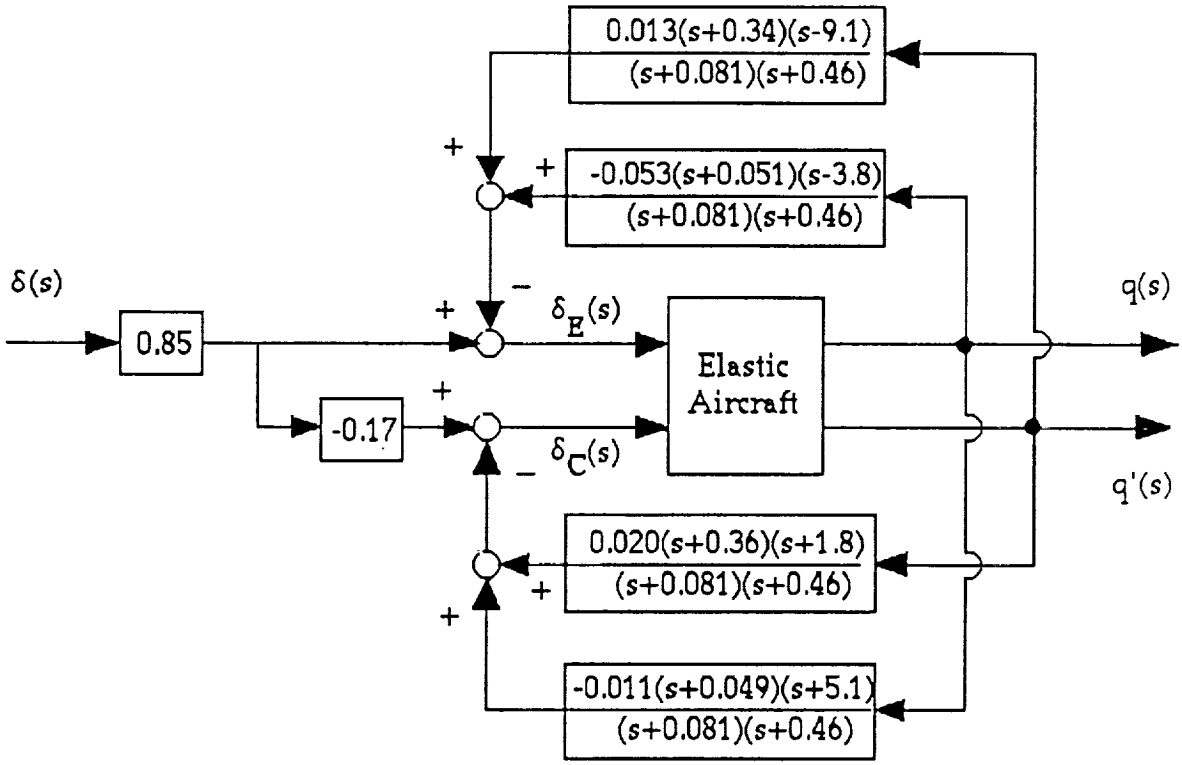

Fig.8, IMF Designed Closed-Loop System

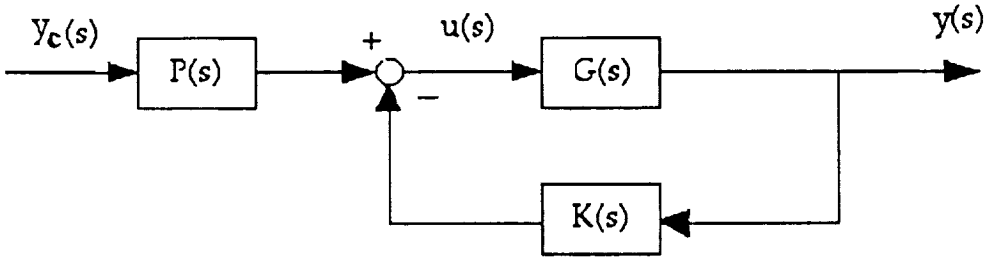

Fig. 9, Generic Closed-Loop System

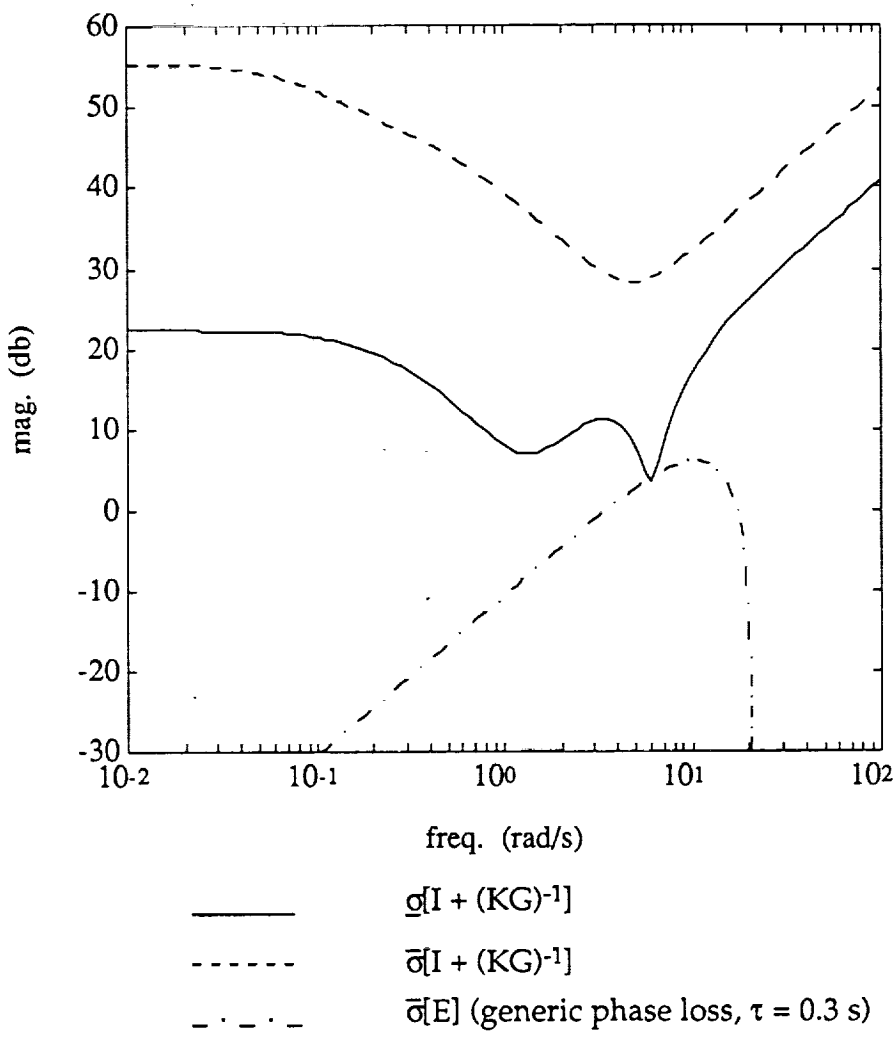

Figure 10. Classical Design Stability Robustness Analysis

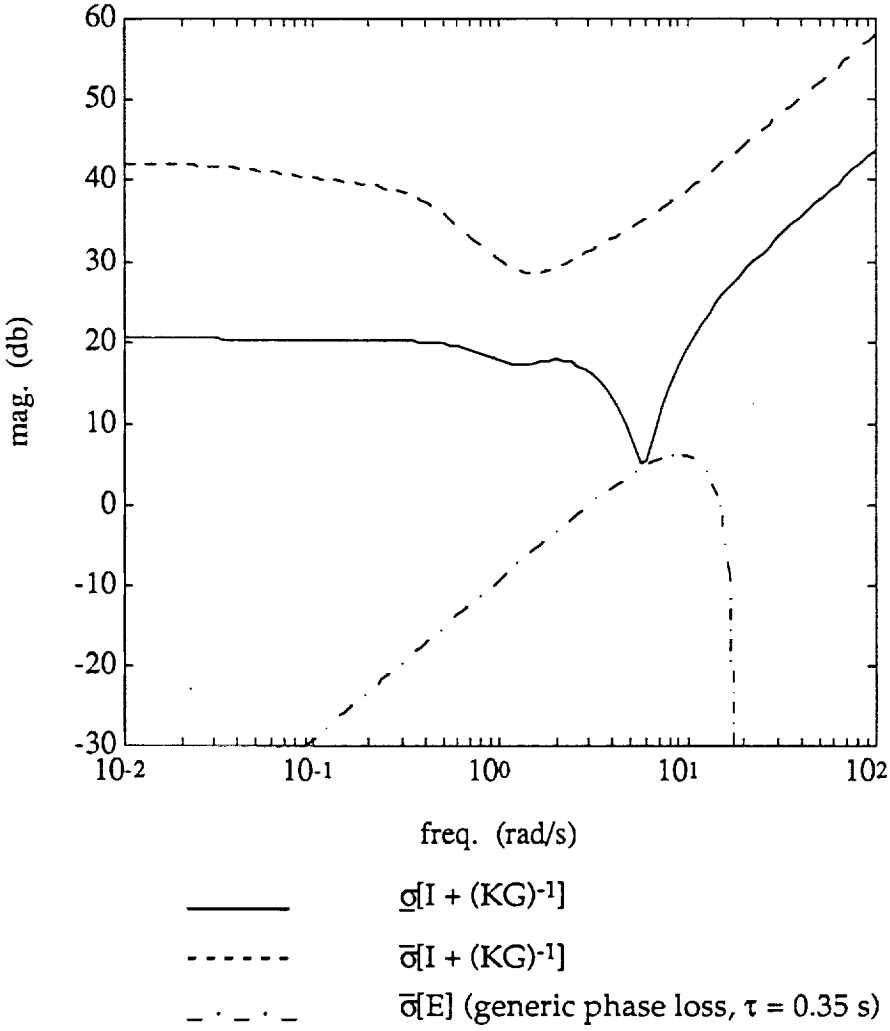

Figure 11. IMF Design Stability Robustness Analysis

Appendix B

G2751

Numerical And Literal Aeroelastic-Vehicle-Model Reduction For Feedback Control Synthesis

Brett Newman* and David K. Schmidt**
Aerospace Research Center
Arizona State University
Tempe, Arizona

Abstract

The simplification of a high-order, literal model for large flexible aircraft is discussed. Areas of model fidelity that are critical if the model is to be used for control law synthesis are presented. Several simplification techniques, some new and some widely available, that can deliver the necessary model fidelity are presented and applied to a model from the literature. The techniques include both numerical and analytical approaches. An analytical approach, based on first-order sensitivity theory, is shown to lead not only to excellent numerical results, but also to closed-form analytical expressions for key system dynamic properties such as the pole/zero factors of the vehicle transfer-function matrix. The analytical results are expressed in terms of vehicle vibrational characteristics and rigid-body and aeroelastic stability derivatives, thus providing insight in the underlying causes for critical dynamic characteristics.

* Research Associate; Doctoral Student, School Of Aeronautics And Astronautics, Purdue University; Student Member AIAA
** Professor Of Mechanical And Aerospace Engineering; Associate Fellow AIAA

Introduction

To simplify the dynamic analysis and control synthesis, or to ease computational burden in simulation, simple low-order models of the vehicle dynamics are sought. These models, however, must possess the requisite validity in modeling the vehicle characteristics significant in the application. If the model will be used in the synthesis of a feedback system, characteristics critical in a feedback system must be well modeled. This is the first goal of this work, and techniques capable of delivering valid models for multivariable control synthesis will be presented.

A second goal is related to the fact that the physics of the vehicle must be well understood, and models which expose the underlining physical causes for critical dynamic characteristics of the vehicle are desired. This is especially significant in light of the fact that many model reduction procedures in the literature rely on numerical techniques and/or transformations which lead to a model in a form such that the physics of the system are far from transparent in the new model structure. Approximate literal expressions for the factored transfer functions are presented herein that aid in understanding the physics of aeroelastic vehicles, and yet constitute model simplifications as well.

Modeling For Dynamic Analysis and Control Synthesis

To accomplish the second goal, a literal model for the vehicle must be available, and the development of such was the subject of Ref. 1. From the nonlinear, literal, time-domain model of an elastic aircraft, the linearized small perturbation longitudinal dynamic equations were developed in the reference. Transformation to the frequency domain leads to the elastic aircraft model in polynomial matrix form[2] given in Table 1, where elevator deflection δ_E and canard deflection δ_C are the assumed inputs (for a specific configuration example to follow). Typically, vertical acceleration a_z' or pitch rate q' at some location along the fuselage axis are measured responses of interest yielding two additional response equations. This model governs the small perturbation dynamics of the rigid-body degrees of freedom consisting of forward speed u, angle of attack α, pitch angle θ, and pitch rate q, and the generalized elastic degrees of freedom η_i, corresponding to the i'th elastic mode in the model. Parameters of interest appearing in Table 1 are trim velocity V_T, a_z' and q' sensor location relative to the vehicle center of mass x, stability derivatives X_i, Z_i, M_i, and F_{i_j}, elastic mode vibration frequencies ω_i and damping ratios ζ_i, and elastic mode shapes $\phi_i(x)$ and mode slopes $\phi_i'(x)$ at the sensor location.

Numerical values for the parameters in Table 1 are also available for the vehicle studied in Ref. 1. This is a large supersonic aircraft, of reasonably conventional geometry with a low-aspect ratio swept wing, conventional tail, and canard (i.e., similar in geometry to the B-1B but much more flexible). The numerical model contains four free-free elastic modes (resulting in a twelfth

order model), and the a_z' and q' sensor location corresponds to that of the cockpit. The in-vacuo vibration frequencies are 6.3, 7.0, 10.6, and 11.0 rad/s (from Ref. 1), and are considered representative for a large supersonic/hypersonic cruise vehicle with considerable flexibility. The reference flight condition taken here is at Mach 0.6 and altitude 5,000 ft. By inclusion of only the first four elastic modes of the structure, a model simplification has already occurred, the implication of which will be discussed below.

Now consider a generic feedback configuration illustrated in Figure 1, representing the flight and/or structural-mode-control loops, for example. It consists of the interconnected plant (vehicle) matrix $G'(s) = G(s) + \Delta G(s)$ and controller matrix K(s), with excitations from commands Y_c, and responses Y. All signals are multivariable, in general, and G'(s) and K(s) are transfer function matrices.

Of paramount importance in control design is that any simplified model G(s) used in the analysis and synthesis accurately reflects the stability robustness of the "true" closed-loop system, where stability robustness here refers to the system's ability to maintain stability in the face of loop uncertainties.[5] The genesis of this uncertainty could be due to parameter variations or unmodeled dynamics in G and due to modeling simplification, specifically.

Stability of the "true" closed-loop system is determined by the zeros of the ("true") return difference matrix determinant

$$\det (I + GK + \Delta GK) = 0$$

Assuming the nominal closed-loop system (GK) is stable and the forward loop perturbation ΔG is stable, the "true" closed-loop system is stable if

$$\det (I + GK + \varepsilon \Delta GK)|_{s=j\omega} \neq 0$$

for all ω, and all ε $0 \leq \varepsilon \leq 1$ or, equivalently, if $(I + GK(j\omega) + \varepsilon \Delta GK(j\omega))$ remains nonsingular for all ω and all ε, $0 \leq \varepsilon \leq 1$.

It can be shown[3] that a sufficient condition to guarantee the above is to require

$$\bar{\sigma}(\Delta GK(j\omega)) < \underline{\sigma}(I + GK(j\omega))$$

for all ω. Here $\underline{\sigma}$ and $\bar{\sigma}$ denote the minimum and maximum singular values of a matrix, respectively. Therefore, the key frequency ranges where stability robustness is potentially a problem is where

$$\bar{\sigma}(\Delta GK(j\omega)) \approx \underline{\sigma}(I + GK(j\omega)) \qquad (1)$$

over the (physically) possible ΔGK.

For SISO systems, Eq. (1) is easily interpreted on a Nyquist diagram. The right-hand side of Eq. (1) corresponds to the distance between a point on the nominal Nyquist contour $GK(j\omega)$ and the critical point at -1. The left-hand side of Eq. (1) corresponds to the distance between the above point on the nominal Nyquist contour and the corresponding point on the perturbed Nyquist contour, $G'K(j\omega)$. Regions where these two distances are approximately equal define the key frequency ranges. The concept generalizes to MIMO systems, and therefore, Eq. (1) defines the only frequency ranges where stability robustness is potentially a problem, and certain frequency ranges are more critical than others.

One frequency range pinpointed by Eq. (1) is of course the crossover frequency (i.e., the frequency range where $\underline{\sigma}(GK) \approx \bar{\sigma}(GK) \approx 1$) where relatively small variations in the loop GK can be destabilizing. Moreover, it also includes frequencies where small changes in G can create large ΔGK satisfying Eq. (1) (e.g., systems with near pole-zero cancellations within G in the vicinity of the $j\omega$-axis).

Introduction of any simplified plant model into the loop alters the loop shape (e.g., open-loop Bode) from the "true" loop shape. If a desirable[3] loop shape is still achieved, however, deviations from the "true" loop shape may occur in the high and low frequency ranges, and not significantly affect the results of the design. At low frequencies, adequate loop gain (in GK) is all that is required for acceptable command following/disturbance rejection. In the high-frequency range, the loop gain (in GK) must have adequate "roll off" for acceptable noise attenuation. Consequently, an extremely accurate approximation of the "true" system (G') is frequently not required in either the low or high frequency range as long as the two above criteria are met. This again leaves the mid-frequency range or crossover region as the critical region that must be accurately approximated by any simplified model. In summary, the primary modeling requirement imposed by feedback synthesis applications is to achieve an accurate approximation for the frequency response of the plant in the range of loop gain crossover, if the loop gain is large above this frequency range and the loop gain is small below this range. Clearly, the control law K(s) affects these loop gains and determines the crossover range.

A measure of how well a simplified plant model G(s) approximates the "true" plant model G'(s) over the crossover frequency range ($\omega_1 < \omega < \omega_2$) is the element by element frequency response error. Let the frequency response error matrix be defined by

$$E(j\omega) = G'(j\omega) - G(j\omega) \qquad (2)$$

Each i-j element in $E(j\omega)$ describes the frequency response error associated with the corresponding element in $G'(j\omega)$. For $G(s)$ to accurately approximate $G'(s)$ over the crossover frequency range, each element of $E(j\omega)$ and $G'(j\omega)$ must satisfy $|E_{ij}(j\omega)| \ll |G'_{ij}(j\omega)|$ for all ω, $\omega_1 < \omega < \omega_2$. This can be visualized graphically by superimposing the frequency responses of each element of $G'(s)$ and $G(s)$, and noting the differences between the two.

A matrix norm defined by the maximum singular value of the matrix $E(j\omega)$ may also be used to provide a measure of "smallness" for the error $E(j\omega)$. Recall that the maximum singular value of E is defined as

$$\bar{\sigma}(E) = \bar{\lambda}^{1/2}(EE^*)$$

where $\bar{\lambda}$ denotes the maximum eigenvalue. It can be shown[4] that this norm bounds the magnitude of each element in $E(j\omega)$, i.e. $|E_{ij}(j\omega)| \leq \bar{\sigma}(E(j\omega))$.

Let the largest value of $\bar{\sigma}(E(j\omega))$ over the crossover frequency range define a "crossover frequency norm"

$$\|E(j\omega)\|_{cf} = \max_{\omega_1 < \omega < \omega_2} \bar{\sigma}(E(j\omega)) \tag{3}$$

and the value of this norm may be taken as a relevant measure of closeness between the true and approximate model. Note that using the "∞ norm", or

$$\|E(j\omega)\|_{\infty} = \max_{0<\omega<\infty} \bar{\sigma}(E(j\omega))$$

would be far too conservative for our purposes here.

Order Reduction and Simplification

Some order reduction techniques that can lead to good approximations meeting the above criteria will now be highlighted.

Frequency-Weighted Internally-Balanced Reduction[5] - Assume the system in Table 1 is described in state space form, or

$$\begin{aligned} \dot{x} &= Ax + Bu \\ y &= Cx + Du \end{aligned} \tag{4}$$

Two frequency-dependent matrices of interest are

$$X(j\omega) = (j\omega I - A)^{-1}B$$
$$Y(j\omega) = C(j\omega I - A)^{-1}$$

$X(j\omega)$ reflects the system's input behavior, since each column is the state vector's frequency response associated with the related input, whereas $Y(j\omega)$ reflects the system's output behavior, since each column is the output frequency response associated with the related state. The controllability and observability grammians are related to $X(j\omega)$ and $Y(j\omega)$ by

$$X = \frac{1}{2\pi}\int_{-\infty}^{\infty} X(j\omega)X^T(-j\omega)d\omega$$

$$Y = \frac{1}{2\pi}\int_{-\infty}^{\infty} Y(j\omega)Y^T(-j\omega)d\omega$$

Note finally that $X(j\omega)$ and $Y(j\omega)$ are ultimately related to the system's frequency response $G(j\omega) = CX(j\omega) + D = Y(j\omega)B + D$.

By definition, the state directions t_i and u_i decompose X and Y into the following outer product sums

$$X = \sum_{i=1}^{n} t_i v_{c_i} t_i^T$$

$$Y = \sum_{i=1}^{n} u_i v_{o_i} u_i^T$$

where v_{c_i} and v_{o_i} are real nonnegative scalars, and where $u_i^T t_i = 1$ and $u_i^T t_j = 0$ for all $i \neq j$. It is known[6] that the importance of the contribution from state direction t_i to the input-output behavior (i.e. frequency response) of the system is reflected by the relative magnitude of the product $v_{c_i}v_{o_i}$ where this product is the i^{th} Hankel singular value of G(s), each of which is real, nonnegative, and invariant to state-space transformation. The matrix product

$$XY = \sum_{i=1}^{n} t_i v_{c_i} v_{o_i} u_i^T$$

shows that the state directions t_i are eigenvectors of XY, and the products $v_{c_i}v_{o_i}$ are the eigenvalues. In other words, state directions t_i most significant to the system's input-output behavior have the larger values for $v_{c_i}v_{o_i}$.

This leads to the so called internally-balanced reduction technique[6]. The reduced-order model is obtained by using the state directions t_i to transform the system to internally balanced states and truncating the least important states, based on the relative size of the eigenvalues $v_{c_i}v_{o_i}$. As noted in Ref. 5, the reduced-order model will inherently lead to a good approximation in the frequency range where the full order system's frequency response magnitude is large, but this may not be the frequency range of interest (i.e., loop crossover may occur in another frequency range).

To correct this situation, frequency weighting has been incorporated into this approach[5,7]. Consider a weighting filter

$$\dot{x}_w = A_w x_w + B_w \delta$$

$$u = C_w x_w$$

which is well-attenuated outside the frequency range of interest. Let this filter be in cascade with the original system. Decomposing the controllability and observability grammians for the cascaded system leads to frequency weighted internally balanced states which can readily be reduced by truncation as before. Table 2 from Ref. 5 summarizes this frequency weighted internally balanced reduction. Note that frequency-weighted internally-balanced reduction can only be applied to asymptotically stable systems or asymptotically stable subsystems of a larger system.[5,7]

Truncation - Assume the system is in polynomial matrix form, as in Table 1, or

$$\begin{bmatrix} A(s) & c(s) \\ r(s) & m(s) \end{bmatrix} \begin{bmatrix} Z(s) \\ z_r(s) \end{bmatrix} = \begin{bmatrix} B(s) \\ b_r(s) \end{bmatrix} U(s) \qquad (5)$$

$$Y(s) = M(s)Z(s) + m_r(s)z_r(s) + P(s)U(s)$$

Here $Y(s)$ is the vector of responses, $U(s)$ the vector of inputs and $[Z^T(s), z_r(s)]^T$ the vector of system degrees of freedom. Assume that $z_r(s)$ is a scalar, and then $m(s)$ is also scalar; $r(s)$ and $b_r(s)$ are row vectors; and $c(s)$ and $m_r(s)$ are column vectors. Define the notation $A_i|B_j$ as the matrix formed from the matrix A, but its i^{th} column is replaced by the j^{th} column of B. Then using the properties of the determinant of a partitioned matrix, along with Cramer's rule, yields

$$\frac{Z_i(s)}{U_j(s)} = \frac{m \det [A_i|B_j - cm^{-1}(r_i|b_{r_j})]}{m \det[A - cm^{-1}r]}$$

$$\frac{z_r(s)}{U_j(s)} = \frac{b_{r_j} \det[A - B_j b_{r_j}^{-1} r]}{m \det[A - cm^{-1}r]}$$

where the (s) denoting functional dependence has been dropped for notational brevity.

Assume now that

$$\begin{aligned} c_k r_l &\ll m \quad ; \; k,l = 1, \ldots, n \\ B_{j_k} r_l &\ll b_{r_j}, \; ; \; k,l = 1, \ldots, n \\ c_k(r_i|b_{r_j})_l &\ll m \quad ; \; k,l = 1, \ldots, n \end{aligned} \tag{6}$$

where dim (Z(s)) = n. Then

$$\begin{aligned} A_i|B_j - cm^{-1}(r_i|b_{r_j}) &\approx A_i|B_j \\ A - B_j b_{r_j}^{-1} r &\approx A \\ A - cm^{-1}r &\approx A \end{aligned}$$

and Z_i and z_r become

$$\begin{aligned} \frac{Z_i(s)}{U_j(s)} &\approx \frac{\hat{Z}_i(s)}{U_j(s)} = \frac{\det [A_i|B_j]}{\det [A]} \\ \frac{z_r(s)}{U_j(s)} &\approx b_{r_j}/m \end{aligned} \tag{7}$$

Note that $Z_i(s)/U_j(s)$ is simply that obtained if the degree of freedom z_r was truncated from the model (or not included in the modeling from the outset).

Now (consistent with the model in Table 1), let $m(s) = a_r s^2 + d_r s + k_r$ and $b_{r_j}(s) = b_{r_j}$ (a_r, d_r, k_r, b_{r_j} scalar constants), and consider a high-frequency approximation, or let $|s| \rightarrow \infty$, leading to $|b_{r_j}(s)/m(s)| \rightarrow 0$. In this case (or if $m_r b_{r_j} \approx 0$ in general), the approximate model is the well-known truncated model

$$Y(s) \approx M(s)\hat{Z}(s) + P(s)U(s)$$

$$\frac{\hat{Z}_i(s)}{U_j(s)} = \frac{\det[A_i|B_j]}{\det[A]}$$

This approximation will produce a model with the desired characteristics when assumptions (6) are valid, and the crossover frequency is well above

$$\sqrt{|k_r/a_r|} \text{ and } \sqrt{|b_{r_j}/a_r|}$$

In the special case with the system transformed into modal coordinates (5) becomes

$$\begin{bmatrix} (sI - \Lambda) & 0 \\ 0 & (sI - \Lambda_r) \end{bmatrix} \begin{bmatrix} N(s) \\ N_r(s) \end{bmatrix} = \begin{bmatrix} B \\ B_r \end{bmatrix} U(s)$$

$$Y(s) = M\,N(s) + M_r N_r(s) + PU(s)$$

with Λ and Λ_r diagonal. Now assumptions (6) are clearly satisfied. Truncation of the modal coordinates N_r will therefore lead to a good approximation in the frequency range well above the magnitude of the associated eigenvalues (Λ_r). In fact, the transfer-function error resulting from this order reduction is

$$E(s) = G'(s) - G(s) = M_r(sI - \Lambda_r)^{-1}B_r$$

It can be seen that each element of E(s) will be small when $|s| \gg |\Lambda_{r_{ii}}|$ and $|s| \gg |(M_r B_r)_{ij}|$.

Residualization - Referring back to (5), and assuming the same structure for m(s) and $b_{r_j}(s)$, consider now a low-frequency approximation such that $|s| \to 0$, leading to $b_{r_j}(s)/m(s) \to b_{r_j}/k_r$, a constant scalar. In this case, the approximation is the well-known residualized model

$$Y(s) \approx M(s)\hat{Z}(s) + m_r(s)\sum_{j=1}^{q}(b_{r_j}/k_r)U_j(s) + P(s)U(s)$$

$$\frac{\hat{Z}_j(s)}{U_j(s)} = \frac{\det[A_j|B_j]}{\det[A]}$$

where dim(U(s)) = q. This model will have the necessary validity when assumptions (6) are satisfied, and crossover frequency is well below $\sqrt{|k_r/a_r|}$.

Again consider the special case where the system is in modal coordinates, and then assumptions (6) are clearly satisfied. This residualized-mode model will therefore lead to a good

approximation in the frequency range well below the magnitude of the associated eigenvalues (Λ_r). In this case, the transfer function error is

$$E(s) = M_r(sI - \Lambda_r)^{-1}B_r + M_r(L_T)^{-1}B_r$$

It can be seen that each element of E(s) will be small when $|s| \ll |\Lambda_{r_{ii}}|$.

Approximate Literal Expressions - The transfer function matrix G(s) for the lower-order model can be computed numerically using the previous methods. Attention will now turn to a simplification technique, related to the technique in Ref. 2, which yields approximate, closed-form literal expressions for the poles and zeros of the system transfer function (matrix).

The method is based on first order sensitivity theory, and can in principle be applied to a model of higher order. The basic ideal is to obtain approximations for the factors of a polynomial by approximating the coefficients of the polynomial by the first two terms of a Taylor series. To keep the algebra tractable here, and to explain the method by means of example, consider an already simplified system in polynomial matrix form, as in Table 3. This particular model may be obtained via reducing the model in Table 1, by truncating the surge velocity u and residualizing the second thru the fourth generalized elastic deflections η_i for the aircraft in Ref. 1.

Consider now the solution for one element of the transfer function matrix, namely

$$G_{q'}^{\delta_E}(s) = \frac{N(s)}{D(s)}$$

Applying Cramer's rule to the model in Table 3 yields

$$\begin{aligned} D(s) = &- \left(\frac{Z_{\dot{\eta}_1}}{V_{T_1}}s + \frac{Z_{\eta_1}}{V_{T_1}}\right)\bullet[M_\alpha F_{1_q} s + F_{1_\alpha}(s^2 - M_q s)] \\ &- (M_{\dot{\eta}_1} s + M_{\eta_1})\bullet[F_{1_q} s(s - \frac{Z_\alpha}{V_{T_1}}) + (1 + \frac{Z_q}{V_{T_1}})F_{1_\alpha} s] \\ &+ (s^2 + (2\zeta_1\omega_1 - F_{1\dot{\eta}_1})s + (\omega_1^2 - F_{1\eta_1}))\bullet[(s - \frac{Z_\alpha}{V_{T_1}})(s^2 - M_q s) - (1 + \frac{Z_q}{V_{T_1}})M_\alpha s] \end{aligned} \qquad (8)$$

$$\begin{aligned} N(s) = &\frac{Z_{\delta_E}}{V_{T_1}}\bullet\{s\bullet[M_\alpha(s^2 + (2\zeta_1\omega_1 - F_{1\dot{\eta}_1})s + (\omega_1^2 - F_{1\eta_1})) + F_{1_\alpha}(M_{\dot{\eta}_1} s + M_{\eta_1})] \\ &- \phi_1's\bullet[M_\alpha F_{1_q} s + F_{1_\alpha}(s^2 - M_q s)]\} \\ &+ M_{\delta_E}\bullet\{s\bullet[(s - \frac{Z_\alpha}{V_{T_1}})(s^2 + (2\zeta_1\omega_1 - F_{1\dot{\eta}_1})s + (\omega_1^2 - F_{1\eta_1})) - F_{1_\alpha}(\frac{Z_{\dot{\eta}_1}}{V_{T_1}}s + \frac{Z_{\eta_1}}{V_{T_1}})] \end{aligned}$$

$$- \phi_1's \bullet [F_{1_q} s(s - \frac{Z_\alpha}{V_{T_1}}) + (1 + \frac{Z_q}{V_{T_1}})F_{1_\alpha} s]]$$

$$+ F_{1_{\delta_E}} \bullet \{s \bullet [(s - \frac{Z_\alpha}{V_{T_1}})(M_{\dot{\eta}_1} s + M_{\eta_1}) + M_\alpha(\frac{Z_{\dot{\eta}_1}}{V_{T_1}} s + \frac{Z_{\eta_1}}{V_{T_1}})]$$

$$- \phi_1's \bullet [\underline{(s - \frac{Z_\alpha}{V_{T_1}})(s^2 - M_q s)} - M_\alpha(1 + \frac{Z_q}{V_{T_1}})s]]$$

Also, consider the numerical solution for the same transfer function obtained via any appropriate means, or

$$G_{q'}^{\delta_E}(s) = \frac{13s(s + 0.23)(s - 3.4)(s + 4.0)}{s(s^2 + 0.88s + 1.6)(s^2 + 1.0s + 36.)} \tag{9}$$

$$= \frac{K_{q'}^{\delta_E} s[s + sp(\frac{1}{T})_{q'}^{\delta_E}][s + f_{1_1}(\frac{1}{T})_{q'}^{\delta_E}][s + f_{1_2}(\frac{1}{T})_{q'}^{\delta_E}]}{s[s^2 + (2\zeta\omega)_{sp} s + (\omega^2)_{sp}][s^2 + (2\zeta\omega)_{f_1} s + (\omega^2)_{f_1}]}$$

$$= \frac{n_4 s^4 + n_3 s^3 + n_2 s^2 + n_1 s}{s^5 + d_4 s^4 + d_3 s^3 + d_2 s^2 + d_1 s}$$

One now selects approximate terms, one from D(s) and one from N(s), in (8) which best satisfy the following two criteria.

1. The literal expressions for the approximate terms must factor into the same structure as found in the numerical model (poles/zeros). For example, the literal expression for the approximate term for D(s) must have 2 pair of complex roots plus one root at the origin, while that for N(s) must have 4 real roots, including one at the origin (see eq. (9)).
2. The numerical factors calculated from those approximate terms should be as close as possible to the true numerical factors in (9).

In this example, the approximate terms are selected as the underlined terms in (8) yielding

$$\tilde{D}(s) = s[s^2 + (-\frac{Z_\alpha}{V_{T_1}} - M_q)s + (\frac{Z_\alpha}{V_{T_1}} M_q - (1 + \frac{Z_q}{V_{T_1}})M_\alpha)] \tag{10}$$
$$\bullet [s^2 + (2\zeta_1\omega_1 - F_{1_{\dot{\eta}_1}})s + (\omega_1^2 - F_{1_{\eta_1}})]$$
$$= s[s^2 + (2\tilde{\zeta}\omega)_{sp} s + (\tilde{\omega}^2)_{sp}][s^2 + (2\tilde{\zeta}\omega)_{f_1} s + (\tilde{\omega}^2)_{f_1}]$$

$$= s(s^2 + 1.2s + 3.8)(s^2 + 0.62s + 35.)$$

$$= s^5 + \tilde{d}_4 s^4 + \tilde{d}_3 s^3 + \tilde{d}_2 s^2 + \tilde{d}_1 s$$

and

$$\tilde{N}(s) = (M_{\delta_E} - \phi_1' F_{1_{\delta E}})s[s + (-\frac{Z_\alpha}{V_{T_1}})] [s + (\frac{b - [b^2 - 4c]^{1/2}}{2})] [s + (\frac{b + [b^2 - 4c]^{1/2}}{2})]$$

$$= \tilde{K}_{q'}^{\delta E} s[s + {}_{sp}(\frac{1}{\tilde{T}})_{q'}^{\delta E}] [s + {}_{f_{1_1}}(\frac{1}{\tilde{T}})_{q'}^{\delta E}] [s + {}_{f_{1_2}}(\frac{1}{\tilde{T}})_{q'}^{\delta E}]$$

$$= 13s(s + 0.42)(s - 3.3)(s + 4.2)$$

$$= \tilde{n}_4 s^4 + \tilde{n}_3 s^3 + \tilde{n}_2 s^2 + \tilde{n}_1 s$$

where

$$b = \frac{(2\zeta_1\omega_1 - F_{1\dot{\eta}_1})M_{\delta_E} + \phi_1' M_q F_{1_{\delta E}}}{M_{\delta_E} - \phi_1' F_{1_{\delta E}}}$$

$$c = \frac{(\omega_1^2 - F_{1\eta_1})M_{\delta_E}}{M_{\delta_E} - \phi_1' F_{1_{\delta E}}}$$

Now, by expanding (9), one can determine the functional dependence of the polynomial coefficients upon the factors. For example,

$$d_1 = (\omega^2)_{sp}(\omega^2)_{f_1} \tag{11}$$

$$n_1 = K_{q'}^{\delta E}\ {}_{sp}(\frac{1}{T})_{q'}^{\delta E}\ {}_{f_{1_1}}(\frac{1}{T})_{q'}^{\delta E}\ {}_{f_{1_2}}(\frac{1}{T})_{q'}^{\delta E}$$

Noting this functional dependence, expand each coefficient in a Taylor series where the leading term in the series is taken as the approximate coefficients in (10). For example,

$$d_1 = \tilde{d}_1 + \frac{\partial \tilde{d}_1}{\partial x}\Delta x + \ldots$$

$$n_1 = \tilde{n}_1 + \frac{\partial \tilde{n}_1}{\partial y}\Delta y + \ldots \qquad (12)$$

where

$$\Delta x = [\ (\omega^2)_{sp} - (\tilde{\omega}^2)_{sp}\ ,\ (2\zeta\omega)_{sp} - (2\tilde{\zeta}\omega)_{sp}\ ,\ (\omega^2)_{f_1} - (\tilde{\omega}^2)_{f_1}\ ,\ (2\zeta\omega)_{f_1} - (2\tilde{\zeta}\omega)_{f_1}\ ]^T$$
$$= [\ \Delta(\tilde{\omega}^2)_{sp}\ ,\ \Delta(2\tilde{\zeta}\omega)_{sp}\ ,\ \Delta(\tilde{\omega}^2)_{f_1}\ ,\ \Delta(2\tilde{\zeta}\omega)_{f_1}\ ]^T$$

$$\Delta y = [\ K_{q'}^{\delta E} - \tilde{K}_{q'}^{\delta E}\ ,\ sp(\frac{1}{T})_{q'}^{\delta E} - sp(\frac{1}{\tilde{T}})_{q'}^{\delta E}\ ,\ f_{1_1}(\frac{1}{T})_{q'}^{\delta E} - f_{1_1}(\frac{1}{\tilde{T}})_{q'}^{\delta E}\ ,\ f_{1_2}(\frac{1}{T})_{q'}^{\delta E} - f_{1_2}(\frac{1}{\tilde{T}})_{q'}^{\delta E}\ ]^T$$
$$= [\ \Delta\tilde{K}_{q'}^{\delta E}\ ,\ \Delta_{sp}(\frac{1}{\tilde{T}})_{q'}^{\delta E}\ ,\ \Delta_{f_{1_1}}(\frac{1}{\tilde{T}})_{q'}^{\delta E}\ ,\ \Delta_{f_{1_2}}(\frac{1}{\tilde{T}})_{q'}^{\delta E})\ ]^T$$

Corrections to the approximate factors (i.e. Δx and Δy) are now sought. Using the Taylor series for each polynomial coefficient such as (12) and neglecting higher order terms, one can solve for Δx and Δy. This calculation requires the literal expressions for $d_i - \tilde{d}_i$ and $n_i - \tilde{n}_i$ obtained from the nonunderlined term in (8) and the literal expressions for

$$\frac{\partial \tilde{d}_i}{\partial x} \quad \text{and} \quad \frac{\partial \tilde{n}_i}{\partial y}$$

obtained from differentiation of expressions obtained similar to (11).

The approximate literal model is finally obtained by summing the approximate factors and the corresponding corrections. For example,

$$G_{q'}^{\delta_E}(s) = \frac{N(s)}{D(s)}$$

where

$$D(s) \approx s[s^2 + \{\ (2\tilde{\zeta}\omega)_{sp} + \Delta(2\tilde{\zeta}\omega)_{sp}\ \}s + \{\ (\tilde{\omega}^2)_{sp} + \Delta(\tilde{\omega}^2)_{sp}\ \}]$$
$$\bullet[s^2 + \{\ (2\tilde{\zeta}\omega)_{f_1} + \Delta(2\tilde{\zeta}\omega)_{f_1}\ \}s + \{\ (\tilde{\omega}^2)_{f_1} + \Delta(\tilde{\omega}^2)_{f_1}\ \}]$$

and

$$N(s) \approx (\tilde{K}_{q'}^{\delta_E} + \Delta\tilde{K}_{q'}^{\delta_E})s[s + \{ {}_{sp}(\frac{1}{\tilde{T}})_{q'}^{\delta_E} + \Delta_{sp}(\frac{1}{\tilde{T}})_{q'}^{\delta_E} \}]$$

$$\bullet[s + \{ {}_{f_{1_1}}(\frac{1}{\tilde{T}})_{q'}^{\delta_E} + \Delta_{f_{1_1}}(\frac{1}{\tilde{T}})_{q'}^{\delta_E} \}] [s + \{ {}_{f_{1_2}}(\frac{1}{\tilde{T}})_{q'}^{\delta_E} + \Delta_{f_{1_2}}(\frac{1}{\tilde{T}})_{q'}^{\delta_E} \}]$$

Example Results

To be obtained now is a reduced order model that is valid in the anticipated crossover frequency range. Assume the control system requirements are such that this range must be 1 to 10 rad/s. The vehicle discussed previously will be modeled, and the "true" model is taken as that in Table 1 with four elastic modes. A fourth-order model will be sought based on the observation that the "true" model has two complex modes in the crossover frequency range.

Two reduced order models will actually be obtained. One model is obtained by truncating the surge velocity u and pitch angle θ, and employing the frequency-weighted internally-balanced technique using a band pass filter with unity magnitude in the 1 to 10 rad/s frequency range, and 40 db/dec magnitude roll off on either side of the pass band. Here, truncation of u was necessary to eliminate an unstable phugoid pole, and truncation of θ was necessary to eliminate the associated pole at the origin. The other reduced-order model (an effective fourth-order model due to a pole/zero cancellation at the origin) is obtained by truncating the surge velocity u (i.e., a short period approximation), and residualizing the second thru the fourth generalized elastic deflections η_i. Tables 4 thru 6 contain the transfer functions for the original full-order and the two reduced-order models, while Figures 2 and 3 show the q'/δ_E and q'/δ_C frequency responses, respectively.

The q'/δ_E and q'/δ_C frequency-response errors (see Eq. (2)) are simply the distances between the Bode magnitudes of the "true" model and the reduced-order models in Figures 2 and 3. Observe that the reduced-order models accurately approximate the "true" model in the 1 to 10 rad/s frequency range as desired. Similar results are obtained for the other transfer functions in Tables 4 thru 6, in that the reduced-order models are highly accurate in the 1 to 10 rad/s frequency range, as desired. Specifically, the "crossover frequency norm" $\|E(j\omega)\|_{cf}$, see Eq. (3)) is 38 for the truncation/frequency-weighted internally-balanced model, and 170 for the truncation/residualization model, for the model units selected.

Discussion of Results

For control synthesis applications, critical features in the q'/δ_E transfer function, for example, are the nonminimum phase zero located near 3.4 rad/s (see Table 6 and Figure 2) and the lightly damped complex poles near 6 rad/s (see Table 6 and Figure 2). These characteristics have

been shown[8] to limit the stability robustness of a candidate multivariable control law, based on a literal singular-value analysis. Also, a critical feature in the q'/δ_C transfer function is the dipole structure near 3 rad/s and 6 rad/s (see Table 6 and Figure 3). Recall that nonminimum phase zeros limit the allowable loop gain and yield undesirable initial time-response behavior. Lightly damped complex poles can also limit stability robustness, as well as contribute to undesirable time responses. Dipole structures can also critically affect closed-loop stability.

To expose the physics behind these critical characteristics, an approximate literal model is developed from the truncation/residualization model given in Table 3. Note a higher order model could conceivably be used. As we shall see, however, this is not required here to obtain valid results.

Table 7 lists the approximate literal expressions for the factored transfer functions where the underlined terms were selected as the approximate terms, and the remaining terms are the corrections. Table 8 also contains the transfer functions obtained from the literal expressions in Table 7, while Figures 4 and 5 show the q'/δ_E and q'/δ_C frequency responses, respectively, for this simplified model along with the "true" model. Observe that the literal model accurately approximates the "true" model in the 1 to 10 rad/s frequency range. By comparing similar results for the other transfer functions in Tables 4, 6, and 8, one observes that the literal approximations are quite accurate.

Now to expose the parameters affecting the nonminimum phase zero in the q'/δ_E transfer function (see Table 6), consider the expression for $f_{1_1}(\frac{1}{T})^{\delta_E}_{q'}$ appearing in Table 7, or

$$f_{1_1}(\frac{1}{T})^{\delta_E}_{q'} \approx \frac{b - [b^2 - 4c]^{1/2}}{2} + \frac{F_{1_q} M_{\delta_E}}{2F_{1_{\delta_E}}} \qquad (13)$$

$$= \quad -3.3 \quad + \quad (-0.23)$$

with the following numerical values:

$M_q = -0.830\ 1/s$	$M_{\delta_E} = -5.12\ 1/s^2$	$F_{1_q} = -78.4\ 1/s$
$F_{1_{\delta_E}} = -866.\ 1/s^2$	$(\omega_1^2 - F_{1_{\eta_1}}) = 34.8\ 1/s^2$	$(2\zeta_1\omega_1 - F_{1_{\dot{\eta}_1}})s = 0.621\ 1/s$
$\phi_1'(x) = 0.0210$ ft/ft	$b = 0.912\ 1/s$	$c = -13.6\ 1/s^2$

As seen from Eq. (13), the zero location is primarily a function of the first term $\frac{b - [b^2 - 4c]^{1/2}}{2}$, which in turn is primarily a function of the parameter c as given in Table 7, or

$$c = \frac{(\omega_1^2 - F_{1\eta_1})M_{\delta_E}}{M_{\delta_E} - \phi_1'(x)F_{1_{\delta E}}} \qquad (14)$$

Evidently, the key parameters are the elevator control derivatives $M_{\delta E}$ and $F_{1\delta_E}$, elastic mode structural frequency and aerodynamic stiffness $(\omega_1^2 - F_{1\eta_1})$, and the elastic mode slope $\phi_1'(x)$. From the denominator in Eq. (14), it is apparent that the nonminimum phase characteristic is directly related to the control power affecting the rigid-body and elastic pitch motions (i.e., "up elevator" induces rigid-body "pitch up" and elastic "pitch down"). Further, it can be seen how the pitch-rate sensor location, thru $\phi_1'(x)$, and the aeroelastic mode frequency $(\omega_1^2 - F_{1\eta_1})$ affect the nonminimum phase characteristics.

Attention is now turned to the lightly damped complex poles in the q'/δ_E transfer function (see Table 6). The expression for the damping term $(2\zeta\omega)_{f_1}$ appearing in Table 7 is

$$(2\zeta\omega)_{f_1} \approx (2\zeta_1\omega_1 - F_{1\dot{\eta}_1}) + \frac{M_{\eta_1}F_{1_q} + [\frac{Z_{\eta_1}}{V_{T_1}} + (1 + \frac{Z_q}{V_{T_1}})M_{\dot{\eta}_1}]F_{1_\alpha}}{(\omega_1^2 - F_{1\eta_1})} \qquad (15)$$

$$= \quad 0.62 \quad + \quad 0.35$$

with the following numerical values:

$$(1 + \frac{Z_q}{V_{T_1}}) = 1.03 \qquad \frac{Z_{\eta_1}}{V_{T_1}} = -0.00267\ 1/s \qquad M_{\eta_1} = -0.0655\ 1/s^2$$

$$M_{\dot{\eta}_1} = -0.00390\ 1/s \qquad F_{1_\alpha} = -1{,}040\ 1/s^2 \qquad F_{1_q} = -78.4\ 1/s$$

$$(\omega_1^2 - F_{1\eta_1}) = 34.8\ 1/s^2 \qquad (2\zeta_1\omega_1 - F_{1\dot{\eta}_1}) = 0.621\ 1/s$$

As seen from Eq. (15), the low damping is primarily due to the low elastic mode structural and aerodynamic damping $(2\zeta_1\omega_1 - F_{1\dot{\eta}_1})$. However, note that approximately 1/3 of the total damping originates from other sources, such as aerodynamic coupling between the rigid and elastic degrees of freedom (i.e., $M_{\eta_1}F_{1_q}$, $\frac{Z_{\eta_1}}{V_{T_1}}F_{1_\alpha}$, $(1 + \frac{Z_q}{V_{T_1}})M_{\dot{\eta}_1}F_{1_\alpha}$).

Finally, consider the dipole structure in the q'/δ_C transfer function (see Table 6). The dipole consists of the lightly damped complex poles $[s^2 + (2\zeta\omega)_{f_1}s + (\omega^2)_{f_1}]$ and lightly damped complex zeros $[s^2 + {}_{f_1}(2\zeta\omega)^{\delta_C}_{q'}s + {}_{f_1}(\omega^2)^{\delta_C}_{q'}]$. The relative location of the pole and zero along the $j\omega$

axis is determined primarily by the difference between the natural frequency terms $(\omega^2)_{f_1}$ and ${}_{f_1}(\omega^2)^{\delta_c}_{q'}$ appearing in Table 7, or

$$(\omega^2)_{f_1} - {}_{f_1}(\omega^2)^{\delta_c}_{q'} \approx (\omega_1{}^2 - F_{1\eta_1}) + \frac{(1 + \frac{Z_q}{V_{T_1}})M_{\eta_1}F_{1_\alpha}}{(\omega_1{}^2 - F_{1\eta_1})} \qquad (16)$$

$$- \{ \frac{(\omega_1{}^2 - F_{1\eta_1})M_{\delta_c}}{M_{\delta_c} - \phi_1'(x)F_{1\delta c}} - \frac{M_{\eta_1} + \phi_1'(x)(1 + \frac{Z_q}{V_{T_1}})M_\alpha}{\phi_1'(x)} \}$$

$$= \quad 35. \quad + \quad 2.0$$

$$- \{ \quad 2.0 \quad - \quad (-6.5) \quad \}$$

with the following numerical values:

$$(1 + \frac{Z_q}{V_{T_1}}) = 1.03 \qquad M_\alpha = -3.33\ 1/s^2 \qquad M_{\eta_1} = -0.0655\ 1/s^2$$

$$M_{\delta_c} = 0.809\ 1/s^2 \qquad F_{1_\alpha} = -1{,}040\ 1/s^2 \qquad F_{1_{\delta c}} = -631.\ 1/s^2$$

$$(\omega_1{}^2 - F_{1\eta_1}) = 34.8\ 1/s^2 \qquad \phi_1'(x) = 0.0210\ ft/ft$$

As seen from Eq. (16), the second and third terms approximately cancel, leaving the dipole structure primarily a function of the elastic mode structural frequency and aerodynamic stiffness $(\omega_1{}^2 - F_{1\eta_1})$, stability derivatives $\frac{Z_q}{V_{T_1}}$, M_α, and M_{η_1}, and the elastic mode slope $\phi_1'(x)$. For fixed stability derivatives $\frac{Z_q}{V_{T_1}}$, M_α, and M_{η_1}, it is apparent the pole location is directly related to the elastic mode structural frequency and aerodynamic stiffness, while the zero location is directly related to the q' sensor location thru the elastic mode slope.

Conclusions

The importance of a dynamic model's validity in the (multivariable) region of crossover was underscored, and three model simplification techniques capable of delivering valid models (in this sense) were presented. Classical truncation and residualization were shown to be capable of yielding a good low-order model, but a newer numerical procedure known as the frequency-weighted balanced technique led to superior results in this case.

A literal simplified model was also shown to yield excellent results, and the procedure was presented herein. This approach, furthermore, was shown to lead to closed-form analytical expression for the key dynamic characteristics, and hence expose the fundamental causes for these characteristics.

Acknowledgements

This research was supported by NASA Langley Research Center under Grant NAG1-758. Mr. Doug Arbuckle has served as the technical monitor. This support is appreciated.

References

1.Waszak, M.R. and Schmidt, D.K., "Flight Dynamics of Aeroelastic Vehicles," *Journal of Aircraft* , Vol. 25, No. 6, June, 1988.

2.Pearce, B.F., et al, "Analytical Study of Approximate Longitudinal Transfer Functions For A Flexible Airframe," ASD - TDR - 62 - 279, June, 1962.

3.Doyle, J.C. and Stein, G., "Multivariable Feedback Design: Concepts For a Classical/Modern Synthesis," *IEEE Transactions On Automatic Control* , Vol. AC-26, February, 1981.

4.Bacon, B.J. and Schmidt, D.K., "A Fundamental Approach to Equivalent Systems Analysis," *Journal of Guidance, Control, and Dynamics* , Vol. 11, No. 6, Nov.-Dec., 1988.

5.Bacon, B.J. and Schmidt, D.K., "Multivariable Frequency-Weighted Order Reduction," *Journal of Guidance, Control, and Dynamics* , Vol. 12, No. 1, Jan.-Feb., 1989.

6.Moore, B.C., "Principal Component Analysis in Linear Systems: Controllability, Observability, and Model Reduction," *IEEE Transactions On Automatic Control* , Vol. AC-26, February 1981.

7.Enns, D.F., "Model Reduction for Control System Design," Ph.D. dissertation, Department of Aeronautics and Astronautics, Stanford University, June, 1984.

8.Schmidt, D. K. and Newman, B., "Multivariable Flight Control Synthesis And Literal Robustness Analysis For An Aeroelastic Vehicle," Proceedings Of The AIAA Guidance, Navigation, And Control Conference, Portland, Oregon, August, 1990

Table 1. Elastic Aircraft Longitudinal Dynamic And Response Equations In Polynomial Matrix Form

$$
\begin{bmatrix}
s - X_u & -X_\alpha & -X_q s - X_0 & -X_{\dot\eta_1} s - X_{\eta_1} & -X_{\dot\eta_2} s - X_{\eta_2} & \cdots & 0 & 0 \\
-\frac{Z_u}{V_{T_1}} & s - \frac{Z_\alpha}{V_{T_1}} & -(1 + \frac{Z_q}{V_{T_1}})s & -\frac{Z_{\dot\eta_1}}{V_{T_1}} s - \frac{Z_{\eta_1}}{V_{T_1}} & -\frac{Z_{\dot\eta_2}}{V_{T_1}} s - \frac{Z_{\eta_2}}{V_{T_1}} & & 0 & 0 \\
-M_u & -M_\alpha & s^2 - M_q s & -M_{\dot\eta_1} s - M_{\eta_1} & -M_{\dot\eta_2} s - M_{\eta_2} & & 0 & 0 \\
-F_{1_u} & -F_{1_\alpha} & -F_{1_q} s & s^2 + (2\zeta_1\omega_1 - F_{1\dot\eta_1})s + (\omega_1^2 - F_{1\eta_1}) & -F_{1\dot\eta_2} s - F_{1\eta_2} & & 0 & 0 \\
-F_{2_u} & -F_{2_\alpha} & -F_{2_q} s & -F_{2\dot\eta_1} s - F_{2\eta_1} & s^2 + (2\zeta_2\omega_2 - F_{2\dot\eta_2})s + (\omega_2^2 - F_{2\eta_2}) & & 0 & 0 \\
\vdots & & & & & & \vdots & \\
-K_u & -K_\alpha & -K_q s & -K_{\dot\eta_1} s - K_{\eta_1} & -K_{\dot\eta_2} s - K_{\eta_2} & & 1 & 0 \\
0 & 0 & -s & \phi_1'(x)s & \phi_2'(x)s & \cdots & 0 & 1
\end{bmatrix}
\begin{bmatrix} u(s) \\ \alpha(s) \\ \theta(s) \\ \eta_1(s) \\ \eta_2(s) \\ \vdots \\ a_z'(s) \\ q'(s) \end{bmatrix}
=
\begin{bmatrix}
X_{\delta_E} & X_{\delta_C} \\
\frac{Z_{\delta_E}}{V_{T_1}} & \frac{Z_{\delta_C}}{V_{T_1}} \\
M_{\delta_E} & M_{\delta_C} \\
F_{1_{\delta E}} & F_{1_{\delta C}} \\
F_{2_{\delta E}} & F_{2_{\delta C}} \\
\vdots & \vdots \\
K_{\delta_E} & K_{\delta_C} \\
0 & 0
\end{bmatrix}
\begin{bmatrix} \delta_E(s) \\ \delta_C(s) \end{bmatrix}
$$

$$K_u = Z_u - xM_u + \sum_i \phi_i(x)F_{i_u} \qquad K_{\eta_i} = Z_{\eta_i} - xM_{\eta_i} - \phi_i(x)(\omega_i^2 - F_{i\eta_i}) + \sum_{j\,j\neq i} \phi_i(x)F_{i_{\eta_j}} \qquad K_{\delta_E} = Z_{\delta_E} - xM_{\delta_E} + \sum_i \phi_i(x)F_{i_{\delta E}}$$

$$K_\alpha = Z_\alpha - xM_\alpha + \sum_i \phi_i(x)F_{i_\alpha} \qquad K_{\dot\eta_i} = Z_{\dot\eta_i} - xM_{\dot\eta_i} - \phi_i(x)(2\zeta_i\omega_i - F_{i\dot\eta_i}) + \sum_{j\,j\neq i} \phi_i(x)F_{i\dot\eta_j} \qquad K_{\delta_C} = Z_{\delta_C} - xM_{\delta_C} + \sum_i \phi_i(x)F_{i_{\delta C}}$$

$$K_q = Z_q - xM_q + \sum_i \phi_i(x)F_{i_q}$$

Table 2. Frequency Weighted Internally Balanced Reduction

Given: System state space description A, B, C, D and weighting filter state space description A_w, B_w, C_w

Find: r^{th} order system

Step 1: Solve for X and Y from

$$\begin{bmatrix} A & BC_w \\ 0 & A_w \end{bmatrix}\begin{bmatrix} X & X_{12} \\ X_{21} & X_{22} \end{bmatrix} + \begin{bmatrix} X & X_{12} \\ X_{21} & X_{22} \end{bmatrix}\begin{bmatrix} A^T & 0 \\ C_w^T B^T & A_w^T \end{bmatrix} + \begin{bmatrix} 0 & 0 \\ 0 & B_w B_w^T \end{bmatrix} = 0$$

$$\begin{bmatrix} A^T & 0 \\ C_w^T B^T & A_w^T \end{bmatrix}\begin{bmatrix} Y & Y_{12} \\ Y_{21} & Y_{22} \end{bmatrix} + \begin{bmatrix} Y & Y_{12} \\ Y_{21} & Y_{22} \end{bmatrix}\begin{bmatrix} A & BC_w \\ 0 & A_w \end{bmatrix} + \begin{bmatrix} CC^T & C^T D C_w \\ C_w^T D^T C & C_w^T D^T D C_w \end{bmatrix} = 0$$

Step 2: Find T and Σ where $XY = T\Sigma^2 T^{-1}$, $T = [T_r, T_{n-r}]$, $T^{-T} = [U_r, U_{n-r}]$

$$\Sigma^2 = \begin{bmatrix} \Sigma_r^2 & 0 \\ 0 & \Sigma_{n-r}^2 \end{bmatrix}$$

$$\Sigma_r^2 = \mathrm{diag}(v_{c_i} v_{o_i}) \quad i = 1, \ldots, r$$

$$\Sigma_{n-r}^2 = \mathrm{diag}(v_{c_i} v_{o_i}) \quad i = r+1, \ldots, n$$

$$v_{c_1} v_{o_1} \geq \ldots \geq v_{c_n} v_{o_n} \geq 0$$

Step 3: r^{th} order system is

$$A_r = U_r^T A T_r$$

$$B_r = U_r^T B$$

$$C_r = C T_r$$

$$D_r = D$$

Table 3. Truncation/Residualization Model

$$
\begin{bmatrix}
s - \frac{Z_\alpha}{V_{T_1}} & -(1 + \frac{Z_q}{V_{T_1}})s & -\frac{Z_{\dot{\eta}_1}}{V_{T_1}}s - \frac{Z_{\eta_1}}{V_{T_1}} & 0 & 0 \\
-M_\alpha & s^2 - M_q s & -M_{\dot{\eta}_1} s - M_{\eta_1} & 0 & 0 \\
-F1_\alpha & -F1_q s & s^2 + (2\zeta_1\omega_1 - F1_{\dot{\eta}_1})s + (\omega_1^2 - F1_{\eta_1}) & 0 & 0 \\
-K_\alpha & -K_q s & -K_{\dot{\eta}_1} s - K_{\eta_1} & 1 & 0 \\
0 & -s & \phi_1'(x)s & 0 & 1
\end{bmatrix}
\begin{bmatrix}
\alpha(s) \\ \theta(s) \\ \eta_1(s) \\ a_z'(s) \\ q'(s)
\end{bmatrix}
=
\begin{bmatrix}
\frac{Z_{\delta_E}}{V_{T_1}} & \frac{Z_{\delta_C}}{V_{T_1}} \\
M_{\delta_E} & M_{\delta_C} \\
F1_{\delta_E} & F1_{\delta_C} \\
K_{\delta_E} & K_{\delta_C} \\
0 & 0
\end{bmatrix}
\begin{bmatrix}
\delta_E(s) \\ \delta_C(s)
\end{bmatrix}
$$

Table 4. Transfer Functions For The True Model

$$G_{a_z}^{\delta_E}(s) = 52s(s+0.0089)(s+0.020\pm j1.7)(s+0.36\pm j11)(s+1.0\pm j11)(s-1.5\pm j12)(s+3.1\pm j14)/D(s) \quad (ft/s^2/rad)$$

$$G_{q}^{\delta_E}(s) = 8.0s(s+0.051)(s+0.20)(s-3.6)(s+4.0)(s+0.36\pm j11)(s+2.8\pm j13)(s-0.57\pm j13)/D(s) \quad (rad/s/rad)$$

$$G_{a_z}^{\delta_C}(s) = -240s(s+0.0081)(s-0.17\pm j1.8)(s+0.90\pm j4.1)(s+0.23\pm j11)(s+0.36\pm j11)(s+2.6\pm j13)/D(s) \quad (ft/s^2/rad)$$

$$G_{q}^{\delta_C}(s) = 16s(s+0.055)(s+0.12)(s+0.60\pm j2.9)(s+0.26\pm j11)(s+0.36\pm j11)(s+2.6\pm j13)/D(s) \quad (rad/s/rad)$$

where

$$D(s) = (s-0.033)(s+0.043)(s+0.45\pm j1.2)(s+0.44\pm j6.0)(s+0.22\pm j11)(s+0.36\pm j11)(s+2.6\pm j13)$$

Table 5. Transfer Functions For The Truncated/FWIB Model

$$G_{a_z}^{\delta_E}(s) = 52(s+0.020\pm j1.7)(s-1.2\pm j14)/D(s) \quad (ft/s^2/rad)$$

$$G_{q}^{\delta_E}(s) = 15(s+0.088)(s-2.9)(s+3.9)/D(s) \quad (rad/s/rad)$$

$$G_{a_z}^{\delta_C}(s) = -240(s-0.18\pm j1.8)(s+0.92\pm j4.1)/D(s) \quad (ft/s^2/rad)$$

$$G_{q}^{\delta_C}(s) = 15(s+0.090)(s+0.70\pm j2.9)/D(s) \quad (rad/s/rad)$$

where

$$D(s) = (s+0.46\pm j1.2)(s+0.44\pm j6.0)$$

Table 6. Transfer Functions For The Truncated/Residulization Model

$$G_{a_z}^{\delta_E}(s) = 46s(s+0.014\pm j1.7)(s-1.7\pm j14)/D(s) \quad (ft/s^2/rad)$$

$$G_{q}^{\delta_E}(s) = 13s(s+0.23)(s-3.4)(s+4.0)/D(s) \quad (rad/s/rad)$$

$$G_{a_z}^{\delta_C}(s) = -240s(s-0.17\pm j1.8)(s+1.0\pm j4.2)/D(s) \quad (ft/s^2/rad)$$

$$G_{q}^{\delta_C}(s) = 14s(s+0.16)(s+0.66\pm j3.0)/D(s) \quad (rad/s/rad)$$

where

$$D(s) = s(s+0.44\pm j1.2)(s+0.50\pm j6.0)$$

Table 7. Approximate Literal Expressions For The Factored Transfer Functions

$$G_{a_z'}^{\delta_F}(s) = \frac{K_{a_z'}^{\delta_F} s[s^2 + {}_{sp}(2\zeta\omega)_{a_z'}^{\delta_F} s + {}_{sp}(\omega^2)_{a_z'}^{\delta_F}][s^2 + {}_{f_1}(2\zeta\omega)_{a_z'}^{\delta_F} s + {}_{f_1}(\omega^2)_{a_z'}^{\delta_F}]}{D(s)}$$

$$G_{a_z'}^{\delta_C}(s) = \frac{K_{a_z'}^{\delta_C} s[s^2 + {}_{sp}(2\zeta\omega)_{a_z'}^{\delta_C} s + {}_{sp}(\omega^2)_{a_z'}^{\delta_C}][s^2 + {}_{f_1}(2\zeta\omega)_{a_z'}^{\delta_C} s + {}_{f_1}(\omega^2)_{a_z'}^{\delta_C}]}{D(s)}$$

$$G_{q'}^{\delta_E}(s) = \frac{K_{q'}^{\delta_E} s[s + {}_{sp}(\frac{1}{T})_{q'}^{\delta_E}][s + {}_{f_{1_1}}(\frac{1}{T})_{q'}^{\delta_E}][s + {}_{f_{1_2}}(\frac{1}{T})_{q'}^{\delta_E}]}{D(s)}$$

$$G_{q'}^{\delta_C}(s) = \frac{K_{q'}^{\delta_C} s[s + {}_{sp}(\frac{1}{T})_{q'}^{\delta_C}][s^2 + {}_{f_1}(2\zeta\omega)_{q'}^{\delta_C} s + {}_{f_1}(\omega^2)_{q'}^{\delta_C}]}{D(s)}$$

where $D(s) = s[s^2 + (2\zeta\omega)_{sp} s + (\omega^2)_{sp}][s^2 + (2\zeta\omega)_{f_1} s + (\omega^2)_{f_1}]$

$$(\omega^2)_{sp} \approx \frac{\frac{Z_\alpha}{V_{T_1}} M_q - (1 + \frac{Z_q}{V_{T_1}}) M_\alpha}{} - \frac{(1 + \frac{Z_q}{V_{T_1}}) M_{\eta_1} F_{1_\alpha}}{(\omega_1^2 - F_{1\eta_1})}$$

$$(2\zeta\omega)_{sp} \approx \frac{-\frac{Z_\alpha}{V_{T_1}} - M_q}{} - \frac{[\frac{Z_{\eta_1}}{V_{T_1}} + (1 + \frac{Z_q}{V_{T_1}}) M_{\dot{\eta}_1}] F_{1_\alpha} + M_{\eta_1} F_{1_q}}{(\omega_1^2 - F_{1\eta_1})}$$

$$K_{a_z'}^{\delta_E} \approx K_{\delta_E}$$

$${}_{sp}(\omega^2)_{a_z'}^{\delta_E} \approx \frac{\frac{Z_\alpha}{V_{T_1}} M_q}{} + \frac{[(\omega_1^2 - F_{1\eta_1}) K_\alpha + F_{1_\alpha} K_{\eta_1}](1 + \frac{Z_q}{V_{T_1}}) M_{\delta_E}}{K_{\eta_1} F_{1_{\delta_E}}}$$

$${}_{sp}(2\zeta\omega)_{a_z'}^{\delta_E} \approx \frac{-\frac{Z_\alpha}{V_{T_1}} - M_q}{} + \frac{[(\omega_1^2 - F_{1\eta_1}) M_{\delta_E} + M_{\eta_1} F_{1_{\delta_E}}] K_q}{K_{\eta_1} F_{1_{\delta_E}}}$$

$${}_{f_1}(\omega^2)_{a_z'}^{\delta_E} \approx \frac{(\omega_1^2 - F_{1\eta_1}) + \frac{K_{\eta_1} F_{1_{\delta_E}}}{K_{\delta_E}}}{} + \frac{(1 + \frac{Z_q}{V_{T_1}}) K_\alpha M_{\delta_E}}{K_{\delta_E}}$$

$${}_{f_1}(2\zeta\omega)_{a_z'}^{\delta_E} \approx \frac{(2\zeta_1\omega_1 - F_{1\dot{\eta}_1}) + \frac{K_{\dot{\eta}_1} F_{1_{\delta_E}}}{K_{\delta_E}}}{} + \frac{[-(\omega_1^2 - F_{1\eta_1}) K_{\delta_E} + K_{\eta_1} F_{1_{\delta_E}}] K_q M_{\delta_E}}{K_{\eta_1} K_{\delta_E} F_{1_{\delta_E}}}$$

$$K_{q'}^{\delta_E} \approx M_{\delta_E} - \phi_1'(x) F_{1_{\delta_E}}$$

$${}_{sp}(\frac{1}{T})_{q'}^{\delta_E} \approx \frac{-\frac{Z_\alpha}{V_{T_1}}}{} - \frac{\frac{Z_{\eta_1}}{V_{T_1}} F_{1_\alpha} M_{\delta_E} + \frac{Z_\alpha}{V_{T_1}} M_{\eta_1} F_{1_{\delta_E}}}{(\omega_1^2 - F_{1\eta_1}) M_{\delta_E}}$$

$${}_{f_{1_1}}(\frac{1}{T})_{q'}^{\delta_E} \approx \frac{b - [b^2 - 4c]^{1/2}}{2} + \frac{F_{1_q} M_{\delta_E}}{2F_{1_{\delta_E}}}$$

$${}_{f_{1_2}}(\frac{1}{T})_{q'}^{\delta_E} \approx \frac{b + [b^2 - 4c]^{1/2}}{2} + \frac{F_{1_q} M_{\delta_E}}{2F_{1_{\delta_E}}}$$

$$b = \frac{(2\zeta_1\omega_1 - F_{1\dot{\eta}_1}) M_{\delta_E} + \phi_1'(x) M_q F_{1_{\delta_E}}}{M_{\delta_E} - \phi_1'(x) F_{1_{\delta_E}}}$$

$$(\omega^2)_{f_1} \approx \underline{(\omega_1^2 - F_{1\eta_1})} + \frac{(1 + \frac{Z_q}{V_{T_1}})M_{\eta_1}F_{1_\alpha}}{(\omega_1^2 - F_{1\eta_1})}$$

$$(2\zeta\omega)_{f_1} \approx \underline{(2\zeta_1\omega_1 - F_{1\dot{\eta}_1})} + \frac{[\frac{Z_{\eta_1}}{V_{T_1}} + (1 + \frac{Z_q}{V_{T_1}})M_{\dot{\eta}_1}]F_{1_\alpha} + M_{\eta_1}F_{1_q}}{(\omega_1^2 - F_{1\eta_1})}$$

$$K_{a_z}^{\delta_c} \approx \underline{K_{\delta_c}}$$

$$sp(\omega^2)_{a_z}^{\delta_c} \approx \underline{\frac{Z_\alpha}{V_{T_1}}M_q} - \frac{[(\omega_1^2 - F_{1\eta_1})M_\alpha + M_{\eta_1}F_{1_\alpha}](1 + \frac{Z_q}{V_{T_1}})K_{\delta_c}}{(\omega_1^2 - F_{1\eta_1})K_{\delta_c} + K_{\eta_1}F_{1\delta c}}$$

$$sp(2\zeta\omega)_{a_z}^{\delta_c} \approx \underline{-\frac{Z_\alpha}{V_{T_1}} - M_q} + \frac{[(\omega_1^2 - F_{1\eta_1})M_{\delta_c} + M_{\eta_1}F_{1\delta c}]K_q - [M_{\eta_1}F_{1_q} + (1 + \frac{Z_q}{V_{T_1}})M_{\dot{\eta}_1}F_{1_\alpha}]K_{\delta_c}}{(\omega_1^2 - F_{1\eta_1})K_{\delta_c} + K_{\eta_1}F_{1\delta c}}$$

$$f_1(\omega^2)_{a_z}^{\delta_c} \approx \underline{(\omega_1^2 - F_{1\eta_1}) + \frac{K_{\eta_1}F_{1\delta c}}{K_{\delta_c}}} + \frac{[M_{\eta_1}F_{1_\alpha}K_{\delta_c} - M_\alpha K_{\eta_1}F_{1\delta c}](1 + \frac{Z_q}{V_{T_1}})}{(\omega_1^2 - F_{1\eta_1})K_{\delta_c} + K_{\eta_1}F_{1\delta c}}$$

$$f_1(2\zeta\omega)_{a_z}^{\delta_c} \approx \underline{(2\zeta_1\omega_1 - F_{1\dot{\eta}_1}) + \frac{K_{\dot{\eta}_1}F_{1\delta c}}{K_{\delta_c}}} + \frac{(\frac{Z_\alpha}{V_{T_1}} + M_q)(1 + \frac{Z_q}{V_{T_1}})M_\alpha K_{\delta_c} - M_{\eta_1}K_qF_{1\delta c}}{(\omega_1^2 - F_{1\eta_1})K_{\delta_c} + K_{\eta_1}F_{1\delta c}}$$

$$K_{q'}^{\delta_c} \approx \underline{M_{\delta_c} - \phi_1'(x)F_{1\delta c}}$$

$$sp(\frac{1}{T})_{q'}^{\delta_c} \approx \underline{-\frac{Z_\alpha}{V_{T_1}}} + \frac{[\phi_1'(x)(1 + \frac{Z_q}{V_{T_1}})\frac{Z_\alpha}{V_{T_1}}M_\alpha + \frac{Z_{\eta_1}}{V_{T_1}}M_\alpha - \frac{Z_\alpha}{V_{T_1}}M_{\eta_1}]F_{1\delta c}}{(\omega_1^2 - F_{1\eta_1})M_{\delta_c}}$$

$$f_1(\omega^2)_{q'}^{\delta_c} \approx \underline{\frac{(\omega_1^2 - F_{1\eta_1})M_{\delta_c}}{M_{\delta_c} - \phi_1'(x)F_{1\delta c}}} - \frac{M_{\eta_1} + \phi_1'(x)(1 + \frac{Z_q}{V_{T_1}})M_\alpha}{\phi_1'(x)}$$

$$f_1(2\zeta\omega)_{q'}^{\delta_c} \approx \underline{\frac{(2\zeta_1\omega_1 - F_{1\dot{\eta}_1})M_{\delta_c} + \phi_1'(x)M_qF_{1\delta c}}{M_{\delta_c} - \phi_1'(x)F_{1\delta c}}} - \frac{\phi_1'(x)(1 + \frac{Z_q}{V_{T_1}})\frac{Z_\alpha}{V_{T_1}}M_\alpha F_{1\delta c}}{(\omega_1^2 - F_{1\eta_1})M_{\delta_c}}$$

$$c = \frac{(\omega_1^2 - F_{1\eta_1})M_{\delta_E}}{M_{\delta_E} - \phi_1'(x)F_{1\delta E}}$$

Table 8. Transfer Functions For The Approximate Literal Model

$$G_{a_z}^{\delta_E}(s) = 46s(s+0.13\pm j2.0)(s-1.9\pm j14)/D(s) \quad (ft/s^2/rad)$$

$$G_{q}^{\delta_E}(s) = 13s(s+0.20)(s-3.5)(s+3.9)/D(s) \quad (rad/s/rad)$$

$$G_{a_z}^{\delta_C}(s) = -240s(s-0.11\pm j1.8)(s+0.72\pm j4.0)/D(s) \quad (ft/s^2/rad)$$

$$G_{q}^{\delta_C}(s) = 14s(s+0.16)(s+0.74\pm j2.8)/D(s) \quad (rad/s/rad)$$

where

$$D(s) = s(s+0.45\pm j1.2)(s+0.48\pm j6.0)$$

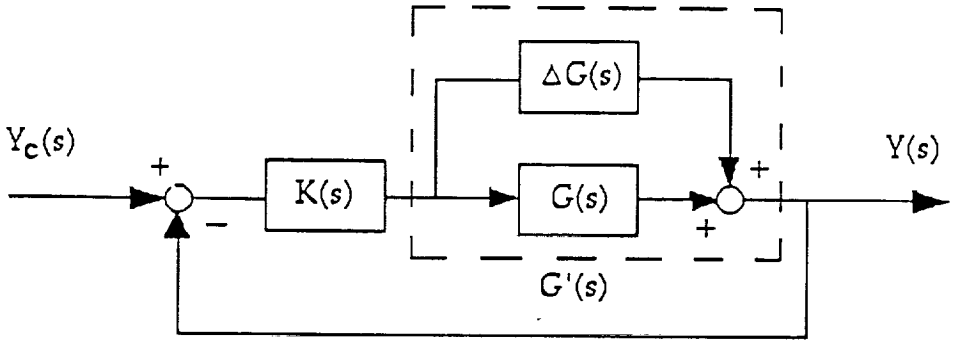

Figure 1. Generic Feedback Configuration

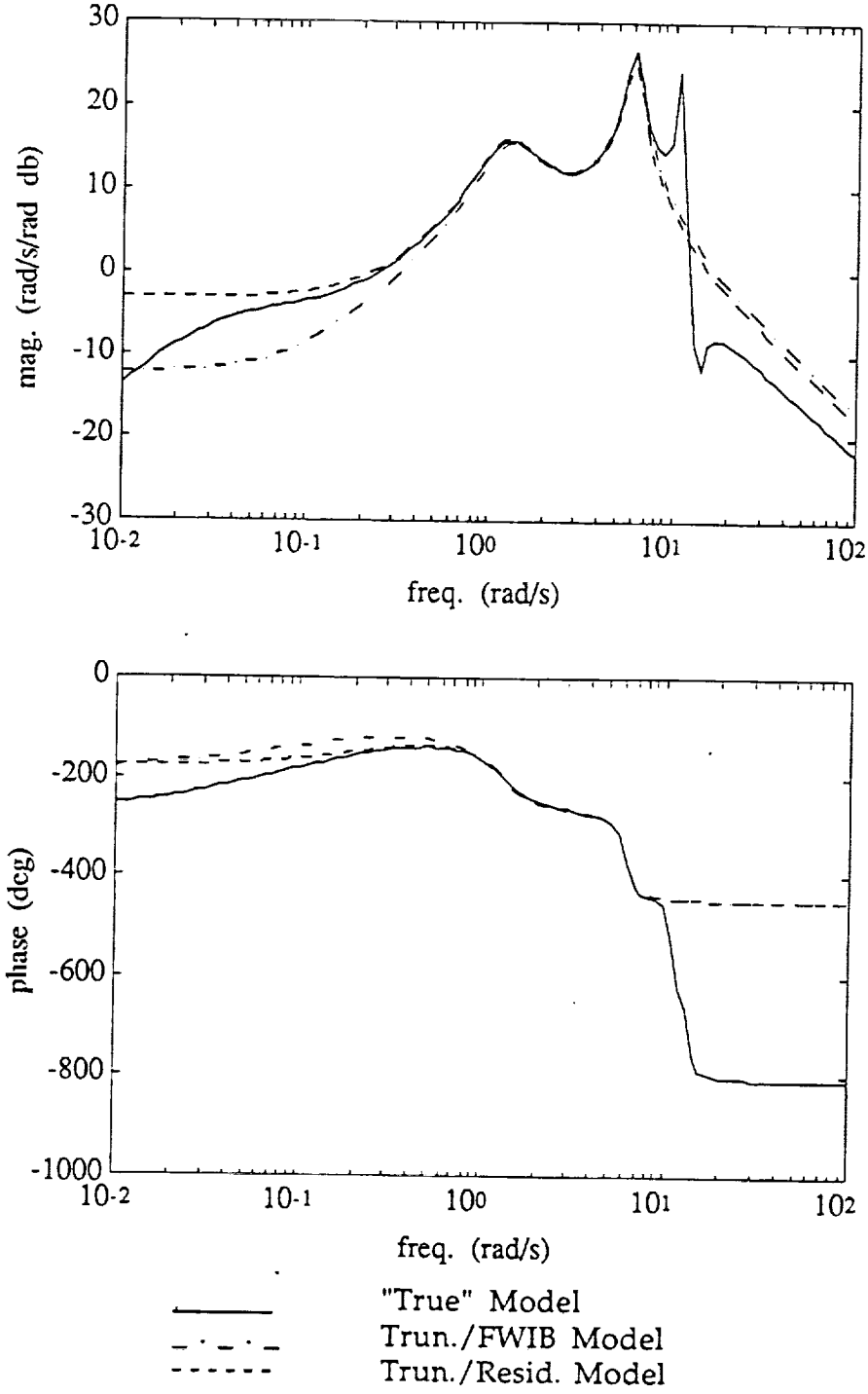

Figure 2. $G_{q}^{\delta_E}(s)$ Frequency Response

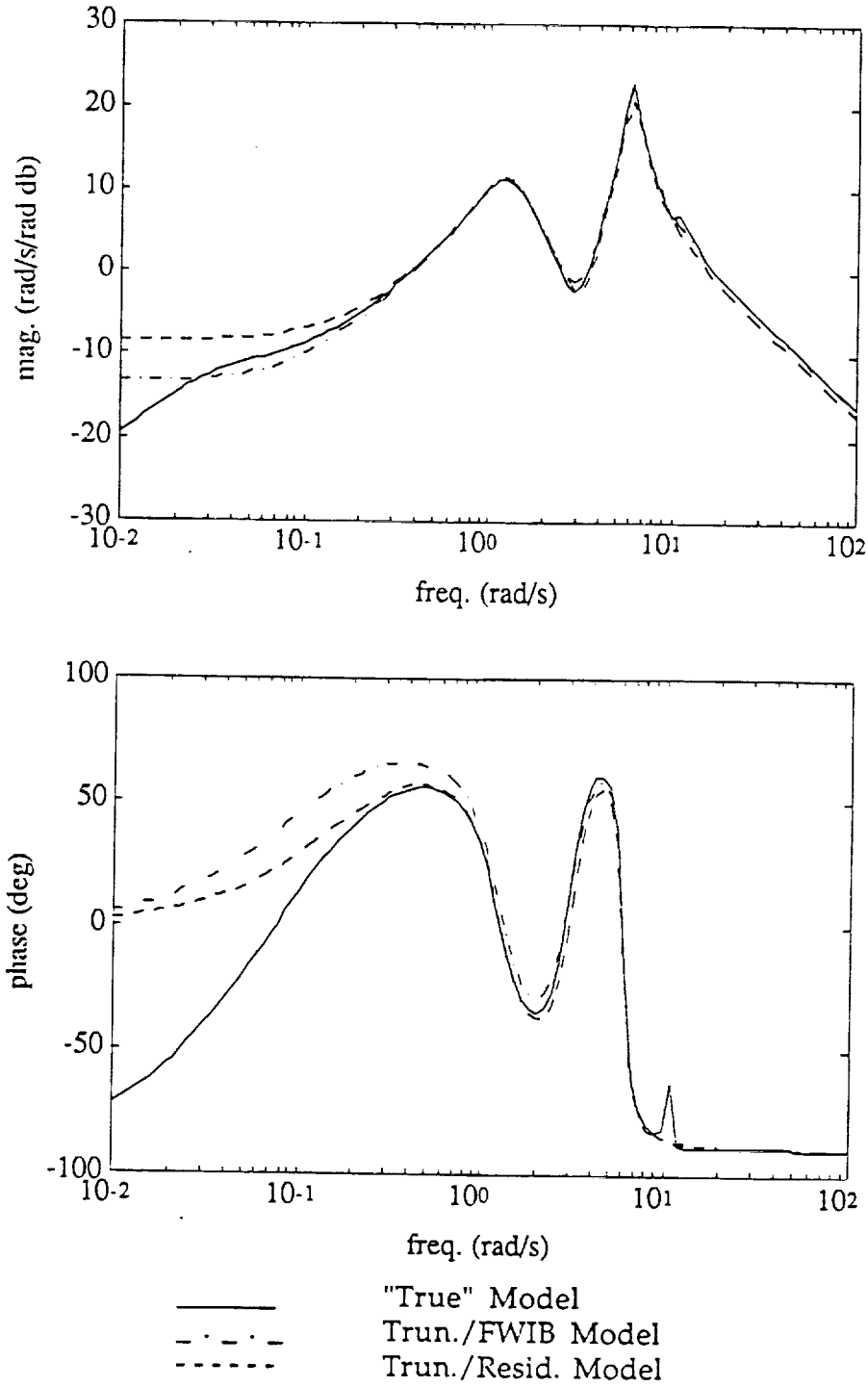

Figure 3. $G_q^{\delta_c}(s)$ Frequency Response

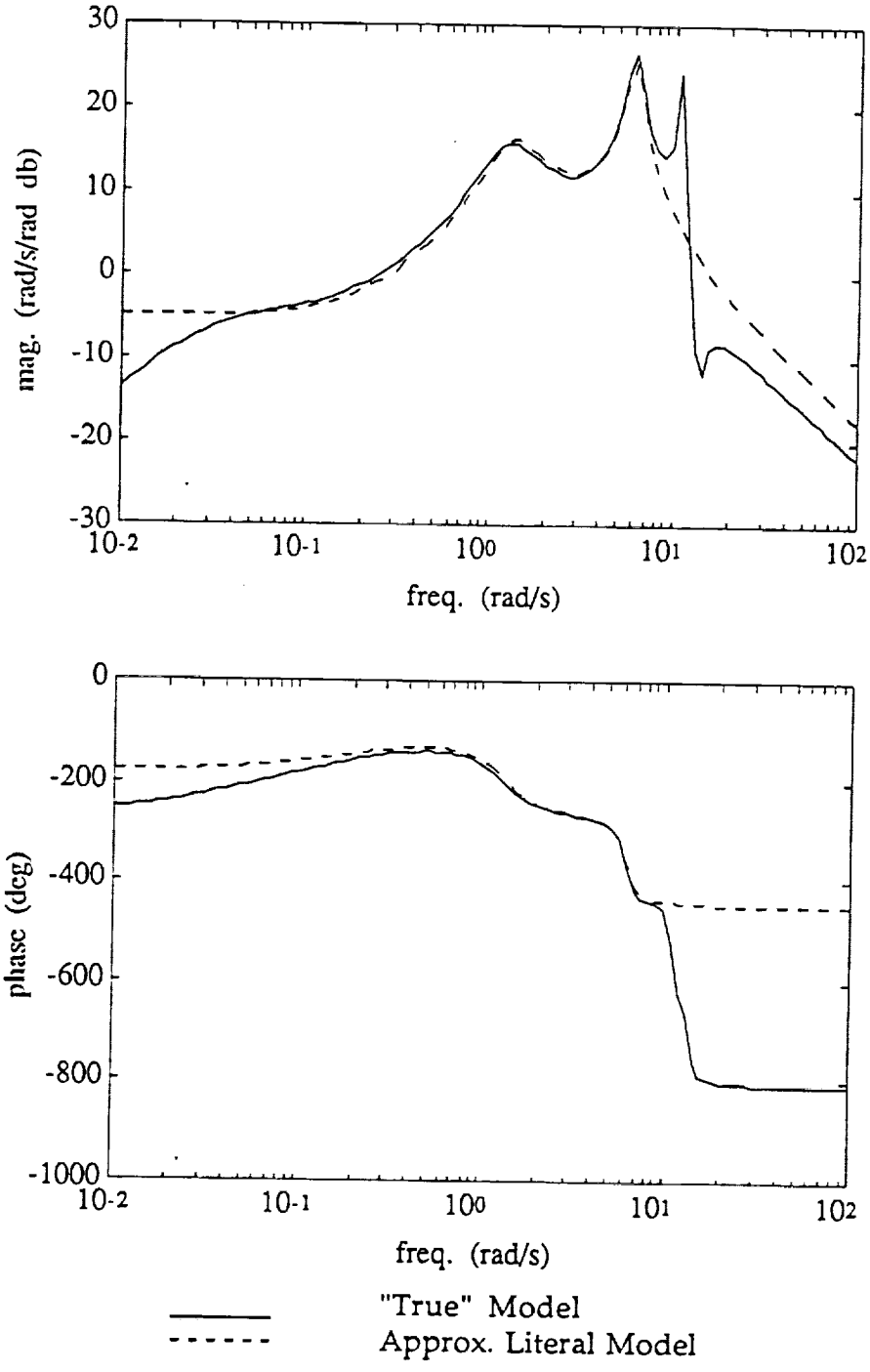

Figure 4. $G_{q}^{\delta_E}(s)$ Frequency Response

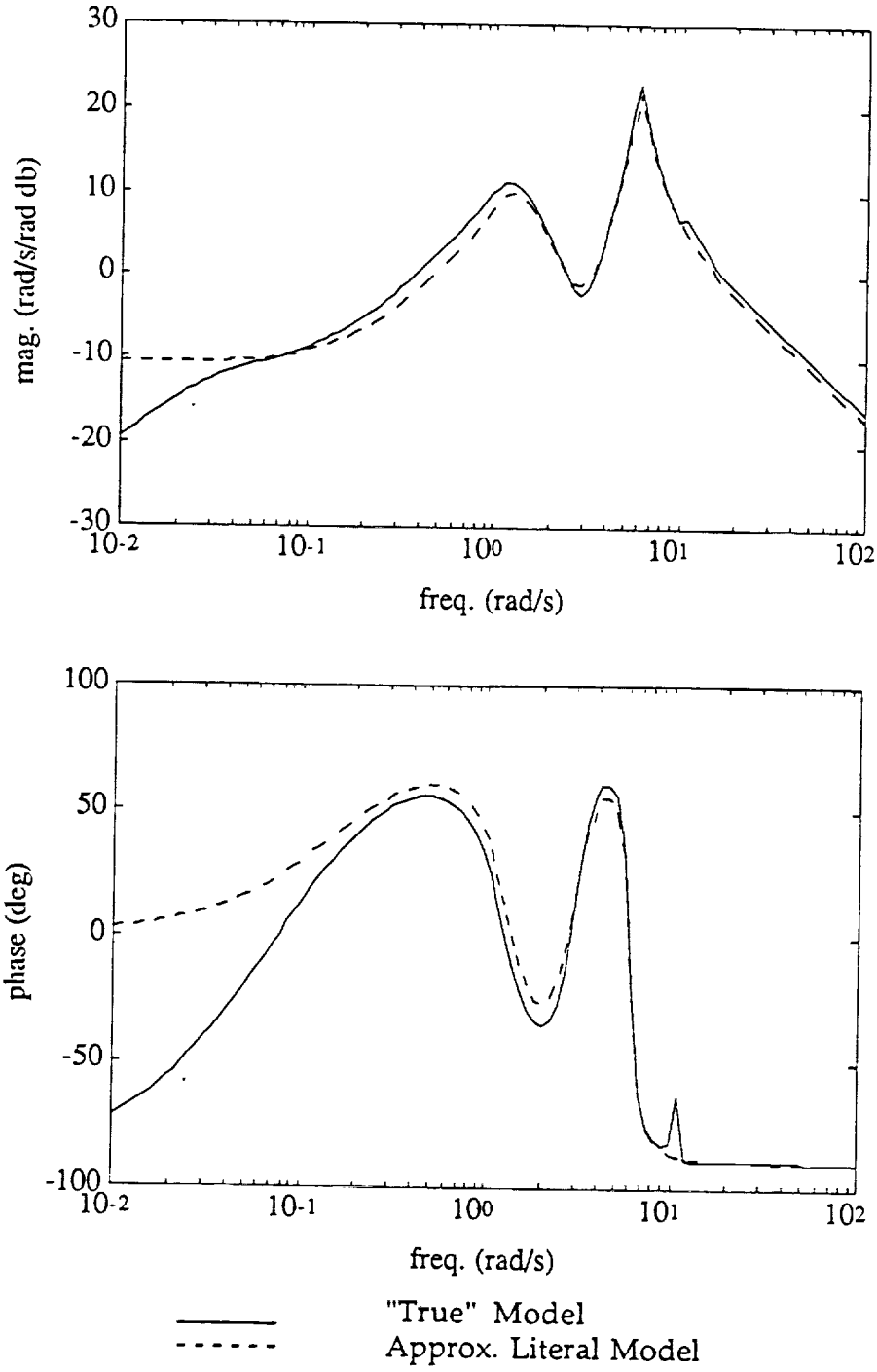

Figure 5. $G_q^{\delta_c}(s)$ Frequency Response

Appendix C

DYNAMICS of AEROSPACE VEHICLES

David K. Schmidt
and
Brett Newman

Dept. of Mechanical And Aerospace Engineering
Arizona State University
Tempe, Arizona

OUTLINE

1. MOTIVATION
2. CRITERIA FOR SIMPLIFICATION
3. METHODOLOGY
4. RESULTS FROM APPLICATIONS
5. CONTROL SYNTHESIS FOR FLEXIBLE AIRCRAFT
6. RESULTING CONTROL LAWS
7. ANALYSIS OF THE CONTROL LAWS
8. SUMMARY AND CONCLUSIONS

CRITERIA FOR SIMPLIFICATION

Model Used In Synthesis And Analysis Of Feedback Systems

Performance Of Full Order System Must Be Preserved

Stability Robustness Of Full Order System Must Be Preserved

Physical Insight Should Be Enhanced

Recognize The Significance Of Model/Controlle Input/Output Characteristics

THE GENERIC CLOSED-LOOP SYSTEM

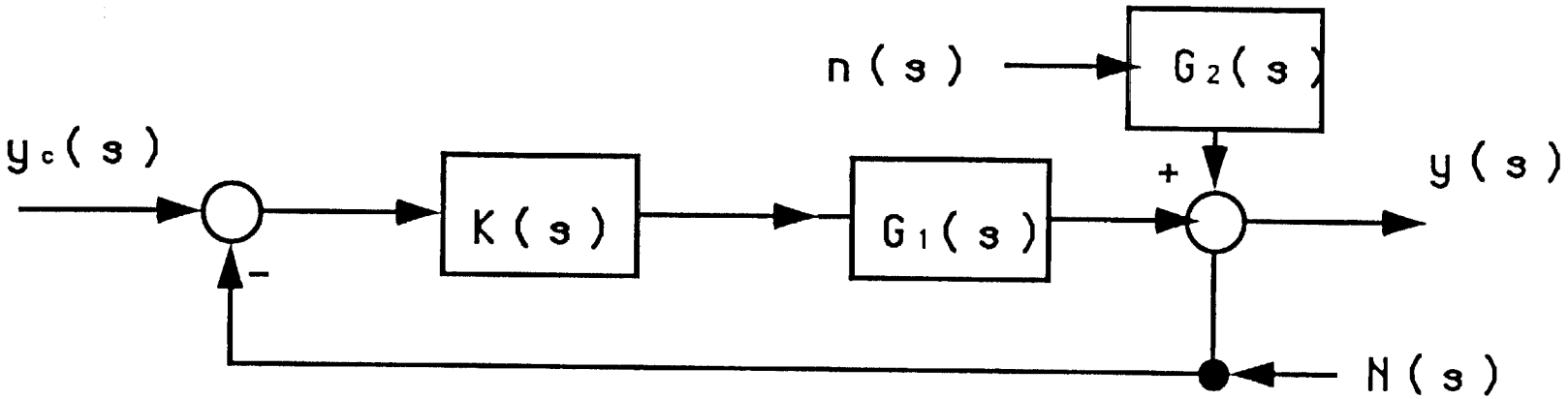

$$Y(s) = [I + G_1K]^{-1} G_1K(Y_c - N) + [I + G_1K]^{-1} G_2 n$$

7/21/89

MODEL SIMPLIFICATION TREATED AS MODEL UNCERTAINTY

Let Full-Order Model $\triangleq G(s)$

Let Reduced-Order Model $\triangleq G_R(s)$

Model "Uncertainty" $\triangleq \Delta G(s) = G(s) - G_R(s)$

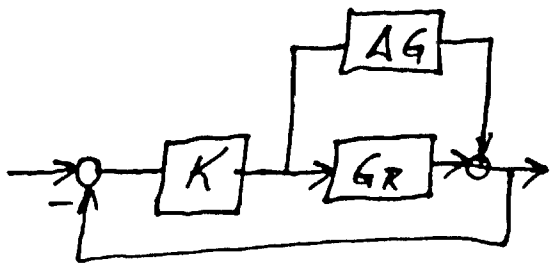

? What ΔG's Are Critical In Model Reduction

→ The Same As Critical Uncertainty In Loop

7/21/89

REVIEW OF CRITICAL ΔG's

→ Multivariable Nyquist Theory

From the Principle of The Argument:

The No. of Zeros OF $\phi_{CL}(s)$ in R.H.P. Are

$$\lim_{R\to\infty} N(0, \phi_{CL}(s), D_R) = Z$$

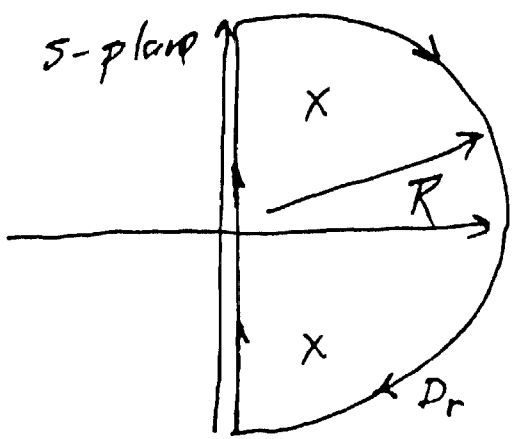

ϕ_{CL} - any analytic function on D_r

$\Rightarrow$ For Feedback Systems, Function of Interest is Closed-Loop Characteristic Polynomial

Let $K(s) = C_K (sI - A_K)^{-1} B_K$

$G(s) = C_G (sI - A_G)^{-1} B_G$

$\Rightarrow GK(s) \triangleq C_{GK} (sI - A_{GK})^{-1} B_{GK}$

As Shown in Kwak. & Sivan (and elsewhere)

$$\phi_{CL}(s) = \det(sI - A_{GK}) \det\left[I + C_{GK}(sI - A_{GK})^{-1} B_{GK}\right]$$

$$\text{or} \quad = \phi_{OL}(s) \det\left[I + GK(s)\right]$$

So If

$$\lim_{R \to \infty} \eta(0, \phi_{OL}(s), D_R) = P$$

Then Stability (And Robustness) May Be Determined Using The Following:

$$\lim_{R \to \infty} \eta(0, \det[I + GK(s)], D_R) = Z - P$$

Implication of Nyquist

Let $G \rightarrow G + \Delta G \triangleq G'$ (e.g. G_R)

$GK \rightarrow (G+\Delta G)K \triangleq \phi_{OL}'(s)$

$\phi_{CL}(s) \rightarrow \phi_{CL}'(s) = \phi_{OL}'(s) \det[I + (G+\Delta G)K]$

Clearly $\phi'(s)$ stable iff $z' = 0$

But if $p' = p$

$z' = z - (z-p) + (z'-p')$

If $\phi_{CL}(s)$ stable $\rightarrow z = 0$

So, $\phi'(s)$ stable iff $(z'-p') = (z-p)$

7/21/89

Imp. N.T. (cont'd)

Therefore $\lim_{R\to\infty}\{\eta(0, \det[I+(G+\Delta G)K], D_R\}$

If $= \lim_{R\to\infty}\{\eta(0, \det[I+GK], D_R)\}$

Then $Z' = 0 \Rightarrow \phi_{CL}'(s) = 0$

? What' ΔG's are critical ?

$\Rightarrow \Delta G$'s that Change Image $[\det(I+(G+\Delta G)K)]\Big|_{s=j\omega}$

From Image $[\det(I+GK)]\Big|_{s=j\omega}$

Near The Origin — s... Could Change Encircl.

This Leads To Bounds On ΔG and ΔGK

Example. $\phi_{CL}'(s)$ stable if

$$\bar{\sigma}(\Delta GK) < \underline{\sigma}(I + GK(j\omega)) \quad \forall\ \omega$$

$\Rightarrow$ Critical ΔG's Are Those Leading To

$$\bar{\sigma}(\Delta GK) \to \underline{\sigma}(I + GK(j\omega)) \quad \text{(from below)}$$

$\Rightarrow$ Critical Frequency Ranges

1. ω's such that $\sigma_i(GK) \approx 1$

and 2. ω's such that $\bar{\sigma}(\Delta GK)$ may be large.

7/21/89

CRITERIA FOR MODEL REDUCTION

Model Reduction Technique Should Lead To ΔG's (Due to Reduction) Such That

$$\bar{\sigma}(\Delta G K)\Big|_{s=j\omega} << \underline{\sigma}(I + GK)\Big|_{s=j\omega}$$

→ Especially Stringent Near Crossover ($\sigma_i(GK) \approx 1$)

⇒ Make $\bar{\sigma}(\Delta G)$ small, especially near crossover

⇐ $|\Delta g_{ij}(j\omega)|$ small near crossover

For Internally Balance Technique (Moore '81)

Enns Showed ('84)

$$\sup_{\omega} \bar{\sigma}(\Delta G(j\omega)) < 2 \sum_{Tr} h_i \quad ; \; h_i - \text{Hankel Singular Values}$$

But That's Not Good Enough!

Other Reduction Techniques Can Lead
To Smaller $\bar{\sigma}(\Delta G)$ Where It's Critical
(But Larger Where It's Not)

$\Rightarrow$ Frequency Weighted, Internally Balanced.
$\Rightarrow$ New Criteria $\sup_{\Delta\omega_c} \bar{\sigma}(\Delta G(j\omega))$ "Crossover Norm"

7/21/89

TYPICAL RESULTS

Swept Wing, Supersonic Transport/Bomber

Flight Condition, $M = 0.6$, $h = 5000$ ft.

Structual Modes — 6.3, 7.0, 10.6, 11.0 rad/s

Inputs — Elevator, Canard, Gust

Responses — Pitch Rate, Accel. at Cockpit

$$G(s) = \overset{\delta_E, \delta_c, \alpha_c}{\begin{bmatrix} 2 \times 3 \end{bmatrix}} \begin{matrix} a_{z_s} \\ q_s \end{matrix} = [g_{ij}(s)]$$

Results:

$12^{th} \rightarrow 4^{th}$ Order Model

Unweighted, Internally Bal. – $\|\Delta G(j\omega)\|_c = \underline{443}$

Weighted, Int. Bal. – $\|\Delta G(j\omega)\|_c = \underline{60}$

(rad, ft, sec)

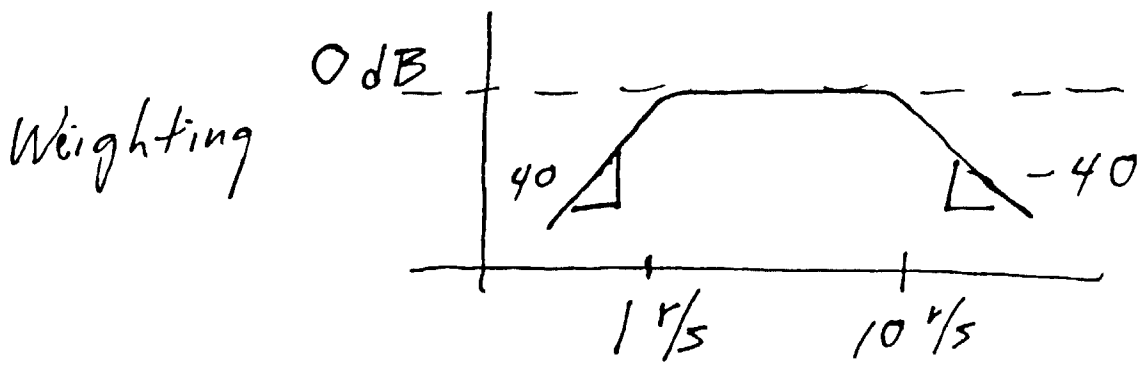

7/21/89

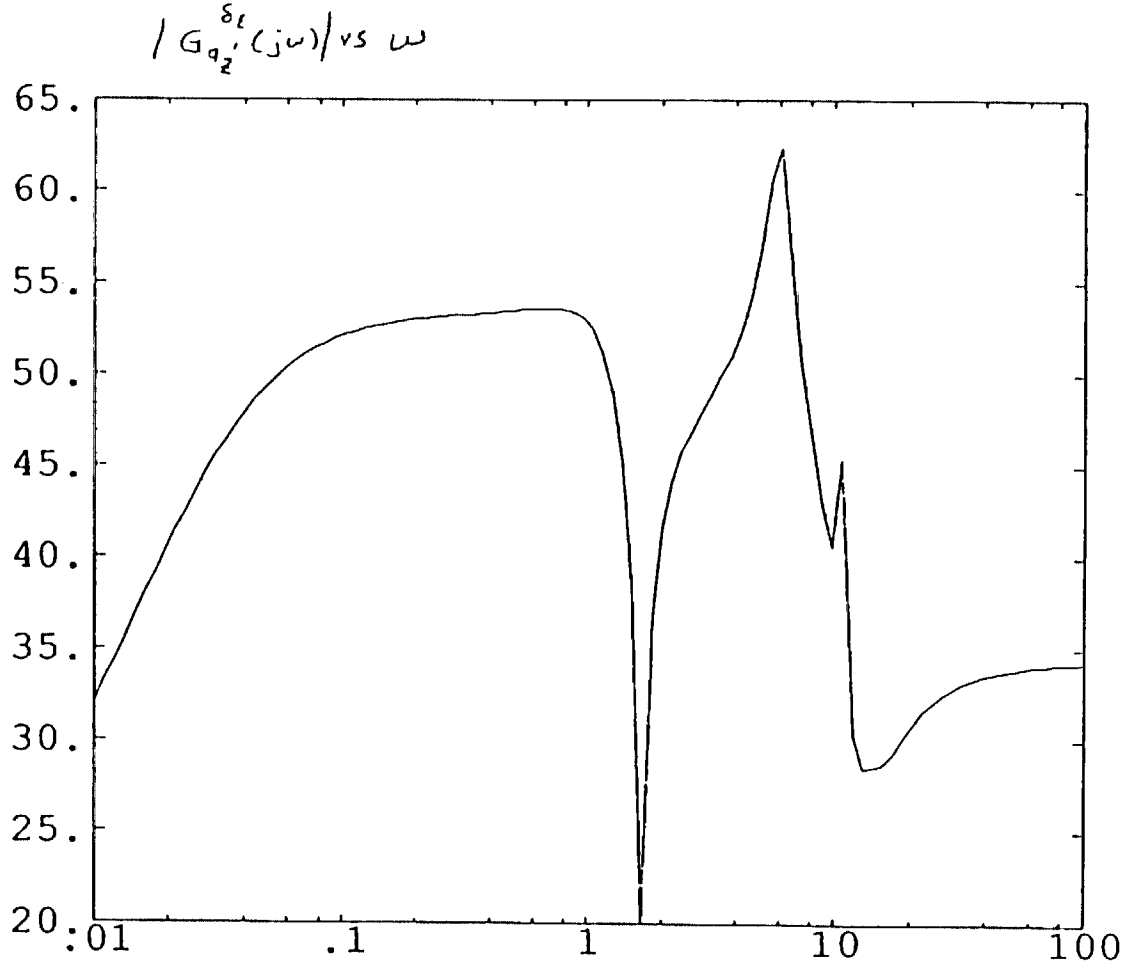

Full-order

a_{z_3}/δ_E

$|G_{a_z}^{\delta_E}(j\omega)|$ vs. ω

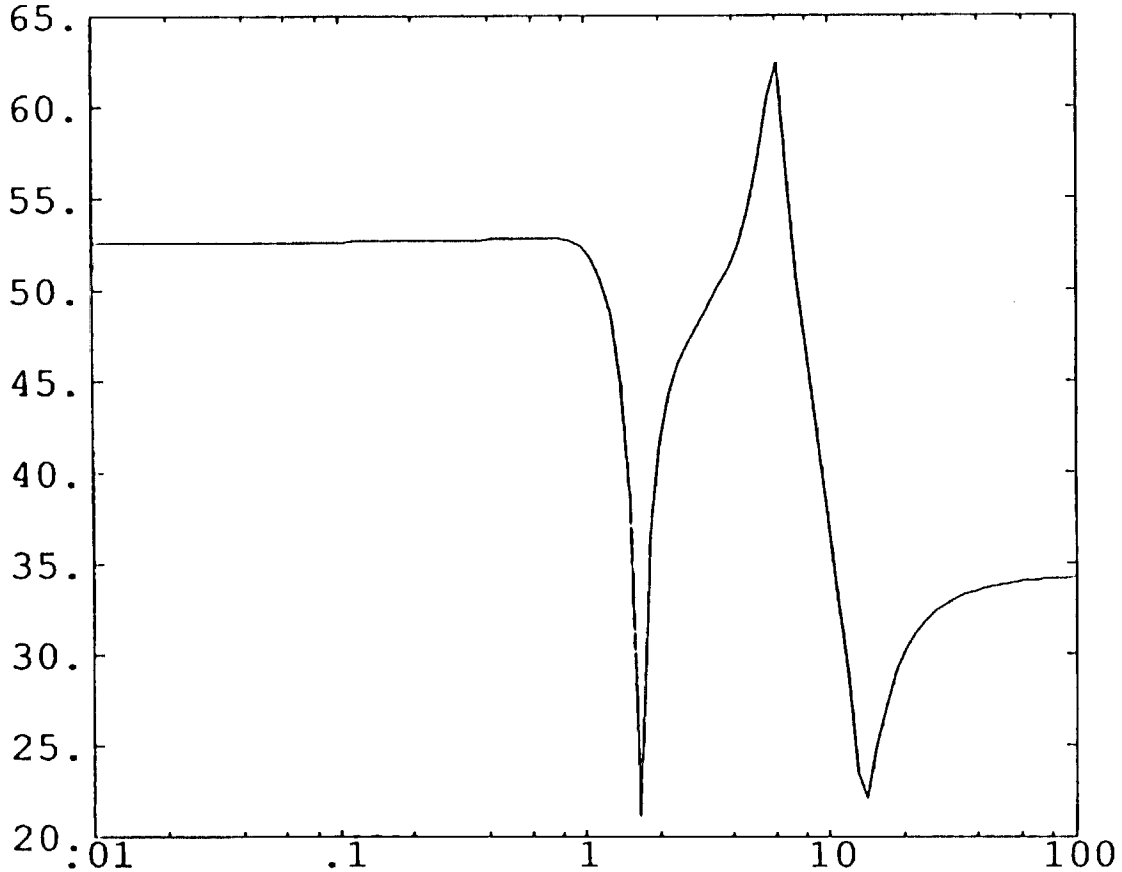

a_{z_s}/δ_E red

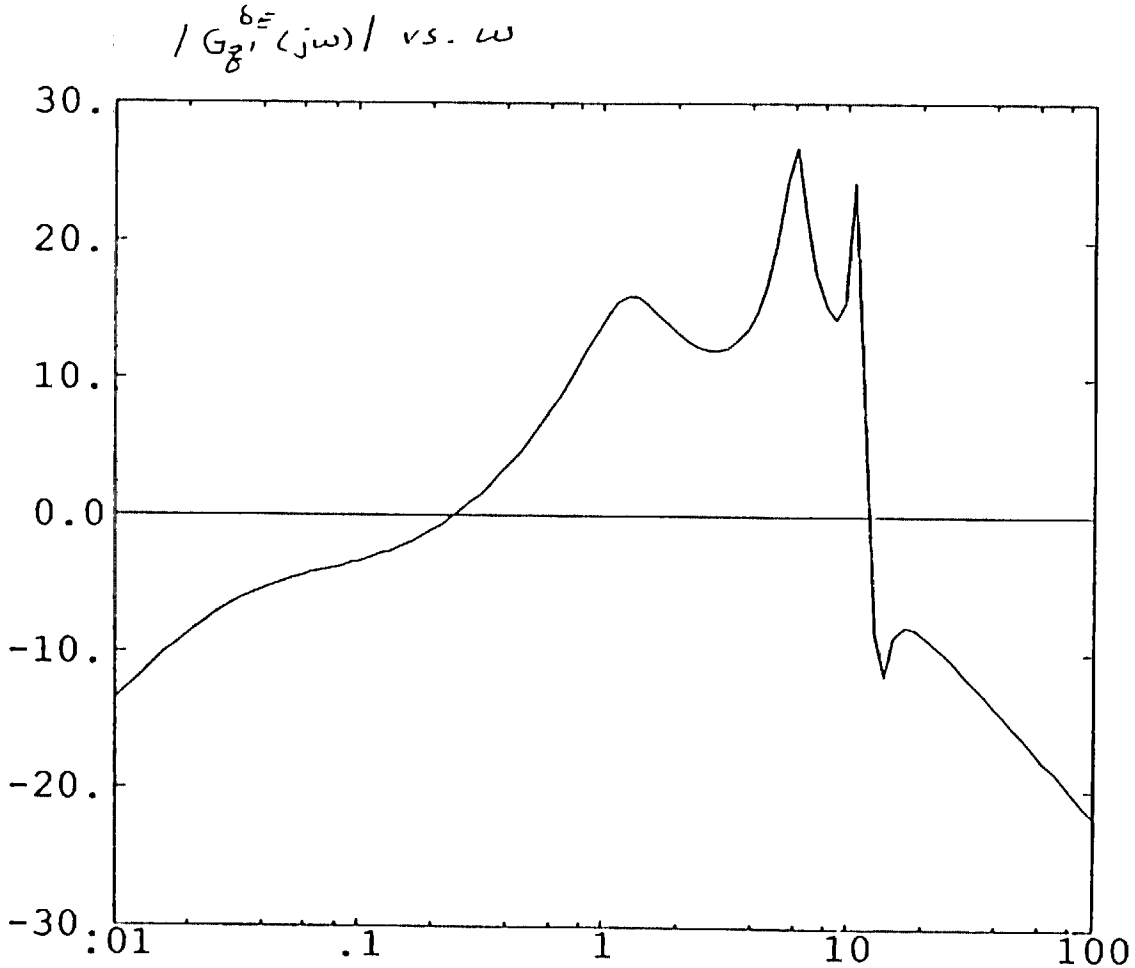

Full-order

q_s/δ_E

$|G_{q}^{\delta_E}(j\omega)|$ vs. ω

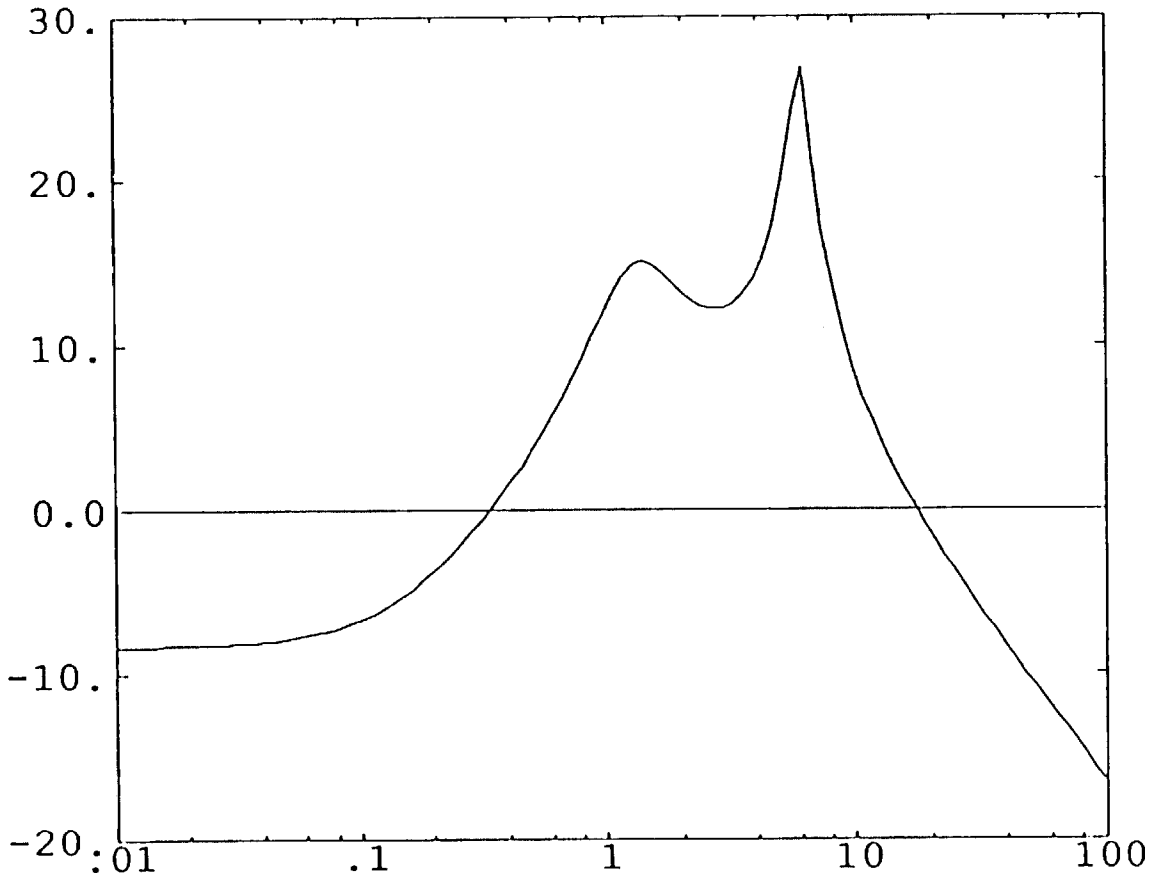

q_s/δ_E rad

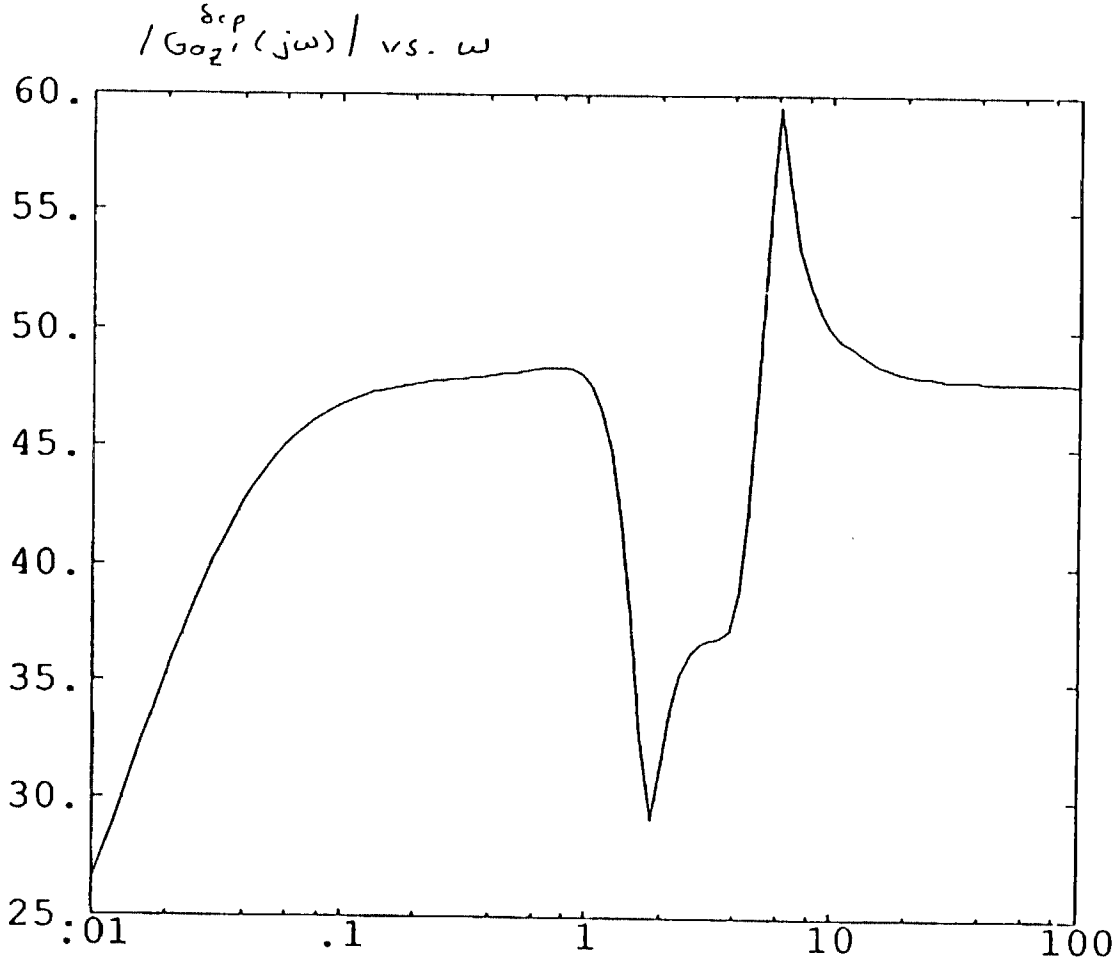

Full order

α_{T_3}/δ_c

7/21/89

$|G_{a_z}^{\delta_{cp}}(j\omega)|$ vs. ω

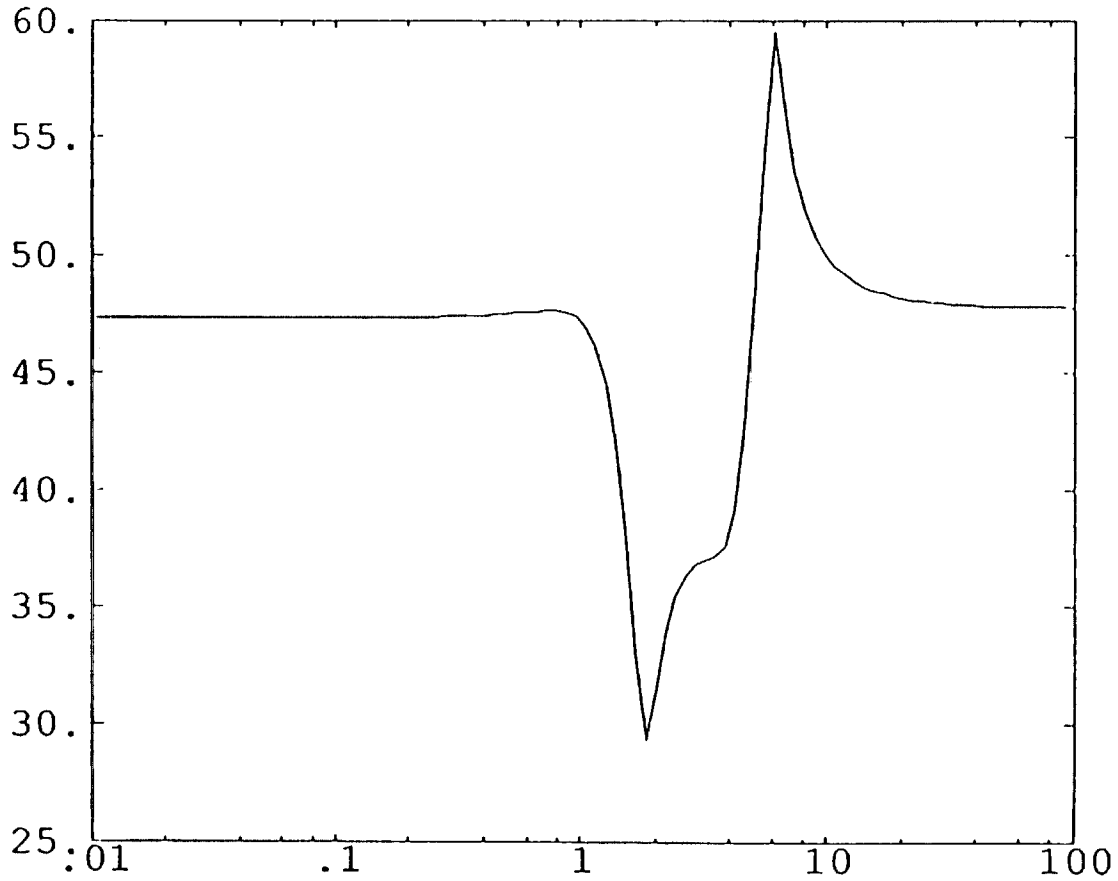

a_{z_s}/δ_c rad

7/21/89

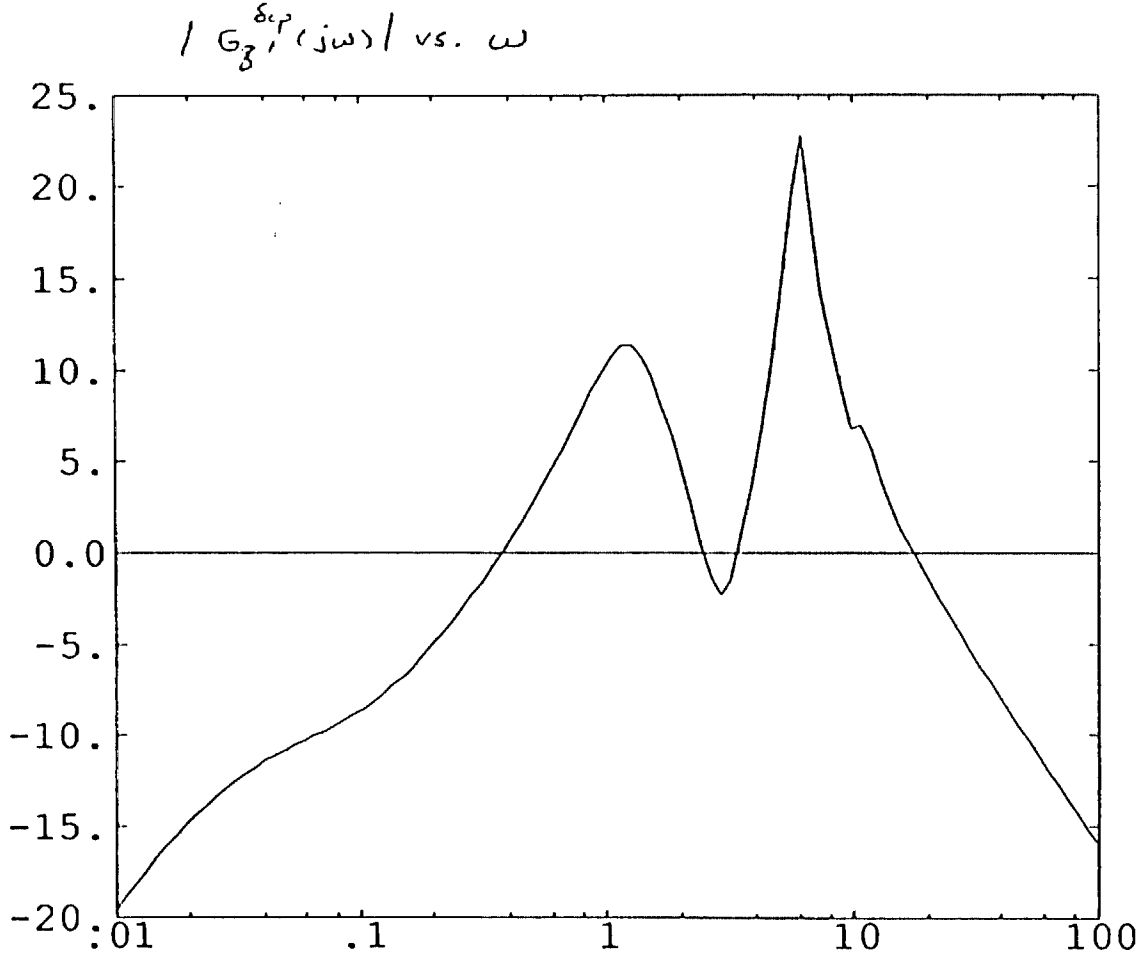

Full-order

δ_s/δ_c

7/21/89

$|G_{g}^{\delta_c p}(j\omega)|$ vs. ω

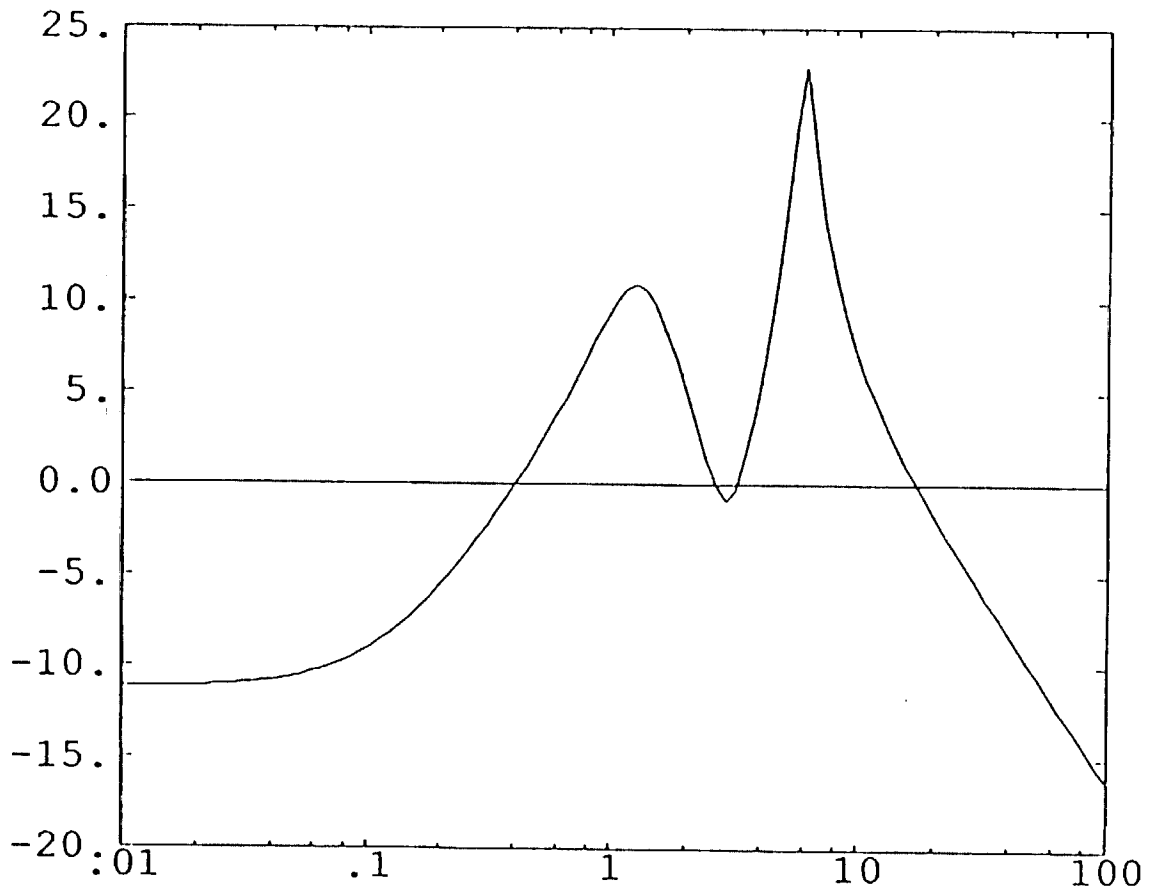

g_s/δ_c Red

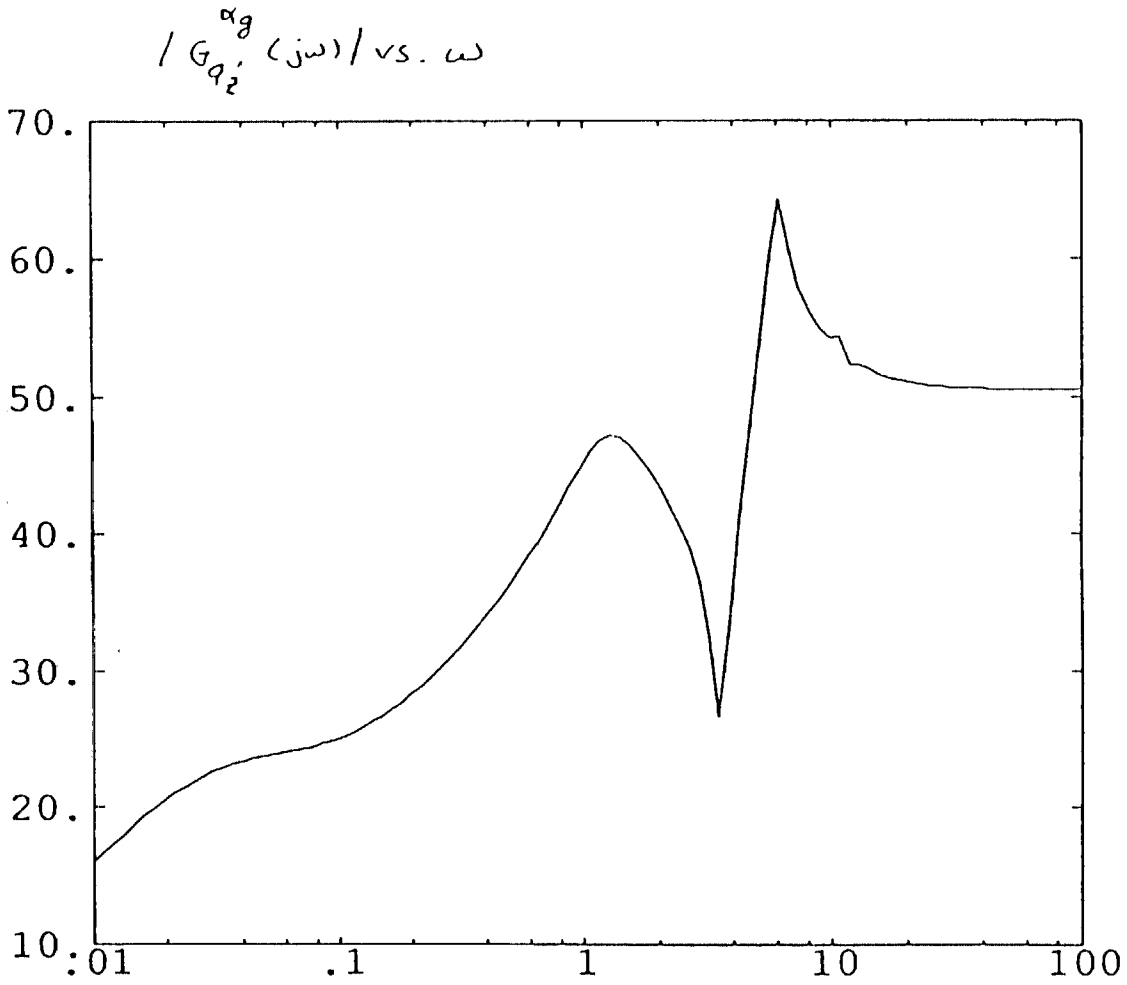

Full order

a_{z_s}/α_g

$|G_{a_z}^{a_g}(j\omega)|$ vs. ω

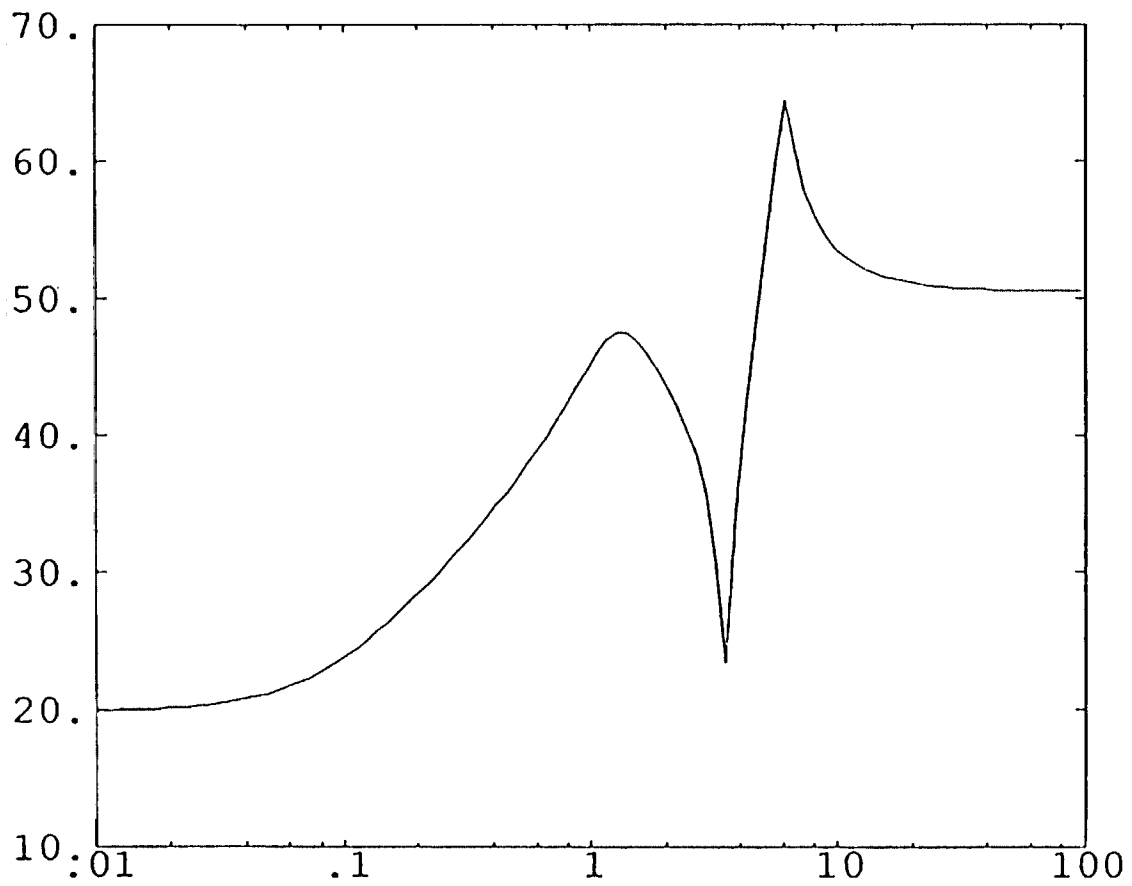

a_{z_s}/d_g rad

7/21/89

$|G_{q,\delta_q}^{\alpha_q}(j\omega)|$ vs. ω

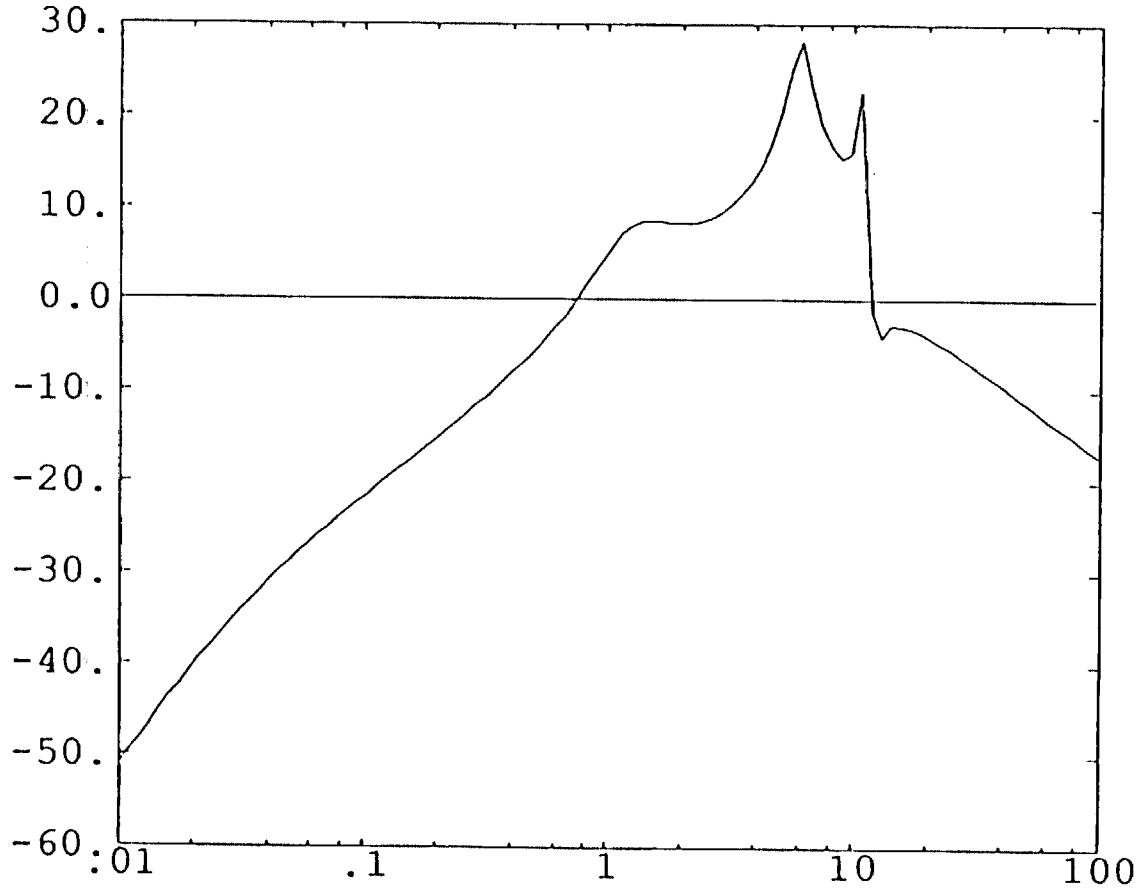

Full-order

q_s/δ_q

7/21/89

$|G_{\beta_s}^{\alpha_g}(j\omega)|$ vs. ω

β_s/α_g red

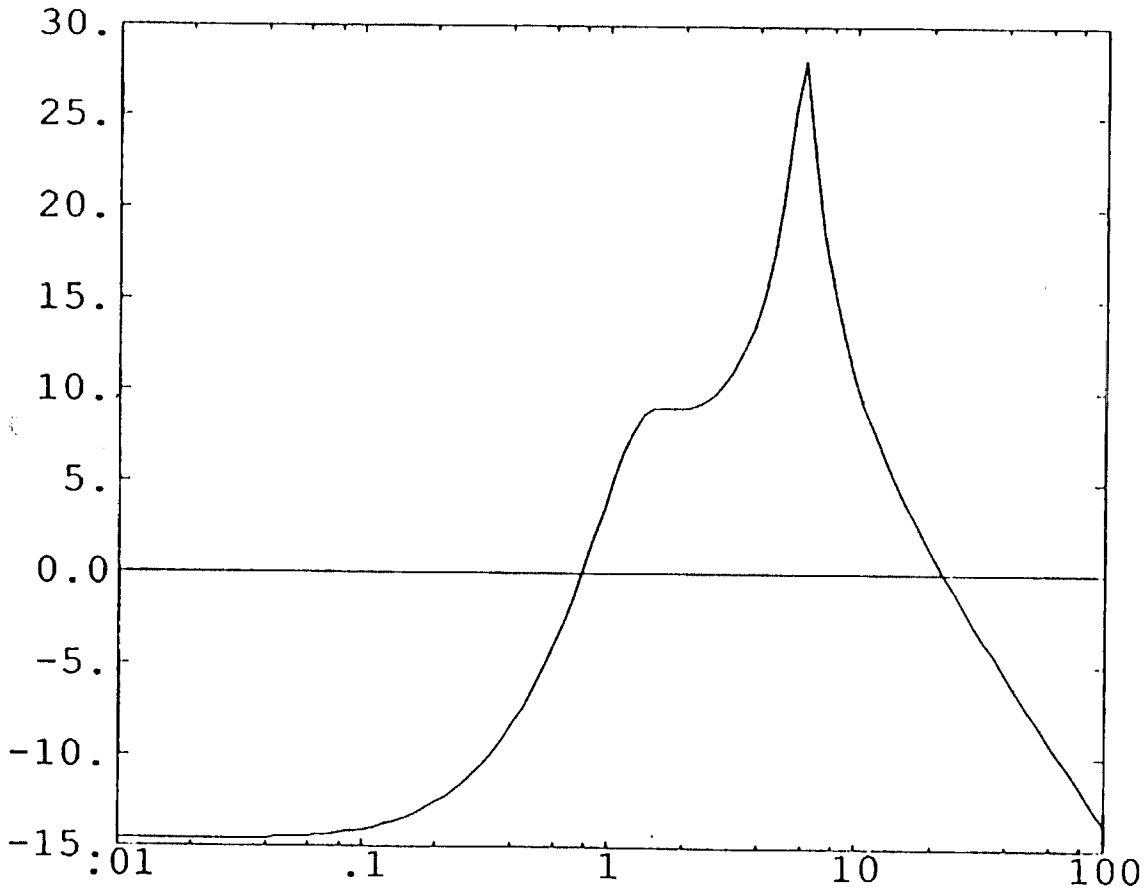

7/21/89

ANOTHER CRITICAL ISSUE

Don't Want Feasible ΔG (or K) To Lead To Large $\bar{\nabla}(\Delta GK)$

→ Notch Filters Vs. Robustness Theory

Demonstrate By Simple Example

Let $G(s) = \dfrac{(s^2 + 2 \cdot .025 + 1.^2)}{s(s^2 + 2 \cdot .0165 + .8^2)}$

→ stable, Min-Phase Plant
Should Be No Problem

Use Robust Control Theory To Obtain

$$K(s) = \frac{8(s^2 + 2 \cdot .0165 + .8^2)}{(s^2 + 2 \cdot .025 + 1.^2)(s + 8)}$$

The Loop-Shape Is Great

$g_m = \infty$, $p_m = 90°$

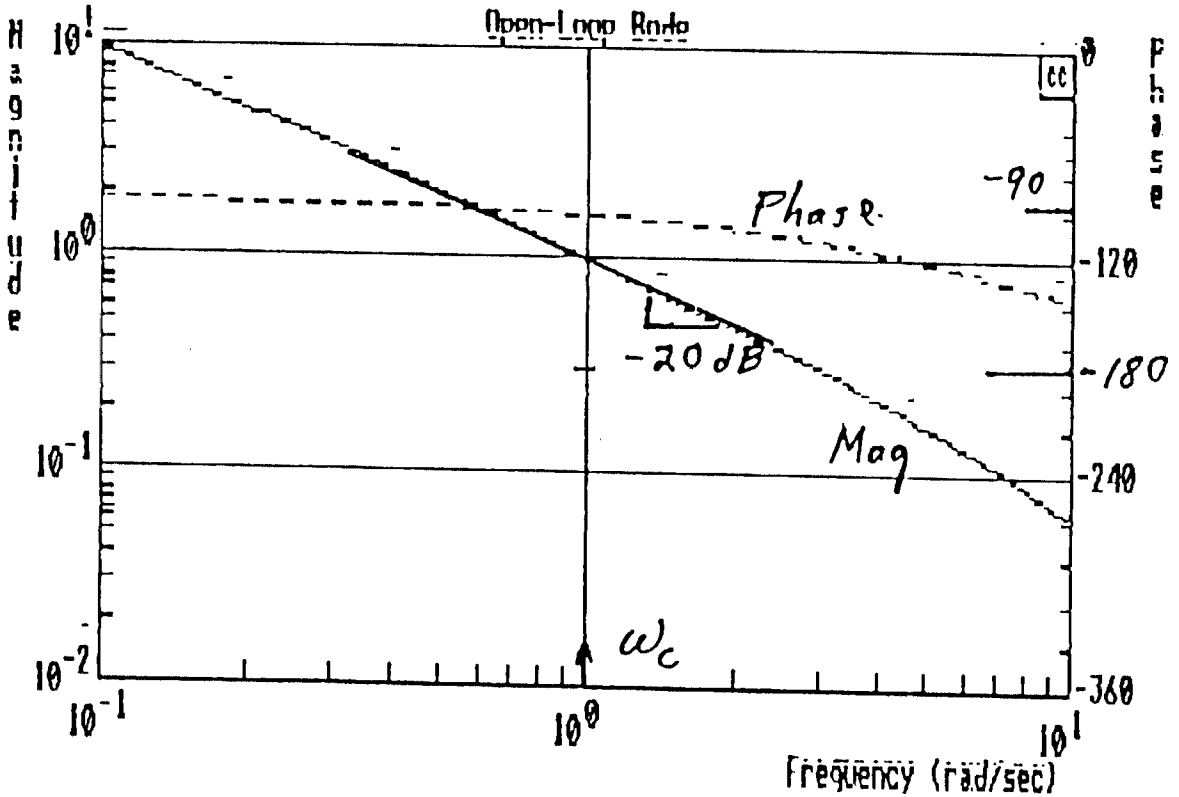

$|1+gK|$

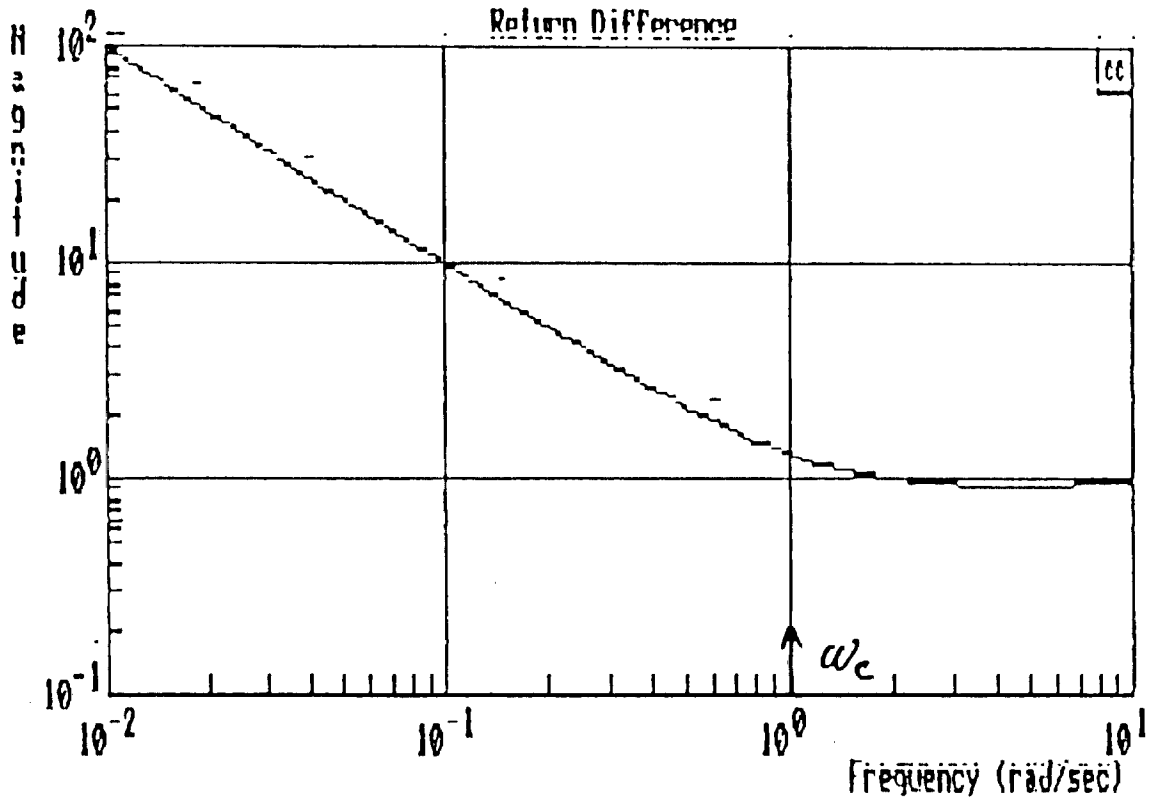
Return Difference
cc
Magnitude
10^2
10^1
10^0
10^{-1}
ω_c
10^{-2}
10^{-1}
10^0
10^1
Frequency (rad/sec)

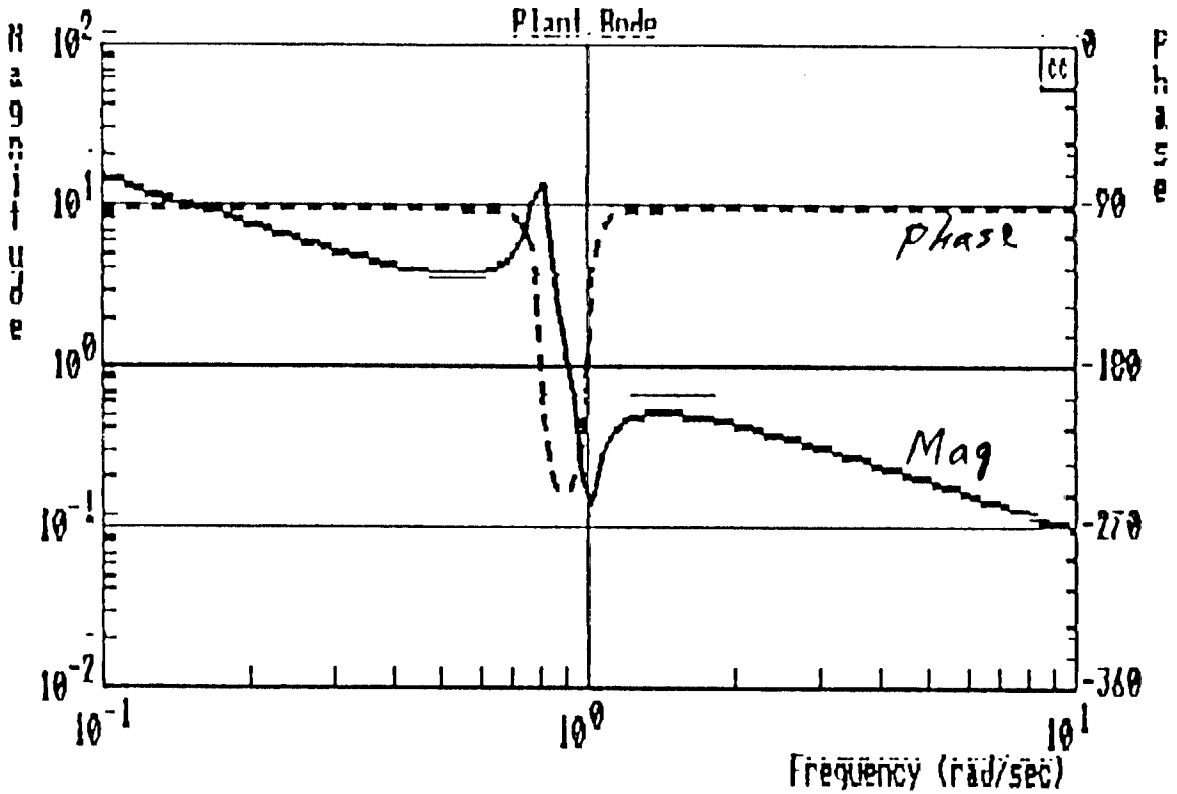
Plant Bode
Magnitude
Phase
10^2
10^1
10^0
10^{-1}
10^{-2}
0
-90
-180
-270
-360
Phase
Mag
10^{-1}
10^0
10^1
Frequency (rad/sec)

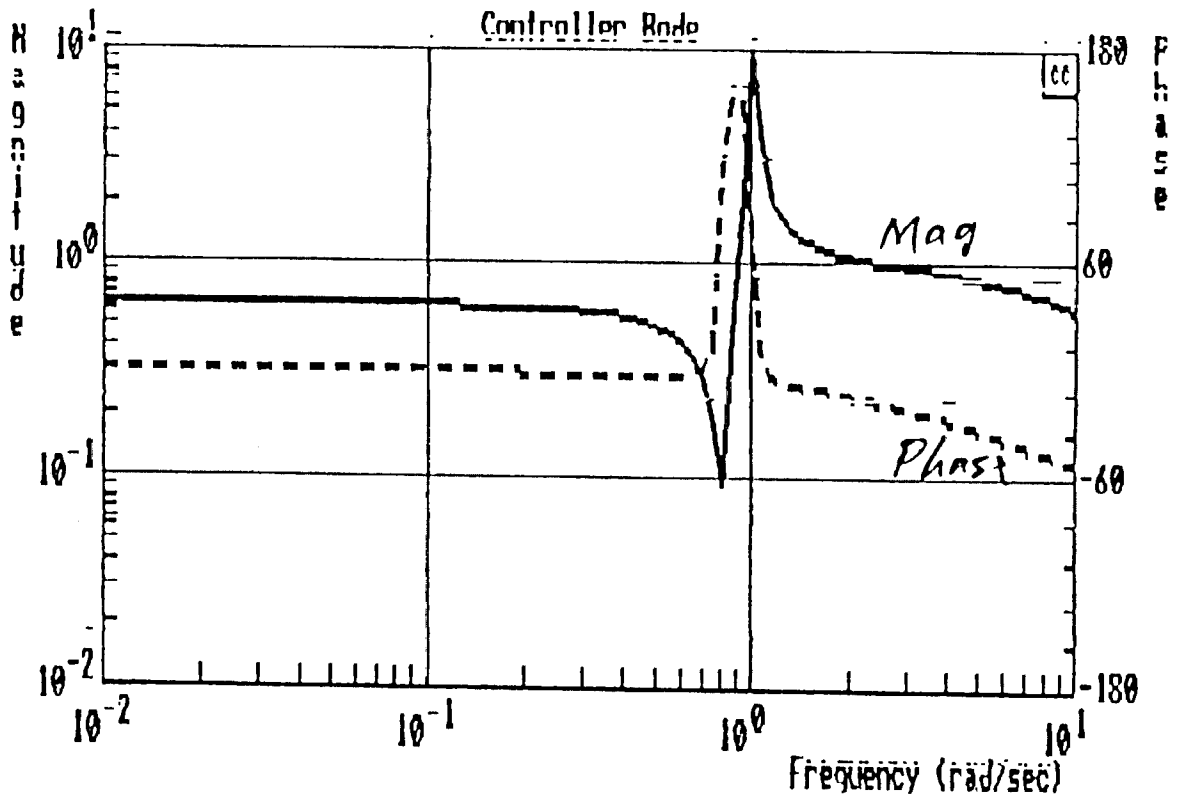
Controller Bode
Magnitude
Phase
Mag
Phase
Frequency (rad/sec)
10^{1}
10^{0}
10^{-1}
10^{-2}
180
60
-60
-180

7/21/89

CONSIDER THE FOLLOWING ΔG

Let $G_{True}(s)$ Be

Rather Than $G_{Design}(s)$

$$\frac{0.7(s^2+2(.0245)+1.2^2)}{s(s^2+2(.0165)+.8^2)}$$

$$G_{Des} = \frac{(s^2+2(.025)+1.^2)}{s(s^2+2(.0165)+.8^2)}$$

Or the "Zero Freqmency" Changes 20%

Let's Take A Look ——

(Note: From Literal Expressions For Flex. Aircraft Transfer Functions, The Above Could Result [illegible])

$|\Delta g K|$

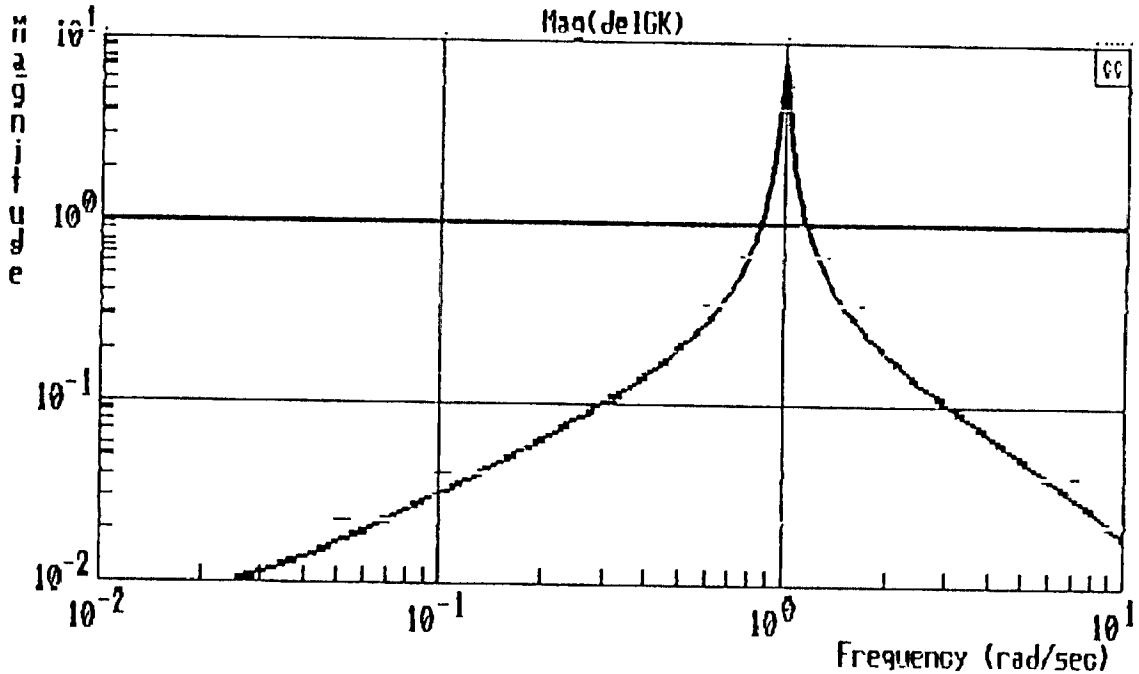

$|\Delta g K|$ is <u>Not</u> $< |1 + gK|$

THE ROOT LOCUS

"Real" Plant
(zeros moved)

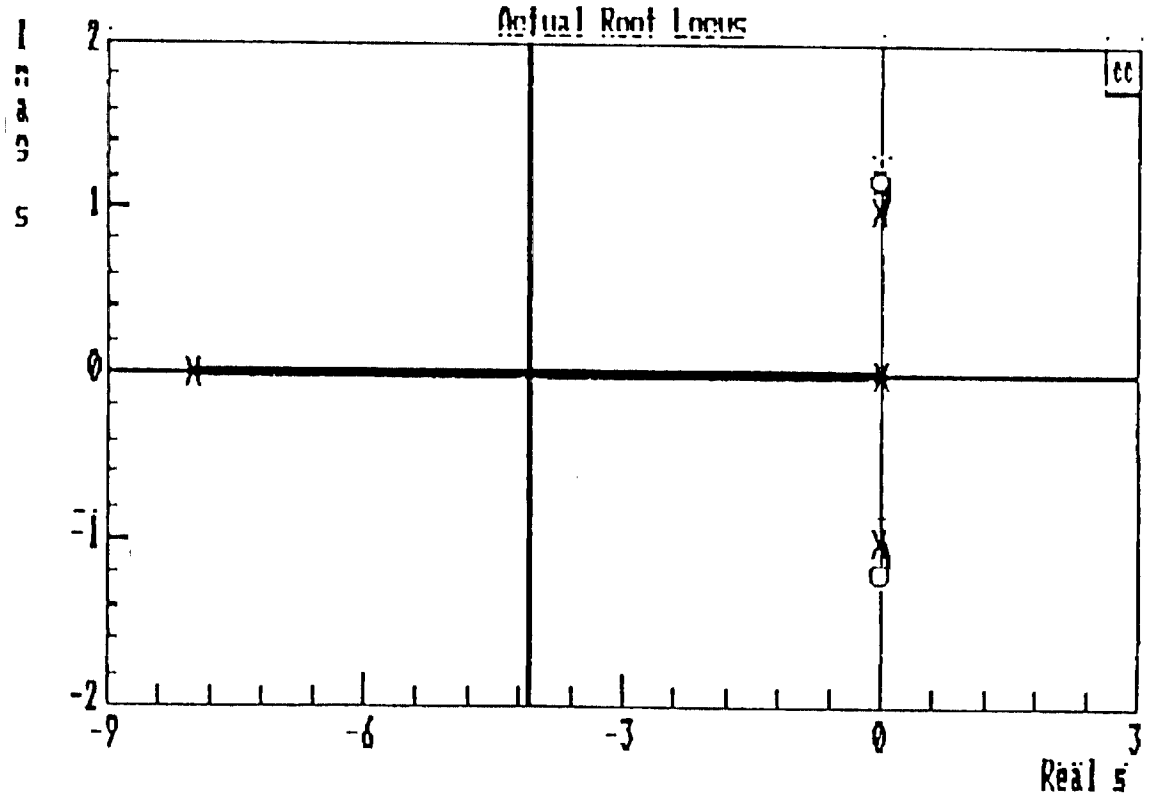

7/21/89

Conclusion - This K(s), although Yielding An Excellent Loop-Shape Was Not Able To Handle This Type Of ΔG

Also

→ The ΔG This Had This Catastrophic Effect Was Due To A Change In G(jω) where |G(jω)| was Small!

→ Model Reduction Must Do A Good Job Here Too!

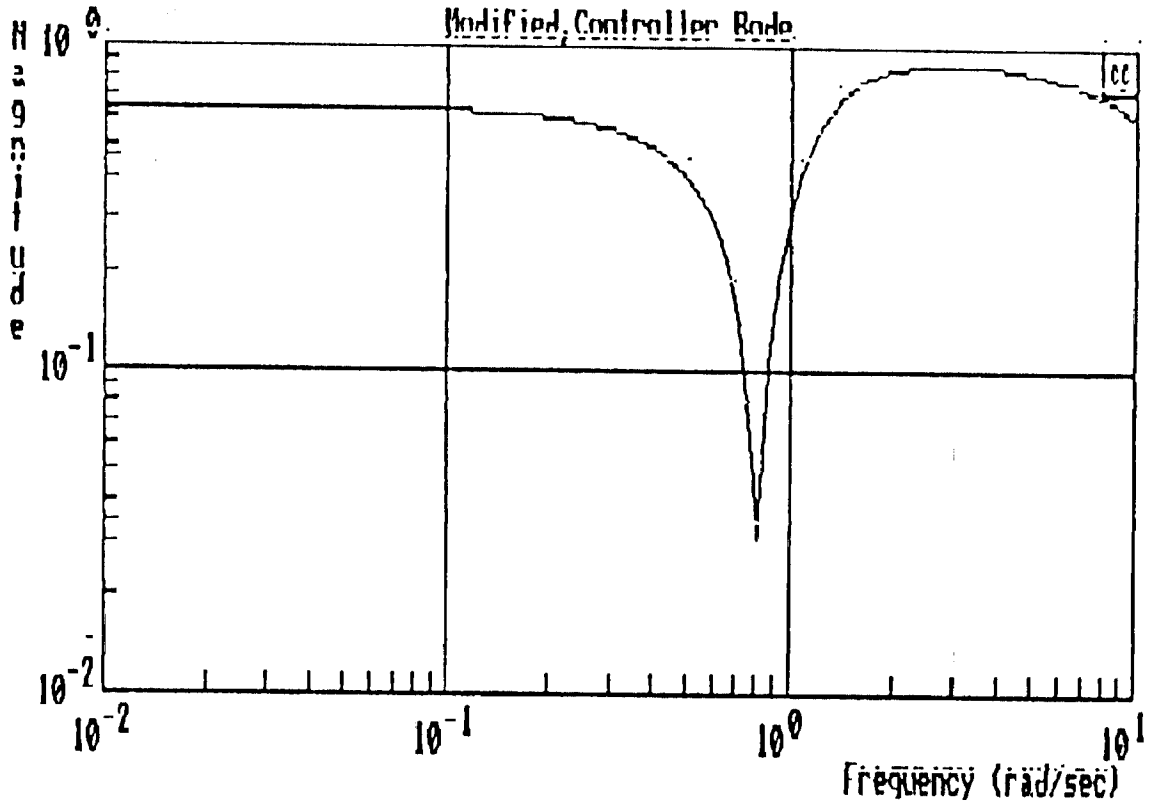
Modified Controller Bode
Magnitude
10^{0}
10^{-1}
10^{-2}
10^{-2}
10^{-1}
10^{0}
10^{1}
Frequency (rad/sec)
cc

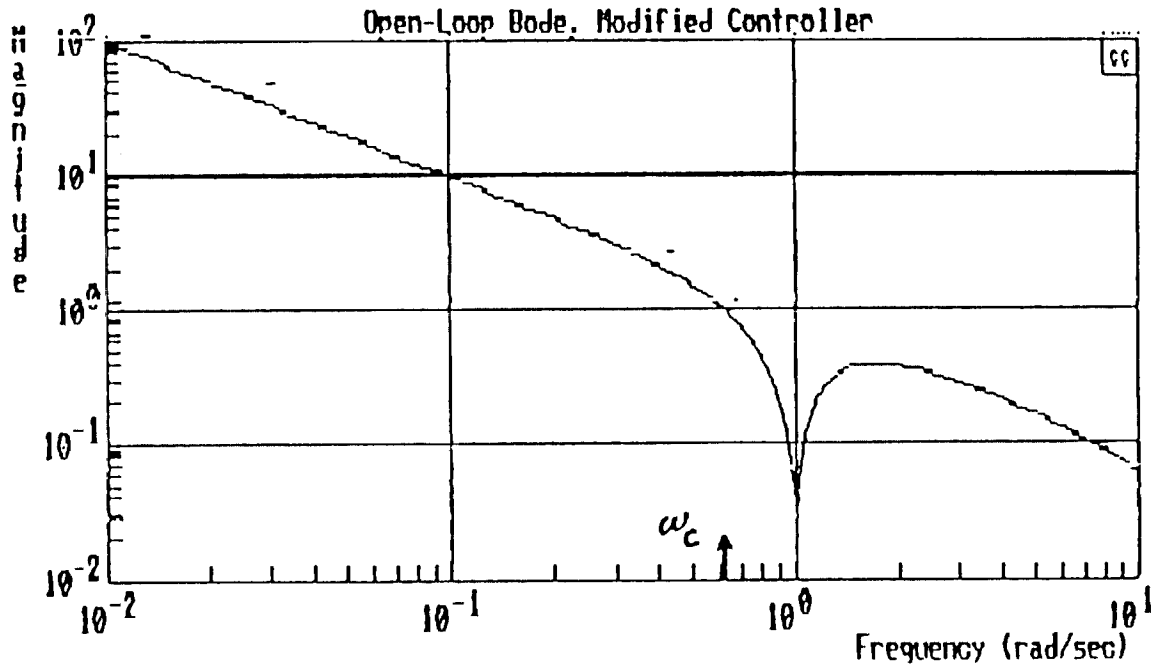
Open-Loop Bode, Modified Controller
cc
magnitude
10^{2}
10^{1}
10^{0}
10^{-1}
10^{-2}
ω_c
10^{-2}
10^{-1}
10^{0}
10^{1}
Frequency (rad/sec)

$|1+gK|$

New Control Law

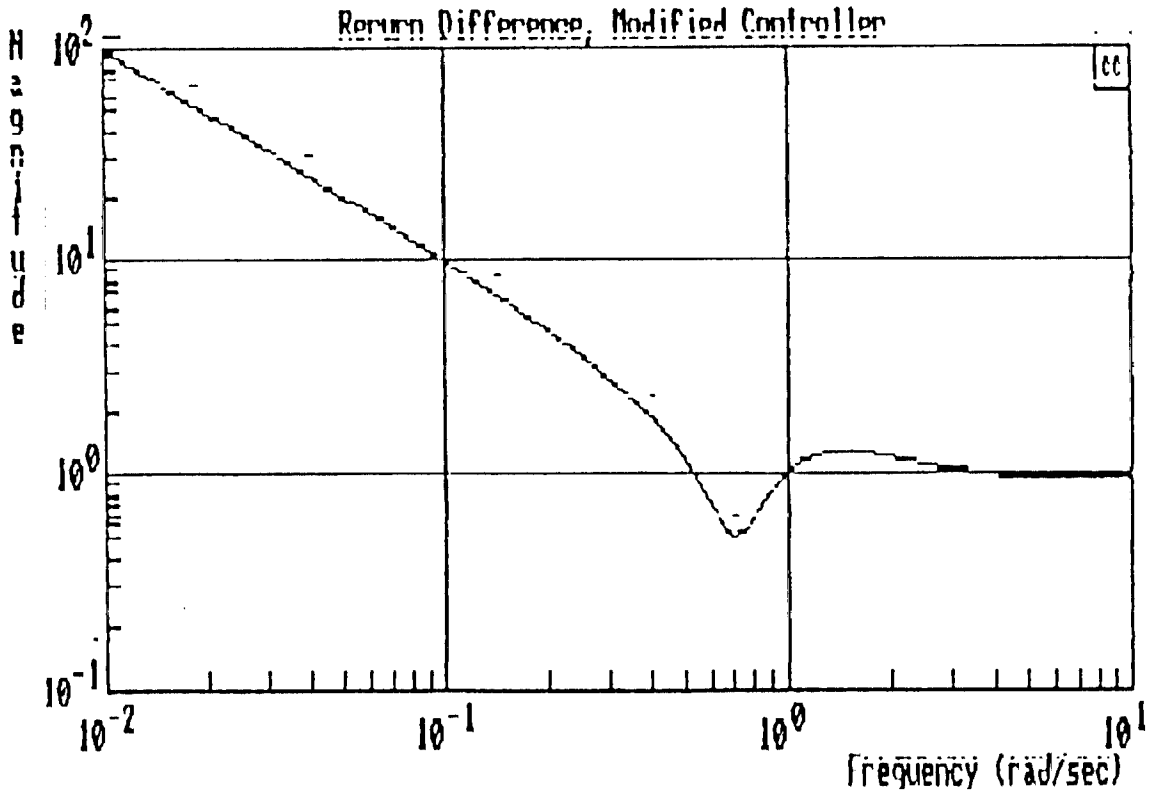

$|\Delta G K|$

New Control Law

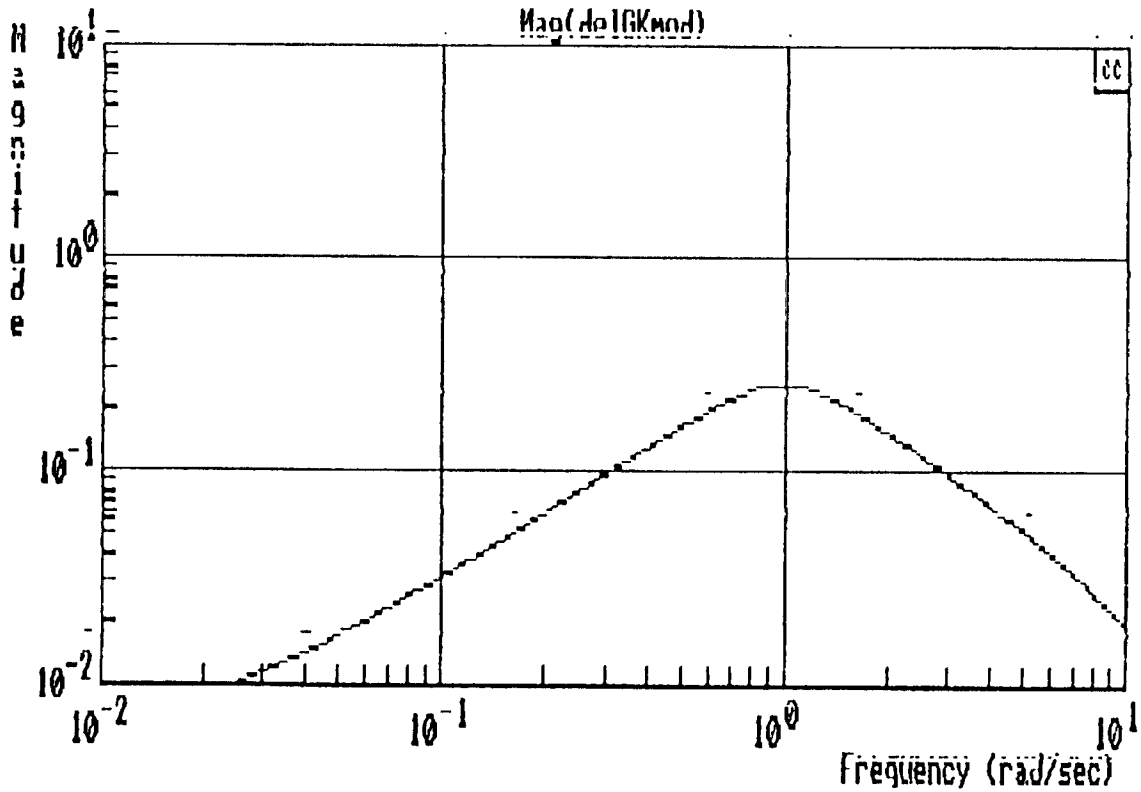

7/21/89

Redesign Control Law –

Don't Amplify This ΔG,

Or Smooth The Peak in K

→ Let $K(s) = \dfrac{8(s^2 + 2 \cdot .016 s + .8^2)}{(s^2 + 2 \cdot .6 s + 1.2^2)(s + 8)}$ "Notch Filter"

Loop-Shape Is Sacrificed But

System Is Robust Against This ΔG

(Note: MIMO Notch Synthesis In Schmidt, Schmidt + Newman '89)

ROOT LOCUS
"Real" Plant
Modified K(s)

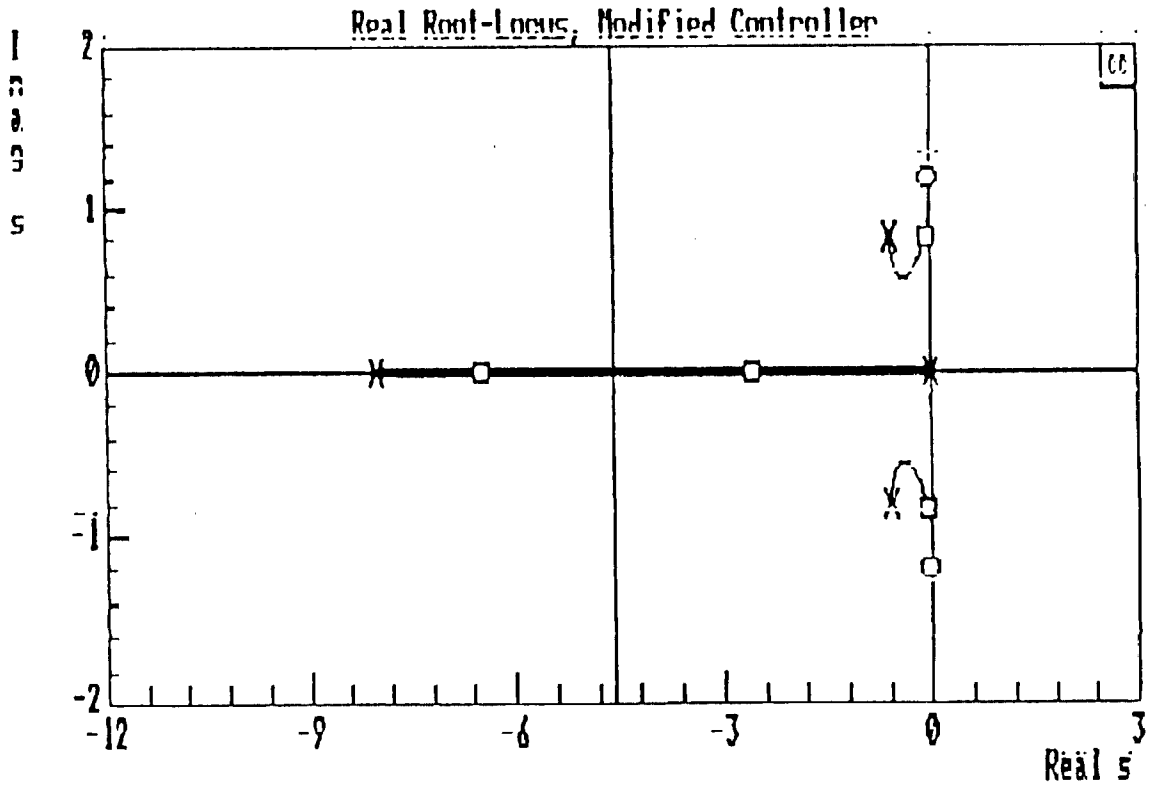

CONCLUSIONS

In Model Reduction, Preserve Classical Crossover Characteristics

Critical Char. Includes Those Where $|G(j\omega)|$ Small Sometimes

Weighted Balanced Procedure Shows Promise

Notch Filters Not Necessarily In Conflict With Robustness Theory - After Revisiting Carefully

Don't Cancel Lightly Damped Zeros